Département du second cycle

Mémoire de Fin d'Etudes

En vue de l'obtention du diplôme d'ingéniorat d'état

Filière : Electrotechnique

Spécialité : Traction électrique

Thème :

Model Predictive Control, application on an induction machine fed by a matrix converter

Présenté par : Mekhilef Aymen A.
Et par : Kasri Sinissa

Encadré par : Dr. Benachour Ali
Co-encadré par : Dr. Dali Ali

Soutenu publiquement, le : 02/09/2020,   Devant le Jury composé de :

M	Iffouzar Koussaila	Président
M	Benachour Ali	Encadreur
M	Dali Ali	Co-encadreur
M	Deboucha Abdelhakim	Examinateur

Binôme N° : 16 / PFE / 2020

Mémoire de Fin d'Etudes

En vue de l'obtention du diplôme d'ingéniorat d'état

Filière : Electrotechnique

Spécialité : Traction électrique

Thème :

Model Predictive Control, application on an induction machine fed by a matrix converter

Présenté par : Mekhilef Aymen A.
Et par : Kasri Sinissa

Encadré par : Dr. Benachour Ali
Co-encadré par : Dr. Dali Ali

Soutenu publiquement, le : 02/09/2020,   Devant le Jury composé de :

M	Iffouzar Koussaila	Président
M	Benachour Ali	Encadreur
M	Dali Ali	Co-encadreur
M	Deboucha Abdelhakim	Examinateur

Binôme N° : 16 / PFE / 2020

<u>ملخص:</u>

الهدف الرئيسي من هذا العمل هو دراسة وتنفيذ التحكم التنبؤي على عزم دوران (MPTC) آلة لا تزامنية ثلاثية الدور يغذيها مموج مصفوفي (MC). نبدأ دراستنا بتقديم نبذة حول المموجات المصفوفية و حول التحكم التنبؤي بتقديم بعض طوبولوجيات MCو بعض تطبيقات التحكم التنبؤي. بعد ذلك ننتقل الى تطبيق التحكم التنؤي على التيارالكهربائي (MPCC) و MPTC على حمولة RLو على آلة لا تزامنية على التوالي يغذيهما عاكس كهربائي في المقام الأول، ثم طبولوجيتين من MC. الجزء الأخير من هذا العمل محجوز للمقارنة بين النتائج التي تم الحصول عليها للمحولات الثلاثة وللمقارنة بين MPTC و بين التحكم المباشر على عزم الدوران (DTC).

<u>كلمات مفتاحية:</u>

مموج مصفوفي (MC)، آلة لا تزامنية، التحكم التنبؤي (MPC)، دالة التكلفة.

<u>Abstract:</u>

The main objective of this topic is to study and implement the Model Predictive Torque Control (MPTC) applied to the three-phase induction machine fed by a Matrix Converter (MC). We begin our study by a state of the art on the matrix converters and the predictive control presenting some topologies of the MC and some applications of the predictive control. Then, Model Predictive Current Control (MPCC) and MPTC have been applied to an RL-load and to an induction machine respectively, driven by an inverter in the first place, and then by two topologies of the MC. The last part of this work is reserved for a comparison between the obtained results of the three converters and for a comparison between MPTC and Direct Torque Control (DTC).

<u>Key words:</u>

Matrix Converter (MC), induction machine, Model Predictive Control (MPC), cost function.

<u>Résumé :</u>

L'objectif principal de ce sujet est d'étudier et implementer la commande predictive du couple à base du modèle (MPTC) appliquée à la machine asynchrone triphasée alimentée par convertisseur matriciel (MC). Nous commençons notre étude par un état de l'art sur les convertisseurs matriciels et sur la commande predictive en présentant quelques topologies du MC et quelques applications de la commande predictive. Ensuite, la commande predictive du courant à base du modèle (MPCC) et la MPTC ont été appliquées à une charge RL et à la machine asynchrone respectivement, alimentée par un onduleur au premier temps, et puis par deux topologies du MC. La dernière partie de ce travail est réservée à une comparaison des résultats obtenus des trois convertisseurs et à une comparison entre la MPTC et la commande direct du couple (DTC).

<u>Mots clès :</u>

Convertisseur Matriciel (MC), machine asynchrone, la commande predictive à base du modèle (MPC), function de coût.

Dedication

In the memory of my grandfather, Seridi Ali, the foremost seeking knowledge supporter whom I have ever known,

To my loving parents, who through thick and thin, have been and still are there for me,

To my sister,

To my family,

To my advisor,

To my co-advisor,

To my project partner,

To my friends in general and to my soul mate, Abderrahmane Kaced in particular,

I dedicate this humble work.

Aymen Abdelmounaim Mekhilef

Dedication

To my dear parents, Lahouas and Farida, for all their sacrifices, their love, their tenderness, their support and their prayers throughout my studies,

To my dear sisters, Ibtissem and Mounia, for their constant encouragement and moral support,

To my brother Yacine and his wife Hawa, for their support and encouragement,

To all my family for their support throughout my university career,

To my advisor Mr. Benachour, and my co-advisor, Mr. Dali for their availability and their supervision during the realization of this modest work,

To my partner in the Final Year Project, Aymen, for his help since the beginning,

To all my friends from the Electric Traction class of 2020,

May this work be the fulfillment of your wishes, and the fruit of your infallible support,

Sinissa Kasri

Table of contents

TABLE OF CONTENTS

LIST OF TABLES

TABLE OF FIGURES

LIST OF SYMBOLS AND ACRONYMS

List of tables

LIST OF TABLES

Table of figures

TABLE OF FIGURES

List of symbols

and acronyms

LIST OF SYMBOLS AND ACRONYMS

MC : Matrix Converter

IMC : Indirect Matrix Converter

DMC : Direct Matrix Converter

SMC : Sparse Matrix Converter

MIMC : Multilevel Indirect Matrix Converter

ZSMC : Z-source Matrix Converter

2LVSI : Two-Level Voltage Source Inverter

NPCC : Neutral-Point Clamped Converter

MPC : Model Predictive Control

MHPC : Model Heuristic Predictive Control

MMPC : Modified Model Predictive Control

DMC : Dynamic Matrix Control

GPC : Generalized Predictive Control

PSC : Predictive Speed Control

P-DPC : Predictive Direct Power Control

MPCC : Model Predictive Current Control

MPTC : Model Predictive Torque Control

DTC : Direct Torque Control

SVM : Space Vector Modulation

PWM : Pulse Width Modulation

T_s : sampling period

UPFC : Unified Power Flow Controller

FCS-MPC : Finite Control Set-Model Predictive Control

FACTS : Flexible AC Transmission Systems

StatComps : Static synchronous compensators

APF : Active Power Filter

SHE : Selective Harmonic Elimination

SHM : Selective Harmonic Mitigation

THD : Total Harmonic Distortion

V_{DC} : DC source voltage

M : Neutral point of the inverter

N : Neutral point of the load

PMSG : Permanent Magnet Synchronous Generator

φ_r : Rotor flux

φ_s : Stator flux

i_s : Stator current

i_r : Rotor current

v_s : Stator Voltage

v_r : Rotor voltage

L_m : Magnetizing inductance

L_s : Stator inductance

R_s : Stator resistance

L_r : Rotor inductance

R_r : Rotor resistance

M_s : mutual inductance between two stator windings

M_r : mutual inductance between two rotor windings

M_{sr} : magnitude of the inductance between the stator and the rotor

Ω : mechanical speed

J : moment of inertia of the mechanical shaft

T_{em} : electromagnetic torque

T_L : load torque

k_f	: dry friction coefficient
ω	: rotor angular speed
p	: number of pole pairs
ξ	: damping coefficient
ω_n	: natural circular pulse
Q	: reactive Power
R_f	: Filter resistance
L_f	: Filter inductance
C_f	: Filter capacitance
α	: Temperature coefficient
T	: Temperature
λ	: weighting factor

General Introduction

General introduction

The use of power converters has become very popular in the recent decades for a wide range of applications, including drives, energy conversion, traction, and distributed generation. The control of power converters has been extensively studied, and new control schemes are presented every year.

For years, induction machines were powered using an AC-DC-AC conversion chain which is often bulky and can be a source of disturbance for the electrical grid [1], [2]. In order to overcome these problems, the matrix converters, which are single stage converters, were proposed in the literature to replace AC-DC-AC converters.

In electric traction and for medium and high power, variable speed drives using induction machines are finding more and more industrial applications. An application can be found in embedded variable speed drives in naval ships [2]. In addition, the choice of converters and their control offers an interesting alternative to the reduction of the constraints related to the design and the generation of current and torque harmonics [2], [3].

Several control schemes have been proposed for the control of power converters and drives. Among these control schemes, hysteresis and linear controls with pulse-width modulation (PWM) are the most established in the literature [4], [5], [6]. However, with the development of faster and more powerful microprocessors, the implementation of new and more complex control schemes became possible [7], [8], [9]. Some of these new control schemes for power converters include fuzzy logic, sliding mode control, and predictive control.

The main objective of this work is the application of predictive control of power converters associated with an induction machine (IM). Indeed, we will be interested in the two topologies of the matrix converter namely the direct and indirect topology and the two-level voltage source inverter.

This thesis is organized into five chapters, it is summarized as follows:

The first chapter is dedicated to an overview on the matrix converters by citing the different topologies proposed in the literature, the chapter is concluded with some applications of the predictive control.

The second chapter is devoted to the analysis and the simulation of predictive control applied to a two-level three-phase inverter feeding an RL-load with evaluation of input and output performance.

In the third chapter, we developed a model predictive torque control (MPTC) of an induction machine that is driven by an inverter. We start by presenting the MPTC and its working principle. After that, a modeling of the induction machine and an analysis of its electromagnetic and electrical performances are presented.

The fourth chapter is dedicated to the analysis and the simulation of the two topologies of the matrix converter (direct and indirect). A model predictive current control has been applied to a matrix converter-fed RL load. The performance of the input and the output variables of each topology is evaluated.

The last chapter of this thesis covers the application of MPTC of an induction machine using direct and indirect topologies of the matrix converter and a comparison between the three converters is presented, while considering the input reactive power controllability and the robustness to the variation of the stator resistance and other aspects.

The general conclusion concerns a brief synthesis of the work carried out with the main obtained results and some perspectives.

Chapter I:

The Matrix Converter and The Model Predictive Control: A state of art

Chapter I : The Matrix Converter and the Model Predictive Control: a state of art

Matrix converters (MC) are a well-known class of direct AC–AC power converter topologies that can be used in numerous applications, where compact volume and low weight are necessary. For good performance, special attention should be paid to the control scheme used for these converters. In 1989, Alesina and Venturini [10] proposed a modulation technique that enables the amplitude of the output voltage of the MC to reach its intrinsic limit. However, the conception of such control algorithm can be overwhelming. The model predictive control strategy is a promising, straightforward and flexible choice for controlling various different matrix converter topologies [11].

This chapter is divided into two main parts, one is devoted to the state of the art of the MC, and the other part is devoted to the state of the art of the Model Predictive Control (MPC). Where some topologies of the converter and some applications of the control strategy have been presented.

I.1. State of the art of the matrix converter

I.1.1. Introduction

Power electronics is a technology that facilitates electrical energy conversion between source and load based on the combined knowledge of energy systems, electronics and control, and this action is made by converters which are electronic circuit based on high power handling semiconductor devices, energy storage elements and magnetic transformer. A well-known example AC-AC frequency converter

Frequency converters convert AC electrical power of one frequency into AC electrical power of different frequency [12]. In addition, this kind of converter also has the capability to control the load voltage amplitude, the displacement angle between source currents and voltages (input power factor) and also, the capability to control bi-directional (or only unidirectional) power flow through the converter [12].

As the popularity of AC motors in the industry continues to grow, AC - AC converters are used in the applications of variable speed drives to control the speed and torque of current motors alternative. AC - AC converters can be divided into two types: Indirect Converters and Direct converters.

I.1.2. Direct AC-AC converters
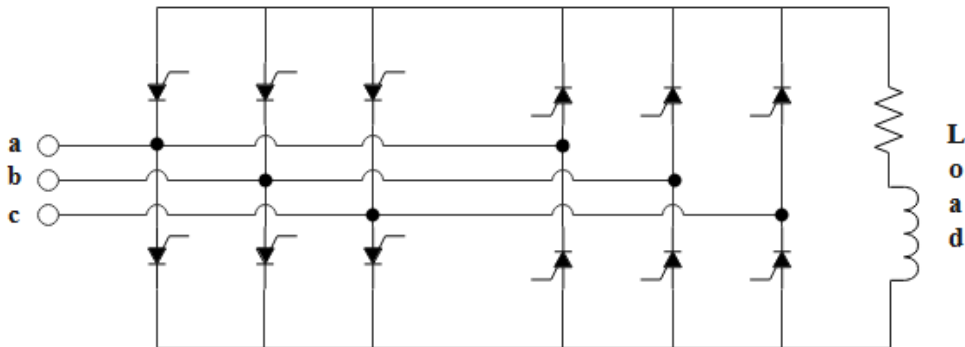
Figure I.1: Cyclo-converter

This structure is very promising, it came to put an end to the problem of energy storage that the indirect structure had suffered before, but it is not too widespread because it uses thyristors as power switches, which are not bidirectional. However, scientists have shown their intense interest in cyclo-converters with forced commutation in other words "matrix converters" to be able to meet industrial requirements, especially when volume, weight, and reliability are basic criteria. the major advantage of a cyclo-converter which was the first direct AC-AC converter is to be able to convert without the need for storage elements [13] .

At the input of this kind of converter, we usually have a fixed amplitude and frequency. On the other hand, at the output the voltage is variable, this means that we can obtain a current supply with an adjustable input power factor whatever was the load. Unlike indirect AC-AC converters (rectifiers-inverters), a cyclo-converter can only build a frequency lower than that of the input.

Without forgetting that by eliminating the energy storage element, we can have a more practical design but this type of converters suffers from the poor quality of the waveforms obtained, which makes its use rare in practice [14].

The first MC was proposed in 1976 by Guygyi-Pelly, and it is a cyclo-converters with a forced commutation and research has devoted to him for thirty years [12], [15].

The three-phase matrix converters are divided into three categories: Direct matrix converters, indirect matrix converters and z-source matrix converters [16].

In 1980, Ventirini and Alesena proposed the first direct Matrix Converter (3x3)[10]. It is a matrix of bidirectional switches, hence the name. And by applying an appropriate modulation strategy, such as space vector modulation (SVM), the matrix converter will be able to generate high quality sinusoidal input and output waveforms.
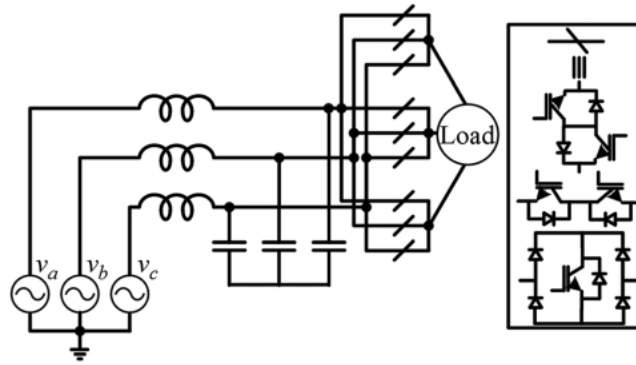
Figure I.2: Direct matrix converter (DMC)

I.1.3. Indirect AC-AC Converters

What characterizes this topology of converters is that there must be an energy storage capacitor and over time this becomes a drawback especially if the storage element is bulky [1]. Also, the duration of life of this element must be taken into consideration because it affects the overall life of the converter. All this makes this topology unsuitable for some applications, such as aerospace applications where the size and weight of the system are critical [13].
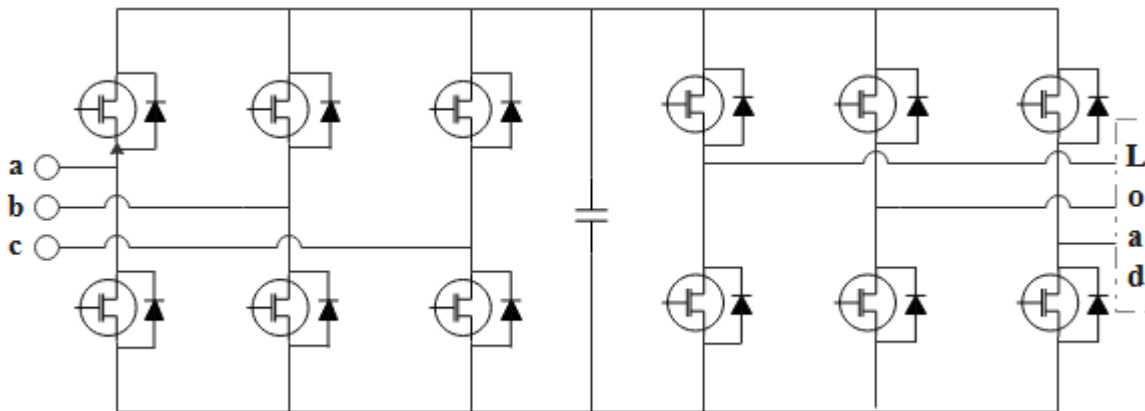
Figure I.3: Indirect AC-AC converter

I.1.4. Different topologies of indirect matrix converters

I.1.4.1.   Conventional Indirect Matrix Converters

In 1989 the Indirect Matrix Converter (IMC) was proposed by Holtz and Boelkens [5]. This structure was capable of producing output waveforms with the same quality as that of direct matrix converters [6], and in some cases it is preferable to use the indirect topology for the simplicity and the safety of switching and the ability to build other more complex topologies from this structure and with multiple inputs and outputs [13].
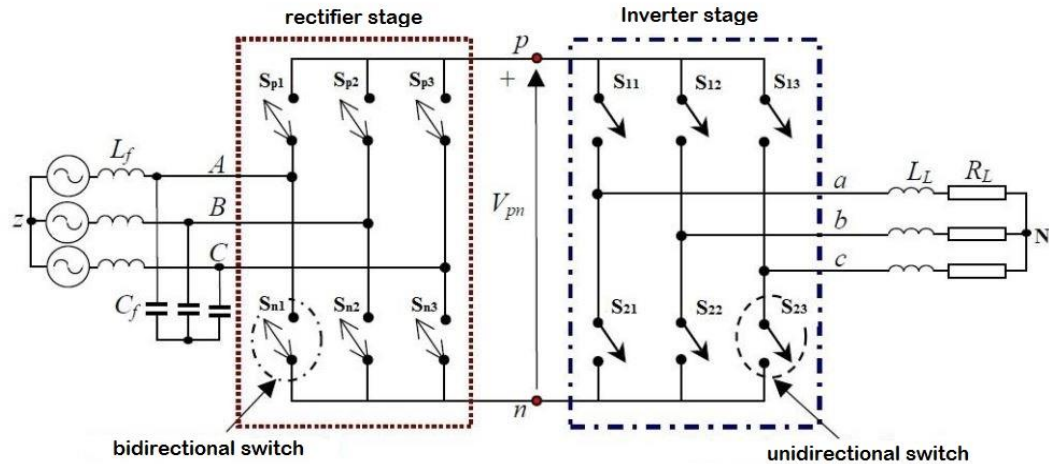
Figure I.4: Indirect Matrix Converter (IMC)

The AC-AC converter is divided into two parts with fictitious DC link. There is a fictitious voltage-fed rectifier on the input side and a fictitious voltage source inverter on the output side.

Conventional IMC structure contains six bidirectional switching devices forming a rectifier and six unidirectional switches forming an inverter, also known as two-stage MC. IMC also provides good voltage regulation and frequency regulation, but, unlike DMC, the commutation strategy is highly simplified. Zero dc-link current commutation is commonly employed in which the inverter stage is modulated into freewheeling mode and then the rectifier will commutate at zero DC link current [16]. This can also reduce the number of active devices, and active clamp circuits become simpler to implement [16].

I.1.4.2.   Sparse Indirect Matrix Converters

The rectifier end of the IMC can operate with both polarities of DC-link voltage, but the converter should have an explicit DC-link voltage polarity due to the inverter side, which leads to the formation of sparse MC (SMC). SMC consists of 15 transistors and 18 diodes as compared with conventional IMC, and it has more considerable conduction losses compared to conventional IMC.[19], it is used in aircraft actuators and in elevator drives [16].

I.1.4.3.   Very Sparse Indirect Matrix Converters

It is important to note that by implementing a zero DC link current control scheme, the IMC switching devices could be further reduced to 12, which would result in a new topology called MC very sparse. [19]. However, the system to be operated is not affected by regeneration and braking (operation in a single quadrant).

I.1.4.4.   Ultra Sparse Indirect Matrix Converters

If only unidirectional power flow is required like in aerospace applications, ultra sparse MC is a good option for providing variable frequency operation. As compared with other IMCs, it consists of only nine unidirectional switches and lower number of diodes [19]. Moreover, we can find this kind of converters in Aircraft's power systems [16].
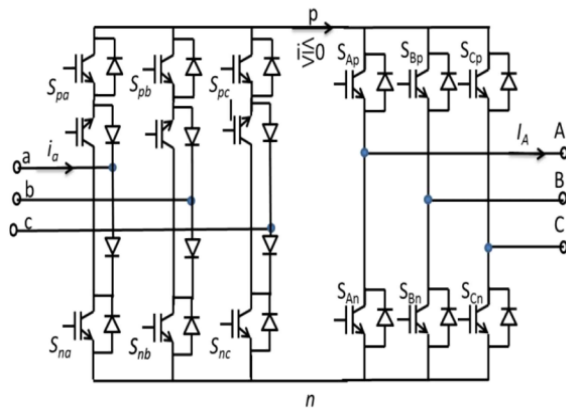
Figure I.5: Sparse Indirect Matrix Converter
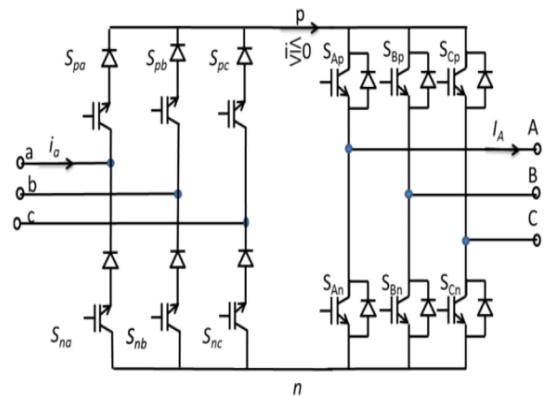
Figure I.6: Very sparse unidirectional IMC
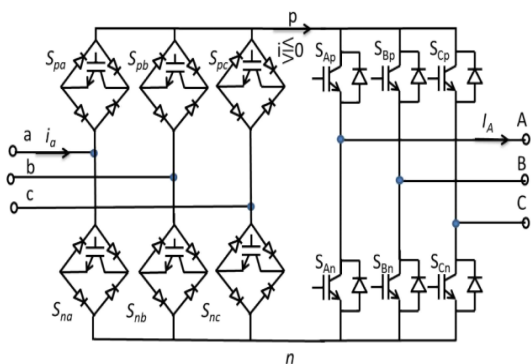
Figure I.8: Very sparse bidirectional IMC
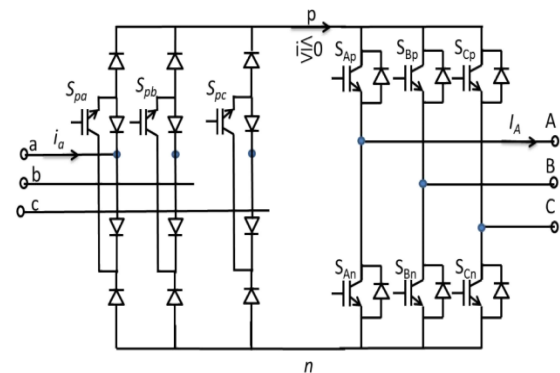
Figure I.9: Ultra sparse IMC

I.1.4.5.   Multilevel Indirect Matrix Converters

An alternative form of the conventional Indirect Matrix Converter, shown in Figure I.4, is the Multilevel indirect matrix converters (MIMC), shown in the Figure I.10. The MIMC is able to produce better quality output waveforms than IMC in terms of harmonic content because of its closer form to a sinusoid wave form but with higher number of power switches [20] in the inverter stage.
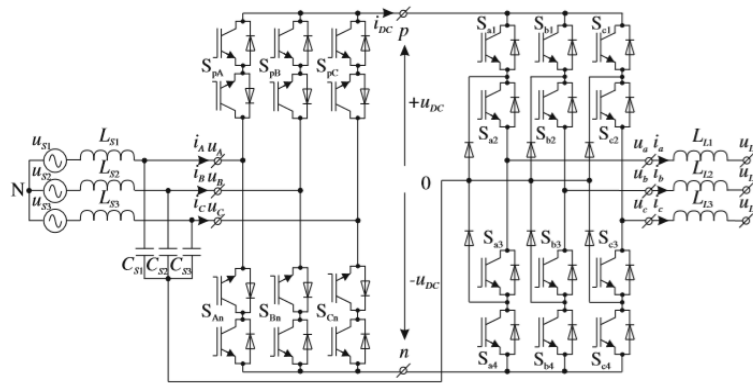
Figure I.10: Multi-Level IMC

Indirect three-level sparse matrix converter was introduced in the literature [21], it has the advantage of lower power switches.

I.1.5. Z-source Matrix Converters

In 2012, the three-phase Z-source MC (ZSMC) was proposed in [22] but it existed long before [23], this structure offers both step-up/step-down functions within a single stage and provides frequency regulation as well. As shown in the figure below, ZSMC has three stages: source side MC, Z-source network, and load side MC. Whenever boost voltage is required, the source side MC is operated in shoot-through interval (all switches are turned on). The longer the interval, the higher is the boost achieved.
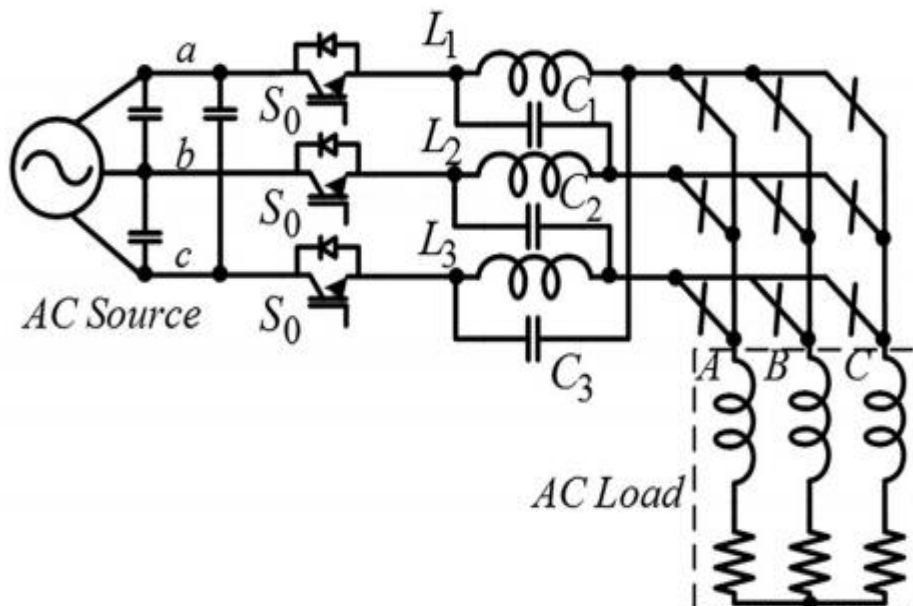
Figure I.11: Z-source Matrix Converter

I.2. State of the art of the Model Predictive Control

I.2.1. Introduction

Model Predictive Control (MPC) has been a topic of research and development for more than three decades [24]. Originally, it was introduced in the process industry, but a very innovative research paper proposed that predictive control can be used in power electronics applications [25], [26] thanks to the evolution of high processing microprocessors which surpassed the drawback of computational burden of the MPC [7].

I.2.2. Development of MPC (History)

The author in [24] reviewed three decades of the MPC development. According to his research, the MPC was first used in industry such as oil and petrochemical industries, which dates back to the 1950s as a computer based supervisory control. At that time, MPC was a promising control strategy yet it wasn't widely embraced by other process industries due to the computational power needed for the MPC until the mid-1970s, when several other techniques were introduced like: Model Heuristic Predictive Control (MHPC) and Dynamic Matrix Control (DMC). These two control algorithms were developed into Generalized Predictive Control (GPC) which is more robust compared to the MHPC and DMC.

In the second decade of the MPC development, during the late 1980s, researchers founded a theoretical approach for the MPC: the discrete-time state-space representation model:

$$\begin{cases} x[i+1] = Ax[i] + Bu[i] \\ y[i+1] = Cx[i] + Du[i] \end{cases} \tag{I.1}$$

During this decade, researchers showed interest in studying the stability of the MPC for the first time. Which can be proven by considering the cost function of the MPC as a Lyapunov function [24]. The cost function is introduced in the next paragraph.

I.2.3. Working principle of MPC

The development seen in these past decades led to multiple applications of the MPC which are different from those seen before, this development covers a very wide class of controllers that found rather recent application in power converters, a classification of the different predictive control methods is shown in the following figure from [6].

The optimization criteria in hysteresis-based predictive control is to keep the controlled variables within the boundaries of a hysteresis area, while in trajectory-based control the variables are forced to follow a predefined trajectory [6]. The deadbeat control theory is based on the inverse discrete model of the controlled system to reach a response with a zero steady-state error within a finite settling-time interval [27].

The difference between these groups of controllers is that deadbeat control and MPC with continuous control set need a modulator in order to generate the required voltage. This will result in having a fixed switching frequency. The other controllers directly generate the switching signals for the converter, do not need a modulator, and present a variable switching frequency [6].

Nonlinearities in the system can be included in the model, avoiding the need to linearize the model for a given operating point, and improving the operation of the system for all conditions. It is also possible to include restrictions on some variables when designing the controller. These advantages can be very easily implemented in some control schemes, such as MPC, but are very difficult to obtain in schemes like deadbeat control [6].
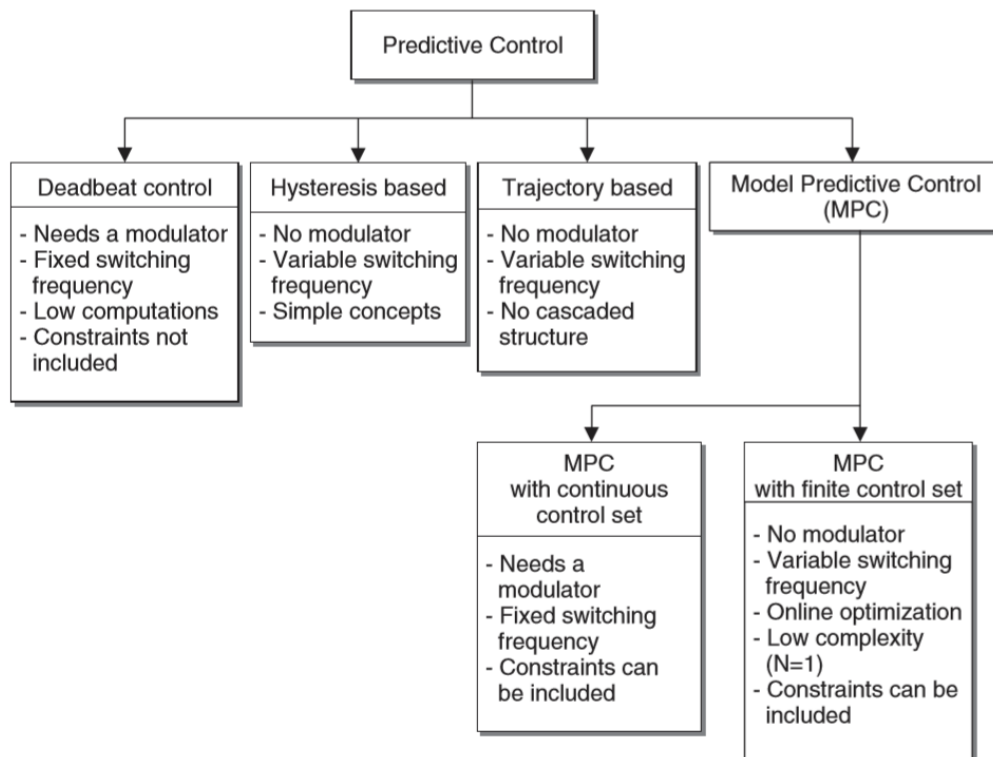
Figure I.12: Classification of predictive control methods used in power electronics

The key element of the MPC is the use of a model of the system for predicting the future behavior of the controlled variables in a predefined horizon in time. This predictive future behavior is used by the controller to obtain the optimal actuation configuration, according to a predefined optimization criterion, which is the "cost function". Then, the optimal actuation is obtained by minimizing this cost function.

Among the advanced control techniques that are more advanced than standard PID control, MPC is one that has been successfully used in industrial applications as mentioned above [28], [29], [30].

The system (I.1) represents a model of the state space representation commonly used in MPC. Notice that the system is discrete, which is mandatory for implementation. To get a discrete-time model it is necessary to use some discretization methods. For first-order systems, the Euler forward method is used because of the simplicity of approximating the derivatives using:

$$\frac{dx}{dt} = \frac{x[k+1] - x[k]}{T_s} \tag{I.2}$$

Where T_s is the sampling period.

The discrete nature of power converters can be considered for implementing MPC control strategies. In this way, finding the solution to the optimization problem can be reduced to evaluate the cost function only for the prediction of the system behavior for the power converters possible switching states. As a finite number of control actions are evaluated, this approach is called finite-control-set MPC (FCS-MPC). This technique has been extensively used for power converters because of the finite number of switching states they present [31].

The cost function definition is one of the most important stages in the design of an MPC, since it allows not only to select the control objectives of the application, but also to include any required constraints that represents the desired behavior of the system [32].
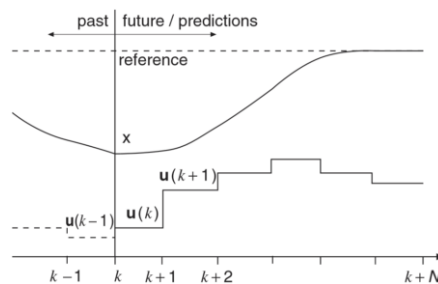
Figure I.13: Working principle of MPC

This function considers the references, future states (or predicted states), and future actuations. In case of a multivariable system, the cost function may be written as:

$$J = \sum_{i}^{n} \lambda_i |x_i^* - x_i^p| \tag{I.3}$$

Where:

- n is the number of controlled variables
- x_i is the controlled variable
- x_i^* is the reference value of the controlled variable
- x_i^p is the predicted value of the controlled variable
- λ_i is the weighting factor

The weighting factor allows for adjusting the importance of each controlled variable according to its priority in the scope statement.

The selected actuation is the one that minimizes the cost function, it is stored so that it can be applied to the converter in the upcoming sampling period [31].

I.2.4. Applications of the MPC

A significant number of applications involving electronic systems are now being reported in the literature, for instance : Predictive current and torque control of power converters [33], [34], motor drives [6], [25], generators for renewable energy applications [8], [9], energy storage applications [35], [36] thanks to the development of microprocessors and other approaches to dealing with the computational burden problem [6].

For GPC controlled power converters, a Pulse Width Modulation (PWM) or Space-Vector Modulation (SVM) is used to generate the voltage in order to optimize some aspects of the power converter [31].

The application of MPC on power converters has extended to grid-connected converters, for instance: flexible AC transmission systems (FACTS), static synchronous compensators (STATCOMs), active power filters (APFs), unified power flow controller (UPFC) or a converter to control the torque and/or speed of a wind turbine for grid integration of renewable energies [31].

Model predictive controlled active-front-end (AFE) rectifiers for energy storage systems, which has been increasingly applied in power distribution sectors and in

renewable energy sources [37], where the main objective of the control strategy is to regulate the output voltage to a given reference [31]. In [37] the authors performed a comparison demonstrating that the MPC controller is more effective than voltage oriented control based PWM (VOC-based-PWM) AFE rectifiers. The structure used for the control of an AFE is cascaded, one outer control loop for regulating the DC-link voltage and one inner control loop for pursuing the reference current and power [31]. Model predictive controlled AFE are used for either controlling the instantaneous active and reactive power, hence the nomenclature predictive direct power control (P-DPC), or for controlling the grid currents [17]. The most used control scheme of a Model predictive controlled AFE is P-DPC uses an external modulator thus it has a fixed switching frequency which means that grid current harmonic spectrum is concentrated around the switching frequency minimizing the cost of the output filter [31]

Another fundamental grid-connected converter is the APF, which is basically a voltage-source inverter whose DC-link is connected to a capacitor's bank [31], [38]. It is for compensating the unbalanced, reactive, and harmonic components of the currents drawn by any load [38]. In [39] the authors investigate the application of MPC to shunt APF. The proposed approach does not require grid synchronization or PWM schemes and provides a single control loop structure enhancing the dynamic performance which is useful for satisfying the dynamic of modern-day smart grids.

MPC has also been applied to Selective Harmonic Elimination (SHE) [40], the technique is called MPC-SHE and its cost function is formulated in a way to follow the voltage reference, to eliminate low-order harmonics, and to reduce switching losses where a sliding discrete Fourier transform is used [31].

Another technique has emerged after the SHE, it is the selective harmonic mitigation (SHM) which also found its application in MPC [41], it is called the MPC-SHM. Its objective is to follow the voltage reference, control the harmonic distortion keeping it below the limits imposed in the grid code, and reduce the switching losses as much as possible [31].

For motor drive applications of the MPC, the measured variables are usually the current and the mechanical speed. And the other variables such as torque, stator or rotor flux are estimated using estimators or the mathematical model of the machine [17]. Estimators are also useful for sensorless MPC [9].

The authors in [9] proposed a predictive speed control (PSC) technique for permanent-magnet synchronous generators (PMSGs) in variable-speed wind turbines. The proposed technique allows to manipulate the mechanical (i.e. speed) and electrical (i.e. current and torque) variables in a single control law to generate the optimal switching state to apply in the next sampling time. In addition, because the cascaded control structure is eliminated, the dynamic performance is enhanced.

To design the predictive current control (PCC) technique, the authors in [9] modeled the PMSG for predicting the currents in the next (future) sampling period. They proposed a discrete-time model to predict the electromagnetic torque and the mechanical speed.

The cost function was expressed as:

$$g_{new} = \lambda_1 \, \omega_{m,ref}[k+1] - \omega_m[k+1] \, + \, i^d_{s,ref}[k+1] - i^d_s[k+1] \qquad \text{(I.4)}$$
$$+ \lambda_2 |T_e[k+1] - T_m[k]|$$

Where λ_1 and λ_2 are called weighting factors, their values depend on the priority of the variable. Since the proposed technique is PSC, the variable that has the most priority is the mechanical speed, therefore λ_1 must be far greater than 1 and λ_2 must be between 0 and 1.

In [17], a comparative study between a conventional control scheme, Proportional-Integral with PWM, and the MPC of a three-level inverter fed RLE load. The MPC scheme showed lower THD of the load voltage, better current tracking and better dynamic response due to the absence of a cascaded structure.

In [17], another comparative study between a conventional control scheme, PWM, and the MPC of a three-level neutral-point clamped (NPC) inverter has been conducted. The cost function of the implemented MPC has for parameters the output current, the input voltage and the switching frequency, which means it can be lowered. The results show that even at the same switching frequency, the predictive strategy reveals a lower tracking error.

Another application of MPC can be found in energy storage systems, particularly in renewable energy. The authors of [36] have presented a model predictive algorithm to control a bidirectional AC-DC converter, which is used in an energy storage system for power transferring between the three-phase AC voltage supply and energy storage devices. The proposed MPC scheme of the AC-DC converter allows bidirectional power flow with instantaneous mode change capability and fast dynamic response. According to their results, the three-phase bidirectional AC-DC converter

can be operated with unity power factor in both the rectifier and inverter modes of operation controlling the reactive power and the MPC has shown better results in terms of total harmonic distortions (THD) and efficiency.

The controlled variables of a predictive torque control (PTC) of an IMC fed induction machine are the torque and the stator flux [19]. And given the possibility to adjust the importance or the priority of a variable by adjusting the weighting factors in the cost function, the authors of [34] have been able to reduce the torque ripples of an IMC fed induction machine by optimizing the weighting factor.

The paper [35] proposes a modified model predictive control (MMPC) method based on Lyapunov function to improve the performance of a bidirectional AC-DC converter, a nonlinear system, of which the stability of the MMPC technique is ensured by the direct Lyapunov method by analyzing a nonlinear model of the converter. The results confirm the stability of the MMPC of the converter and has an advantage of a lower execution time than that of the conventional MPC.

The paper [42] shows that the MPC is simpler than SVM to implement in a DMC from a conceptual and theoretical point of view and provides better source current behavior particularly with a distorted source voltage. In addition, MPC assures a high PF for different loads which does not happen with SVM. This is due to the fact that MPC considers the input filter in order to control the wave form of the source currents, unlike classical SVM.

When it comes to the matrix converter (MC), usually the controlled variables are the output current and the reactive power [17], allowing for applications such as Digital Predictive Current Control Fed by Three Level Indirect Matrix Converter (IMC) under Unbalanced Power Supply Condition. In [33], the authors proposed a three-level indirect matrix converter controlled by FCS-MPC to ensure load current reference tracking and instantaneous reactive power reduction. It also means that the converter can work with capacitive, unity, or inductive power factor [17].

The controlled variables of a predictive torque control (PTC) of an IMC fed induction machine are the torque and the stator flux [19]. And given that it possible to adjust the importance or the priority of a variable by adjusting the weighting factors in the cost function, the authors of [34] have been able to reduce the torque ripples of an IMC-fed induction machine by optimizing the weighting factor.

I.3. Conclusion

In this chapter a brief state of the art of the matrix converter and of the predictive control has been presented with some of their applications.

AC-AC converters are of two kinds: direct and indirect AC-AC converters, the difference between them is that the indirect AC-AC converters need a storage capacitor for the DC-link

The three-phase matrix converter has been divided into three categories: direct matrix converter, indirect matrix converter and Z-source matrix converter.

According to the study, each topology has its special requirements and issues, especially when some conditions have to be met for some particular applications.

A brief introduction and history of development of the MPC have been presented.

The predictive control schemes have been divided into four categories: deadbeat control, hysteresis-based control, trajectory-based control and model predictive control.

MPC is able to achieve high-performance results in a wide range of applications. For decades, it has successfully broadened its applications from chemical processes to renewable energy, power converters and motor drives.

Chapter II:

Model Predictive Current Control of a Three-Phase, Two Level, Inverter-Fed RL-Load

Chapter II : Model Predictive Current Control of Three-Phase, Two Level, Inverter-Fed RL-Load

II.1. Introduction

Current control of a three-phase inverter is one of the most important and classical subjects in power electronics [43]. And with the technological advancement in microprocessors, interest has been shown to Model Predictive Current Control (MPCC) [8], [9].

This chapter presents an MPC scheme for a three-phase, two-level, inverter-fed RL-load. The modeling of the two-level voltage source inverter (2LVSI) and of the load will be presented, the working principle will be explained and both simulation and experimental results will be shown.

II.2. Model Predictive Current Control

In Model Predictive Current Control (MPCC), the current is the variable that should be controlled. In order to control it, we use the model of the system (inverter + load) to predict at each sampling period all the possible output current values according to each possible switching state of the inverter and compare them to a reference. The predicted value that optimize a predefined optimization criterion (the cost function) will be selected, and the corresponding switching states will be applied.

II.3. Inverter Model
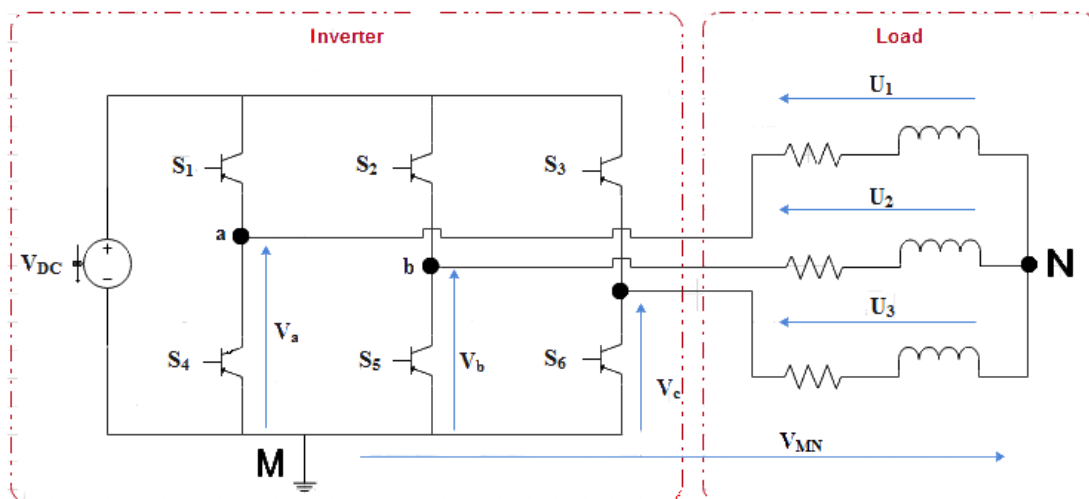
Figure II.1: Voltage source inverter power circuit

The power circuit of the three-phase inverter converts electrical power from DC to AC form using the electrical scheme shown in Figure II.1. Considering that the two switches in each inverter phase operate in a complementary mode in order to avoid

short-circuiting the DC source, the possible switching states are reduced to 8, they are shown in Table II.1.

The model doesn't take into account the switch saturation voltage and diode forward voltage drop for the simplicity of the study.

Where:

- V_{DC} is the DC source voltage.
- v_a, v_b and v_c are the phase-to-neutral (M) voltages of the inverter
- u_1, u_2 and u_3 are the phase-to-neutral (N) voltages of the load
- S_1, ..., S_6 are the gate signals

The power switches operate in a complementary mode; thus, the connection function can be expressed as follows:

$$S_a = \begin{cases} 1 \text{ if } S_1 \text{ on and } S_4 \text{ off} \\ 0 \text{ if } S_1 \text{ off and } S_4 \text{ on} \end{cases}$$

$$S_b = \begin{cases} 1 \text{ if } S_2 \text{ on and } S_5 \text{ off} \\ 0 \text{ if } S_2 \text{ off and } S_5 \text{ on} \end{cases} \tag{II.1}$$

$$S_c = \begin{cases} 1 \text{ if } S_3 \text{ on and } S_6 \text{ off} \\ 0 \text{ if } S_3 \text{ off and } S_6 \text{ on} \end{cases}$$

By applying Kirchhoff's first law we get:

$$\begin{cases} u_1 = v_{MN} + v_a \\ u_2 = v_{MN} + v_b \\ u_3 = v_{MN} + v_c \end{cases} \tag{II.2}$$

Adding the three equations we get:

$$v_{MN} = -\frac{1}{3}(v_a + v_b + v_c) \tag{II.3}$$

Replacing v_{MN} in (II.2) and considering that the load is balanced, we result in the following system:

$$\begin{pmatrix} u_1 \\ u_2 \\ u_3 \end{pmatrix} = \frac{1}{3} V_{DC} \begin{pmatrix} 2 & -1 & -1 \\ -1 & 2 & -1 \\ -1 & -1 & 2 \end{pmatrix} \begin{pmatrix} S_a \\ S_b \\ S_c \end{pmatrix} \tag{II.4}$$

(II.4) is the mathematical model of the inverter which can be easily implemented in MATLAB as a function with three inputs and three outputs.

Table II.1: Possible switching states of a three-phase, two level, voltage source inverter

S_a	S_b	S_c	u_1	u_2	u_3
0	0	0	0	0	0
1	0	0	$\frac{2}{3}V_{DC}$	$\frac{-1}{3}V_{DC}$	$\frac{-1}{3}V_{DC}$
1	1	0	$\frac{1}{3}V_{DC}$	$\frac{1}{3}V_{DC}$	$\frac{-2}{3}V_{DC}$
0	1	0	$\frac{-1}{3}V_{DC}$	$\frac{2}{3}V_{DC}$	$\frac{-1}{3}V_{DC}$
0	1	1	$\frac{-2}{3}V_{DC}$	$\frac{1}{3}V_{DC}$	$\frac{1}{3}V_{DC}$
0	0	1	$\frac{-1}{3}V_{DC}$	$\frac{-1}{3}V_{DC}$	$\frac{2}{3}V_{DC}$
1	0	1	$\frac{1}{3}V_{DC}$	$\frac{-2}{3}V_{DC}$	$\frac{1}{3}V_{DC}$
1	1	1	0	0	0

II.4. Load Model

By applying Kirchhoff's first law to the RL-load in Figure II.1 we get:

$$\begin{cases} u_1 = L\dfrac{di_a}{dt} + Ri_a \\[2mm] u_2 = L\dfrac{di_b}{dt} + Ri_b \\[2mm] u_3 = L\dfrac{di_c}{dt} + Ri_c \end{cases} \tag{II.5}$$

In order to obtain a model for this RL load for simulation in MATLAB/Simulink environment we need to transform (II.5) into Laplace domain as transfer functions:

$$\begin{cases} \dfrac{i_a}{u_1} = \dfrac{1}{sL+R} \\[2mm] \dfrac{i_b}{u_2} = \dfrac{1}{sL+R} \\[2mm] \dfrac{i_c}{u_3} = \dfrac{1}{sL+R} \end{cases} \tag{II.6}$$

For discretizing the system (II.5), the forward Euler method is used. Which is easy to implement and is accurate when the sampling period T_s is small enough. So $\frac{di}{dt}$ is replaced by $\frac{i[k+1]-i[k]}{T_s}$ and after some arrangements, (II.5) becomes:

$$\begin{cases} i_a[k+1] = \left(1 - \dfrac{RT_s}{L}\right) i_a[k] + \dfrac{u_1 T_s}{L} \\[2mm] i_b[k+1] = \left(1 - \dfrac{RT_s}{L}\right) i_b[k] + \dfrac{u_2 T_s}{L} \\[2mm] i_c[k+1] = \left(1 - \dfrac{RT_s}{L}\right) i_c[k] + \dfrac{u_3 T_s}{L} \end{cases} \qquad \text{(II.7)}$$

Where, in the control algorithm, $i_a[k]$ is evaluated as the measured current of *phase a* at the sample k and $i_a[k+1]$ is evaluated as the predicted value of the current of *phase a* at the sample $k+1$.

II.5. Cost Function

In this chapter, the goal is to control the load current. So, the cost function must minimize the error between the measured currents and the reference values.

Thus, the cost function is expressed as:

$$J = |i_a[k+1] - i_a^*[k+1]| + |i_b[k+1] - i_b^*[k+1]| + |i_c[k+1] \\ - i_c^*[k+1]| \qquad \text{(II.8)}$$

Where $i_a^*[k+1], i_b^*[k+1]$ and $i_c^*[k+1]$ are the reference values of the phase currents at the sample $k+1$.

II.6. Working Principle

The goal of the MPCC scheme is to select an actuation (i.e. state) that minimizes the cost function (II.8). The selected actuation is called the optimal switching state x_{opt}. The working principle is explained in the following figures:
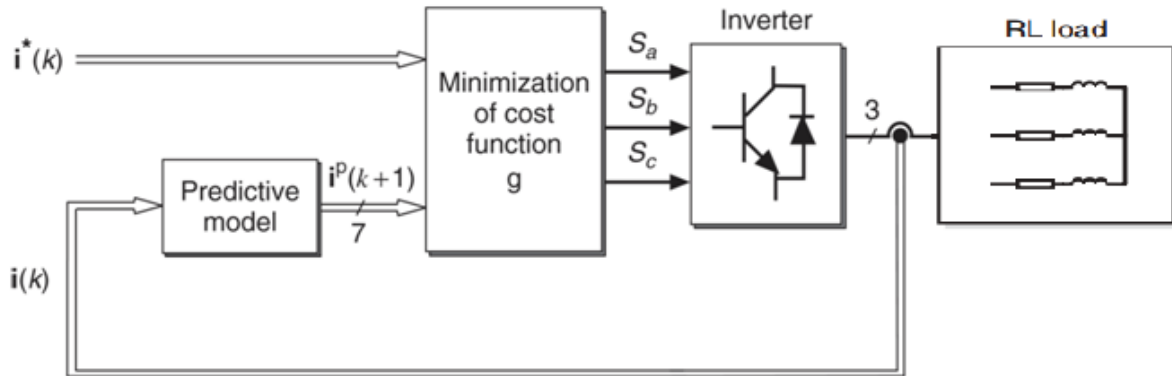
Figure II.2: Predictive current control block diagram

The working principle of this control strategy is explained in detail in *Figure II.3*. The MPCC scheme uses finite number of valid switching states of the inverter in order to find the x_{opt} by using the following steps:
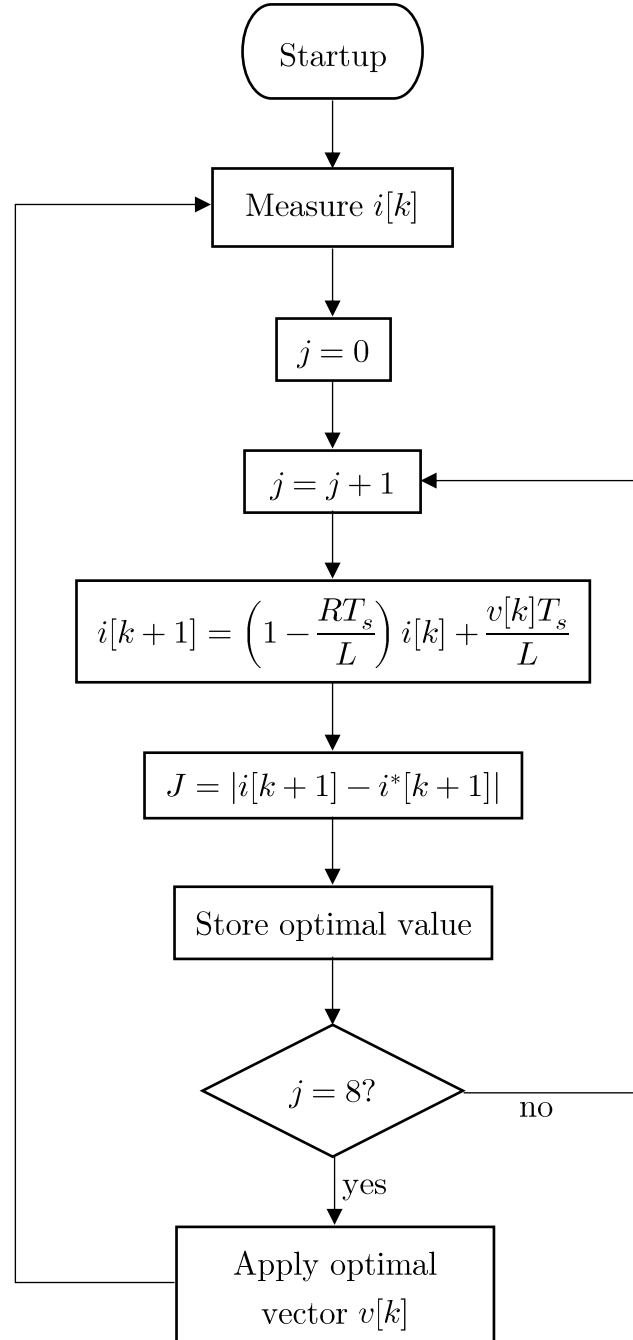
Figure II.3: Flow diagram of MPCC

Step 1: Measure load current $i[k]$ and read input reference $i^*[k+1]$.

Step 2: For each valid switching state, calculate the output voltage of the inverter $v[k]$ using the inverter model.

Step 3: Predict the current of the next sampling period $i[k+1]$ using the load model.

Step 4: Evaluate the cost function by comparing the predictive value with its reference and selecting the switching state that corresponds to the minimum value of the cost function.

Step 5: Apply the optimal switching state x_{opt} to the inverter.

II.7. Implementation

For the sake of simplifying the calculation and minimizing computation time, the currents and the output voltage of the inverter are expressed in $\alpha\beta$ coordinate system.

Considering the unitary vector $a = e^{j2\pi/3} = -\frac{1}{2} + j\frac{\sqrt{3}}{2}$, which represents the 120° phase displacement between the phases. The output voltage vector and the load current can be defined as:

$$v = \frac{2}{3}(v_a + av_b + a^2 v_c) \tag{II.9}$$

$$i = \frac{2}{3}(i_a + ai_b + a^2 i_c) \tag{II.10}$$

Where $i_\alpha = \text{Re}(i)$ and $i_\beta = \text{Im}(i)$

Instead of calculating the output voltage of the inverter for each possible switching state at every iteration, we can calculate them in advance and apply them to the load model.

Table II.2: Possible switching states and output vector voltage

S_a	S_b	S_c	v
0	0	0	$v_0 = 0$
1	0	0	$v_1 = \dfrac{2}{3}V_{DC}$
1	1	0	$v_2 = \dfrac{1}{3}V_{DC} + j\dfrac{\sqrt{3}}{2}V_{DC}$
0	1	0	$v_3 = \dfrac{-1}{3}V_{DC} + j\dfrac{\sqrt{3}}{2}V_{DC}$
0	1	1	$v_4 = \dfrac{-2}{3}V_{DC}$
0	0	1	$v_5 = \dfrac{-1}{3}V_{DC} - j\dfrac{\sqrt{3}}{2}V_{DC}$
1	0	1	$v_6 = \dfrac{1}{3}V_{DC} - j\dfrac{\sqrt{3}}{2}V_{DC}$
1	1	1	$v_7 = 0$
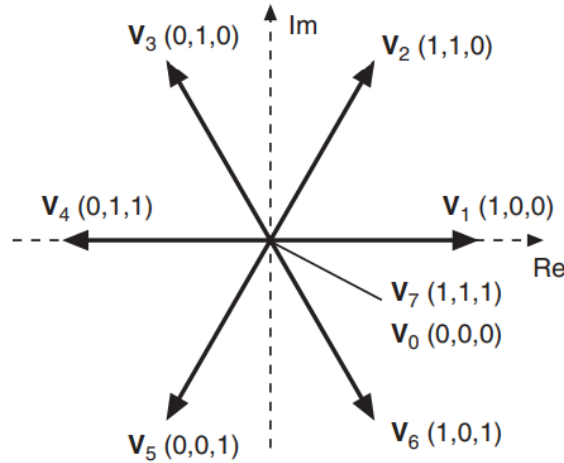
Figure II.4: Voltage vectors in the complex plane

In order to reduce the number of calculations for the output current, we can transform the three equations in (II.7) into one equation using (II.10). We obtain:

$$i[k+1] = \left(1 - \frac{RT_s}{L}\right) i[k] + \frac{vT_s}{L} \tag{II.11}$$

Thus, the cost function (II.8) becomes:

$$J = |i[k+1] - i^*[k+1]| \tag{II.12}$$

The output voltage vectors of the inverter are stored and selected rather than calculated each sampling period of the algorithm. The calculation of the cost function is a subtraction of two one-dimensional complex variables rather than three-dimensional variables. So, the number of calculations is considerably reduced.

II.8. Simulation Results and analysis

The control strategy is simulated in the MATLAB/Simulink environment using the models (II.4), (II.6) and (II.11) considering that the voltage source is constant.

Reference and output current of one phase are shown in Figure II.5. The simulation parameters are listed in Table A.1 in Appendix A

(a)

(b)

(c)
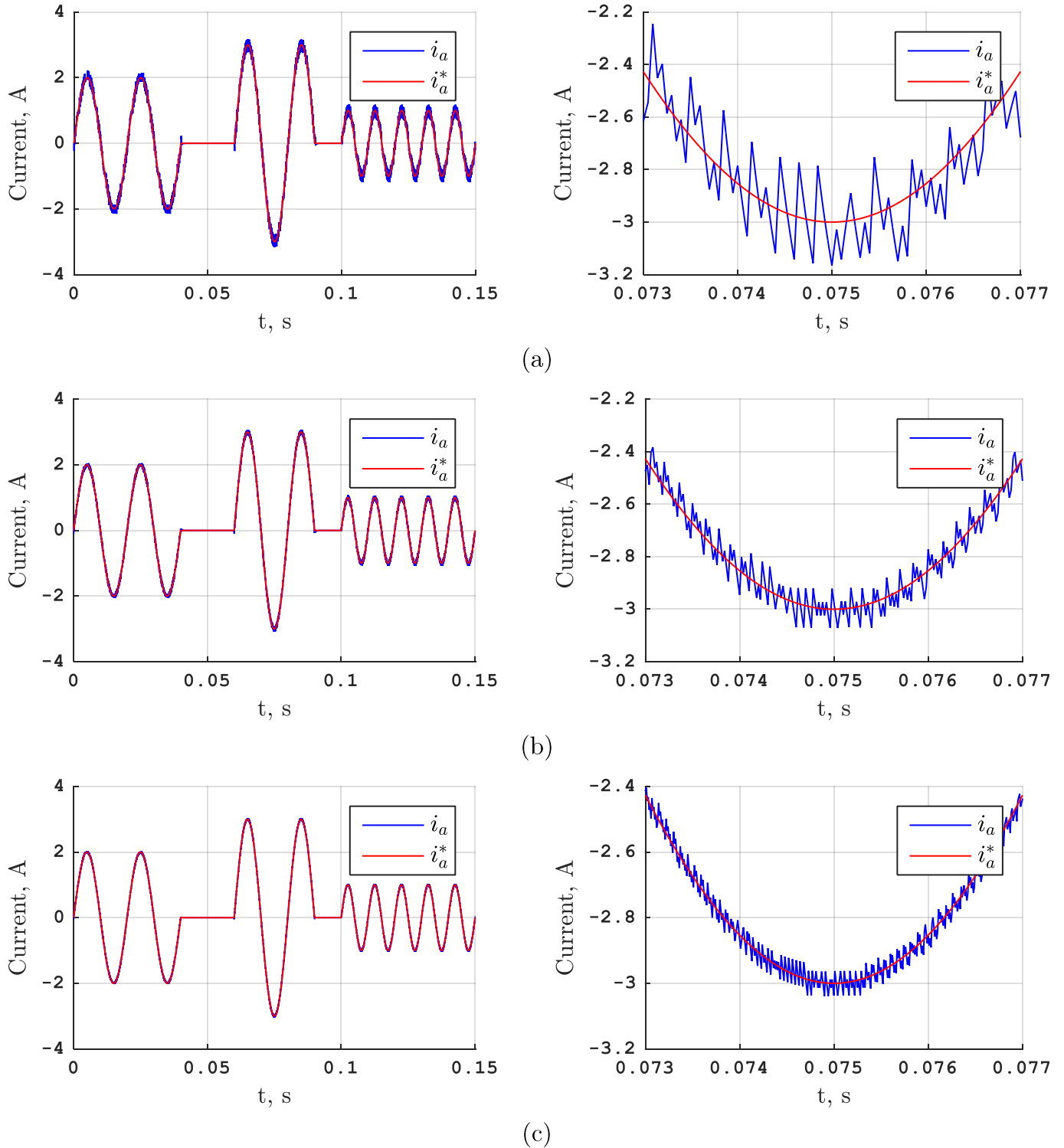
Figure II.5: Simulation results of MPCC of a two-level inverter-fed RL-load:
Reference and output current of phase A and their zoom with a sampling frequency
of: **(a)** 20 kHz, **(b)** 50 kHz, **(c)** 100 kHz
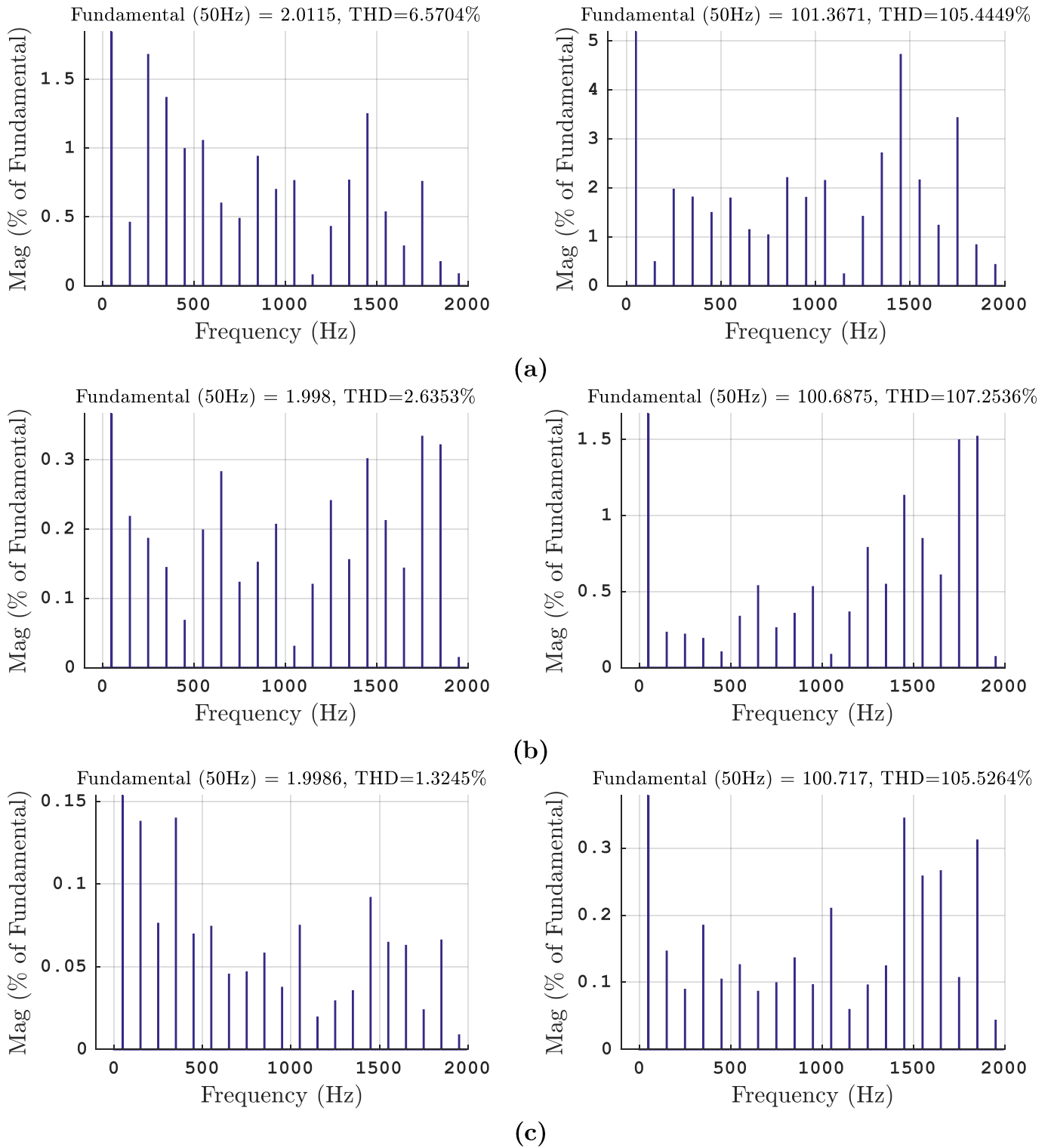
Figure II.6: Simulation results of MPCC of a two level inverter-fed RL-load: Output current and output voltage spectra expressed as percentages of fundamental magnitude, $|I^*| = 2$ A and f* = 50 Hz with a sampling frequency of **(a)** 20 kHz, **(b)** 50 kHz, **(c)** 100 kHz
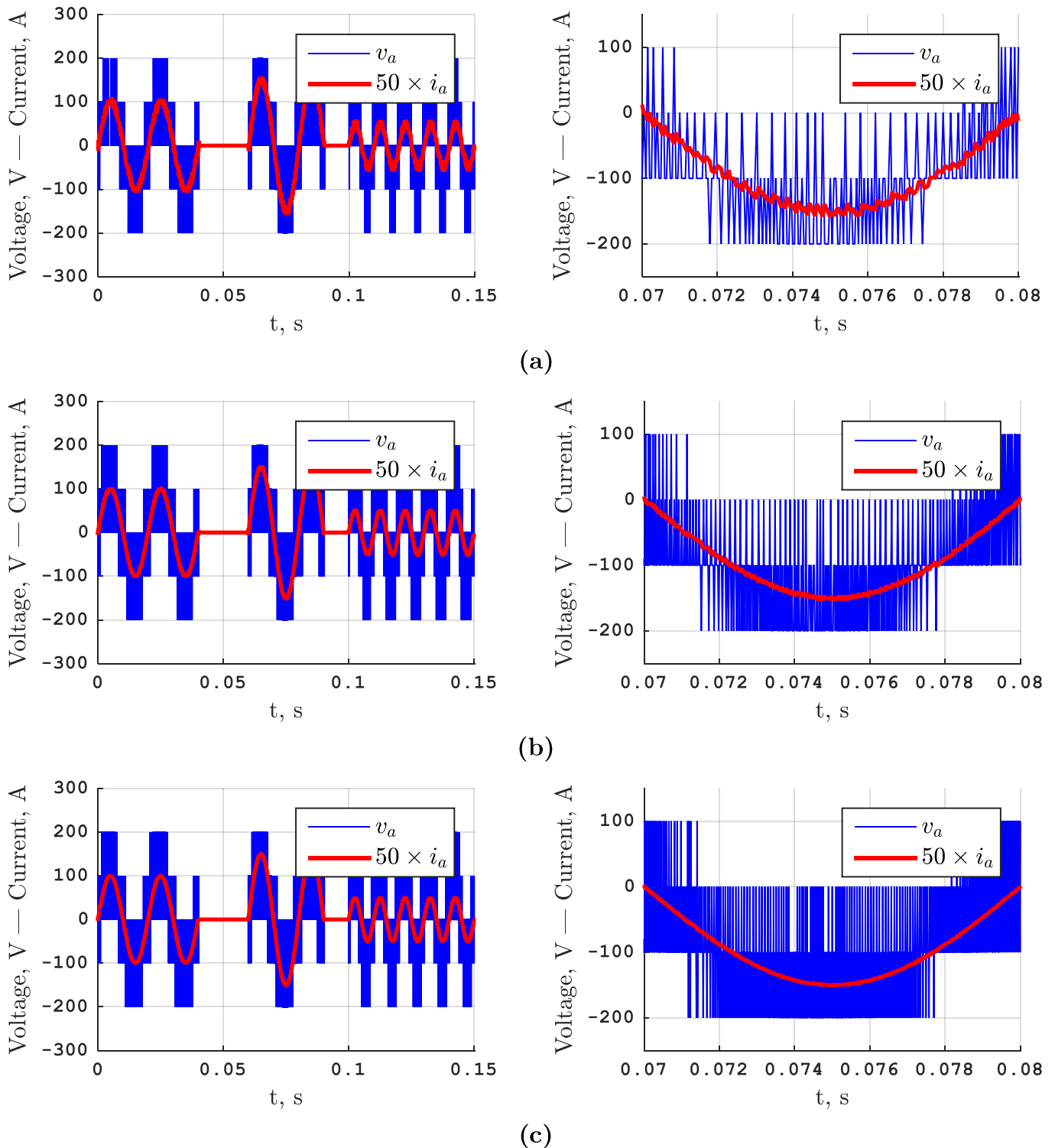
Figure II.7: Simulation results of MPCC of a two-level inverter-fed RL-load: Output voltage of the inverter and 50 ×the load current of phase A with a sampling frequency of: **(a)** 20 kHz, **(b)** 50 kHz, **(c)** 100 kHz

(a)

(b)

(c)
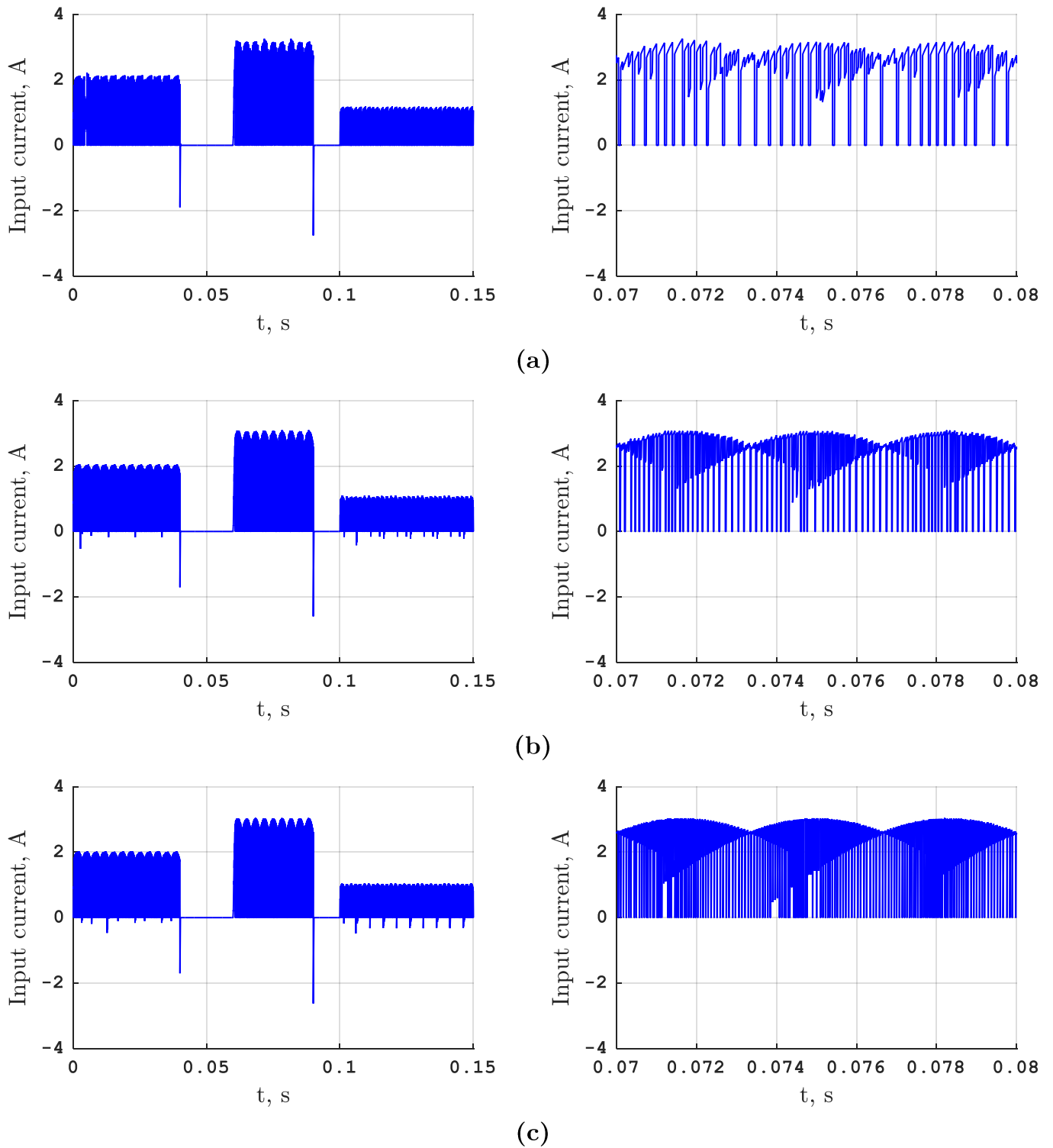
Figure II.8: Simulation results of MPCC of a two-level inverter-fed RL-load: Input current of the inverter and its zoom with a sampling frequency of: **(a)** 20 kHz, **(b)** 50 kHz, **(c)** 100 kHz

Figure V.5, Figure V.6, Figure V.7 and Figure II.8 present the simulation results of the MPCC of a two-level inverter-fed RL-load.

Figure II.5 shows that for the five references (different magnitudes and frequencies), the output current tracks the reference (magnitude, frequency and phase) in a short response time. The output current oscillates around its reference forming a ripple, or a band, around the reference. The magnitude of these oscillations can be reduced by increasing the sampling frequency, which is not ideal for the power switches and the controller circuit.

Figure II.6 represents the output current and output voltage spectra expressed as percentages of fundamental magnitude with a fixed reference frequency and magnitude. It is also observed that the THD of the output current decreases with higher sampling frequencies.

Figure II.7 represents the output voltage of the inverter and its spectra. It shows that the output voltage has a high THD. A phase shift is observed between the output current and the output voltage, it is due to the inductive nature of the RL-load.

Figure II.8 represents the input current of the inverter and its zoom. The input current has six pulses per fundamental output period in accordance to the six sextants on a vector diagram (Figure II.4). Some negative spikes of the input current are observed.

II.9. Conclusion

In this chapter, the predictive current control strategy was introduced, both the converter and the load have been modelled and a cost function has been expressed. The MPCC working principle was explained in detail.

The control scheme was simulated in MATLAB/Simulink environment for different sampling frequencies and different references. The load current manages to track its reference and its quality gets better with high sampling frequencies (low THD).

The higher sampling frequencies help reduce the ripples of the output current, the error between the reference value and the output value of the load current in steady-state got reduced from 0.2675 A (20 kHz) to 0.0577 A (100 kHz).

The inverter is controllable in both magnitude and frequency of the output current.

Even though the MPC can work with non-linear loads, it requires at least one derivative or integral in the load model in order to predict the value of the controlled variable.

MPCC of an RL-load is one of the simplest predictive control schemes. It allows us to apply this control scheme to other loads, like an induction machine for example, which is the subject of the following chapter.

Chapter III:

Model Predictive Torque Control of a Three-Phase, Two Level, Inverter-Fed Induction Machine

Chapter III : Model Predictive Torque Control of Three-Phase, Two Level, Inverter-Fed Induction Machine

III.1. Introduction

In recent years, new control strategies have been developed for the control of power inverters. Among them is the MPC scheme. Which was applied for the control of power converters due to its several advantages, the fast-dynamic response, easy inclusion of non-linearities and system constraints, and flexibility to include other system restrictions and constraints in the controller according to the scope statement [42].

In this chapter, a Model Predictive Torque Control (MPTC) scheme has been applied to the system (inverter + machine), which is one the most common electrical motor drive. The control scheme is described in detail from machine modelling to simulating the system along with inverter model that is described in the previous chapter.

III.2. Model Predictive Torque Control

As shown later in the modeling of the induction machine, both the stator flux φ_s and electromagnetic torque T_{em} can be controlled by selecting the proper voltage as used in the Direct Torque Control (DTC) [2], [44].
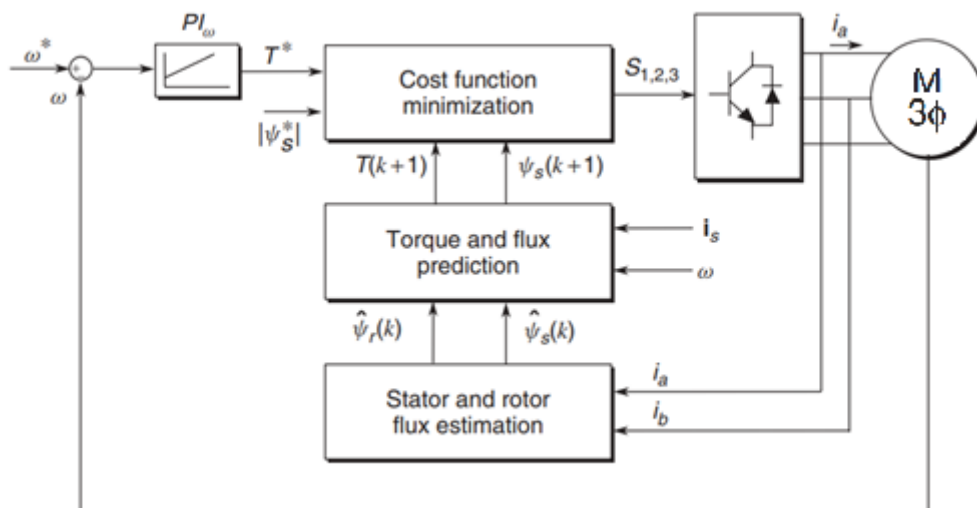
Figure III.1: MPTC scheme

The MPTC selects a voltage vector which results in a stator flux φ_s and electromagnetic torque T_{em} that satisfies the objective of the control. To do so, the control scheme uses models of the converter and the machine to calculate predictions of the controlled variables which are then compared to their references at each sampling

period. The voltage vector is selected based on predefined conditions that are implemented in the cost function.

III.3. Modeling of the induction machine

Modeling the asynchronous motor is the first essential step for its identification and its control [45]. The mathematical model of the machine should have a structure that fully describes the characteristics of the machine and, on the other hand, it should be practical for the implementation of the MPC algorithm.

As shown in the Figure below, the three-phase induction machine has a fixed part, called a stator, consisting of a stack of sheets with low loss rate, supporting three-phase symmetrical windings supplied with three-phase alternating current. A mobile part, called rotor, is not powered, it is short-circuited and it can be of two kinds:

- Wire-wound (with rings) fitted with a generally three-phase winding connected to rings on which brushes rub;
- Squirrel cage, formed of a set of conductive rings connected to each other each end by circular rings.
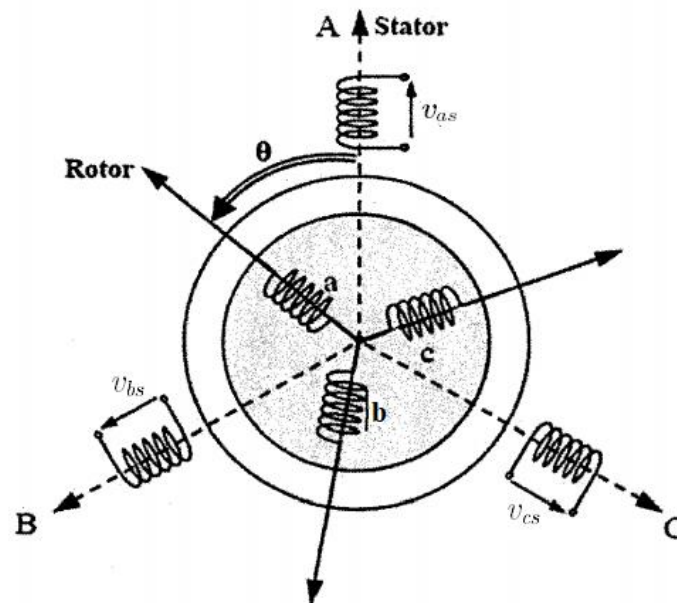
Figure III.2: Schematic representation of the three-phase asynchronous machine

We are interested in the squirrel cage asynchronous motor, because it is characterized by its robustness and its simplicity of construction [2]. However, to establish simple relations between the supply voltages of the motor and its currents, it is necessary to rely on a number of assumptions:

- The air gap is of uniform thickness and the notching effect is negligible;

- We neglect the eddy current and the saturation of the magnetic circuit and its hysteresis, which leads to a sinusoidal magnetic field;
- The resistance of the windings does not vary with the temperature and we neglect skin effect (uniform current density in the conductor section);
- We only consider the first space harmonic created by each of the phases of the two frames (neglecting space harmonics that do not contribute to the average torque. This assumption entails a sinusoidal magneto-motive force (MMF) distribution) [45].

Among the important consequences of these hypotheses, we can cite:

- The flux is additive;
- Self-inductance is constant;
- The law of sinusoidal variation of mutual inductances between the windings of the stator and rotor as a function of the electrical angle of their magnetic axes.

III.3.1. Electrical equations

The electric equations of the asynchronous squirrel cage machine (short-circuited rotor), are written as follows:

$$\text{Stator:} \begin{cases} v_{as} = R_s I_{as} + \frac{d\varphi_{as}}{dt} \\ v_{bs} = R_s I_{bs} + \frac{d\varphi_{bs}}{dt} \\ v_{cs} = R_s I_{cs} + \frac{d\varphi_{cs}}{dt} \end{cases} \tag{III.1}$$

Or in vector form: $[V_{sabc}] = [R_s][I_{sabc}] + \frac{d[\varphi_{sabc}]}{dt}$

$$\text{Rotor:} \begin{cases} v_{ar} = R_r I_{ar} + \frac{d\varphi_{ar}}{dt} = 0 \\ v_{br} = R_r I_{br} + \frac{d\varphi_{br}}{dt} = 0 \\ v_{cr} = R_r I_{cr} + \frac{d\varphi_{cr}}{dt} = 0 \end{cases} \tag{III.2}$$

Or in vector form: $[V_{rabc}] = [R_r][I_{rabc}] + \frac{d[\varphi_{rabc}]}{dt} = \begin{bmatrix} 0 \\ 0 \\ 0 \end{bmatrix}$

Where:

- $v_{as}, v_{bs}, v_{cs}, v_{ar}, v_{br}$ and v_{cr} are the three stator and rotor voltages
- $i_{as}, i_{bs}, i_{cs}, i_{ar}, i_{br}$ and i_{cr} are the three stator and rotor currents
- $\varphi_{as}, \varphi_{bs}, \varphi_{cs}, \varphi_{ar}, \varphi_{br}$ and φ_{cr} are the fluxes through the three phases of the stator and the rotor

III.3.2. Magnetic equations

The magnetic equations of the asynchronous squirrel cage machine are written as follows:

Stator:
$$\begin{cases} \varphi_{as} = L_s I_{as} + M_s I_{bs} + M_s I_{cs} + M_1 I_{ar} + M_3 I_{br} + M_2 I_{cr} \\ \varphi_{bs} = M_s I_{as} + L_s I_{bs} + M_s I_{cs} + M_2 I_{ar} + M_1 I_{br} + M_3 I_{cr} \\ \varphi_{cs} = M_s I_{as} + M_s I_{bs} + L_s I_{cs} + M_3 I_{ar} + M_2 I_{br} + M_1 I_{cr} \end{cases} \quad \text{(III.3)}$$

Rotor:
$$\begin{cases} \varphi_{ar} = L_r I_{ar} + M_r I_{br} + M_r I_{cr} + M_1 I_{as} + M_2 I_{bs} + M_3 I_{cs} \\ \varphi_{br} = M_r I_{ar} + L_r I_{br} + M_r I_{cr} + M_3 I_{as} + M_1 I_{bs} + M_2 I_{cs} \\ \varphi_{cr} = M_r I_{ar} + M_r I_{br} + L_r I_{cr} + M_2 I_{as} + M_3 I_{bs} + M_1 I_{cs} \end{cases} \quad \text{(III.4)}$$

Where:

$M_1 = M_{sr} \cos \theta$

$M_2 = M_{sr} \cos(\theta - 2\pi/3)$

$M_3 = M_{sr} \cos(\theta + 2\pi/3)$

- L_s : stator inductance
- R_s : stator resistance
- L_r : rotor inductance
- R_r : rotor resistance
- M_s : mutual inductance between two stator windings
- M_r : mutual inductance between two rotor windings
- M_{sr} : magnitude of the inductance between the stator and the rotor

III.3.3. Mechanical equation

The mechanical equations of the asynchronous squirrel cage machine are written as follows:

$$\frac{d\Omega}{dt} = \frac{1}{J} \left(T_{em} - T_L - k_f \Omega \right) \quad \text{(III.5)}$$

Where:

- Ω : mechanical speed
- J : moment of inertia of the mechanical shaft
- T_{em} : electromagnetic torque
- T_L : load torque
- k_f : dry friction coefficient

The mathematical model established so far (systems (III.1), (III.2), (III.3) and (III.4)) is a linearly dependent system that can be represented a three-axis coordinate

system. However, the number of equations, inputs and outputs makes the model inappropriate for implementation.

The linear dependence means that only two variables are necessary to describe three physical quantities. Hence, a complex variable can replace the three-phase systems as shown in Figure III.3.

For example, instead of representing the stator currents by a three-equations system, we can represent it using only one equation

$$i_s = \frac{2}{3}(i_{as} + ai_{bs} + a^2 i_{cs}) \text{ where: } a = e^{\frac{j2\pi}{3}} \tag{III.6}$$

Instead of:

$$\begin{cases} i_{as} = I_s \sin(\theta) \\ i_{bs} = I_s \sin(\theta - 2\pi/3) \\ i_{cs} = I_s \sin(\theta + 2\pi/3) \end{cases} \tag{III.7}$$

(a)   (b)
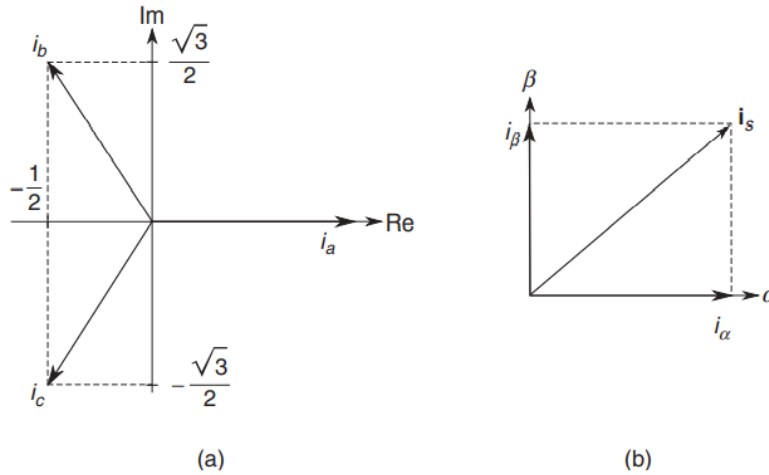
Figure III.3: Coordinate transformation

The same coordinate transformation shown above is used for the other electrical and electromagnetic variables. Thus, the equations of an induction machine can be represented in any arbitrary reference frame rotating at an angular pulse ω_k. The variable ω denotes the rotor angular speed:

$$v_s = R_s i_s + \frac{d\varphi_s}{dt} + j\omega_k \varphi_s \tag{III.8}$$

$$v_r = R_r i_r + \frac{d\varphi_r}{dt} + j\ \omega_k - \omega\ \varphi_r = 0 \tag{III.9}$$

$$\varphi_s = L_s i_s + L_m i_r \tag{III.10}$$

$$\varphi_r = L_m i_s + L_r i_r \tag{III.11}$$

$$T_{em} = \frac{3}{2}pRe\ \overline{\varphi_s} i_s\ = -\frac{3}{2}pRe\ \overline{\varphi_r} i_r\ = \frac{3}{2}pIm(\overline{\varphi_r} i_s) \tag{III.12}$$

Where:

- ω : rotor angular speed ($\omega = p\Omega$)
- p : number of pole pairs
- $\overline{\varphi}$: the complex conjugate value of φ

In order to develop an appropriate control strategy, it is convenient to write the equations of the machine in terms of state variables [6], [45]. The stator current i_s and the rotor flux vectors φ_r are selected as state variables.

From (III.11) we have:

$$i_r = \frac{\varphi_r - L_m i_s}{L_r}$$

(III.13)

By replacing (III.13) in (III.9) and by putting:

$$\tau_r = \frac{L_r}{R_r}$$

we get:

$$\varphi_r + \tau_r \frac{d\varphi_r}{dt} = -j\ \omega_k - \omega\ \tau_r \varphi_r + L_m i_s$$

(III.14)

For the other equation, we replace φ_s in (III.8) by $L_s i_s + L_m i_r$:

$$v_s = R_s i_s + \frac{d(L_s i_s + L_m i_r)}{dt} + j\omega_k(L_s i_s + L_m i_r)$$

Replacing (III.13) in (III.10) yields to:

$$v_s = R_s i_s + L_s \frac{di_s}{dt} + L_m \frac{di_r}{dt} + j\omega_k(L_s i_s + \frac{L_m}{L_r}\varphi_r - \frac{L_m^2}{L_r}i_s)$$

By putting:

$$\tau_s = \frac{L_s}{R_s}$$

$$\sigma = 1 - \frac{L_m^2}{L_s L_r}$$

$$k_r = \frac{L_m}{L_r}$$

$$R_\sigma = R_s + R_r k_r^2$$

$$\tau_\sigma = \sigma L_s / R_\sigma$$

We get: $$i_s + \tau_\sigma \frac{di_s}{dt} = -j\omega_k \tau_\sigma i_s + \frac{k_r}{R_\sigma}\left(\frac{1}{\tau_r} - j\omega\right)\varphi_r + \frac{v_s}{R_\sigma}$$

(III.15)

Equations (III.12), (III.14) and (III.15) form the model of the induction machine used in this thesis. It has two inputs and two outputs that are mandatory for the control scheme to work.

$$\begin{cases} i_s + \tau_\sigma \dfrac{di_s}{dt} = -j\omega_k\tau_\sigma i_s + \dfrac{k_r}{R_\sigma}\left(\dfrac{1}{\tau_r} - j\omega\right)\varphi_r + \dfrac{v_s}{R_\sigma} \\[2ex] \varphi_r + \tau_r \dfrac{d\varphi_r}{dt} = -j\ \omega_k - \omega\ \tau_r\varphi_r + L_m i_s \\[2ex] T_{em} = \dfrac{3}{2}pIm(\overline{\varphi_r}i_s) \end{cases} \qquad \text{(III.16)}$$

Other outputs can be extracted from the model, such as stator flux, rotor flux and electromagnetic torque because these variables are calculated inside the block of the induction machine. However, for experimental purposes, the stator flux and the rotor flux are estimated using estimators.

III.4. Simulation of the model of the machine

In order the verify the mathematical model of equation (III.16), an open-loop simulation has been done in MATLAB/Simulink environment with and without load torque at start-up. The induction machine is fed by its nominal three-phase voltage source. The machine parameters are given in Table B.1 in Appendix B.

(a)   (b)

(c)

(d)
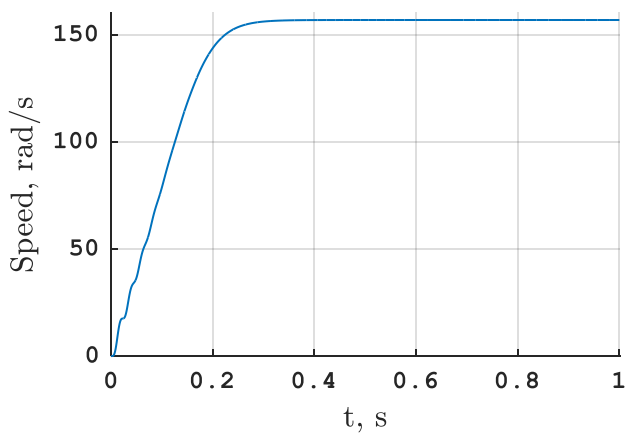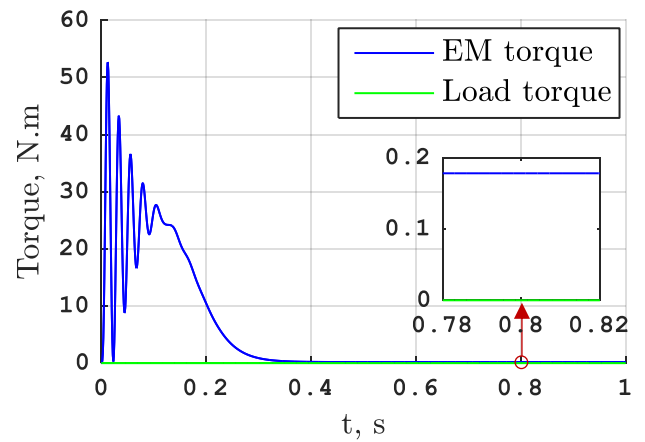
Figure III.4: Open-loop, no load simulation results of the induction motor model: **(a)** mechanical speed, **(b)** electromagnetic and load torque, **(c)** stator currents, **(d)** stator flux magnitude

(a)

(b)

(c)

(d)

Figure III.5: Open-loop, with load simulation results of the induction motor model: **(a)** mechanical speed, **(b)** electromagnetic and load torque, **(c)** stator currents, **(d)** stator flux magnitude
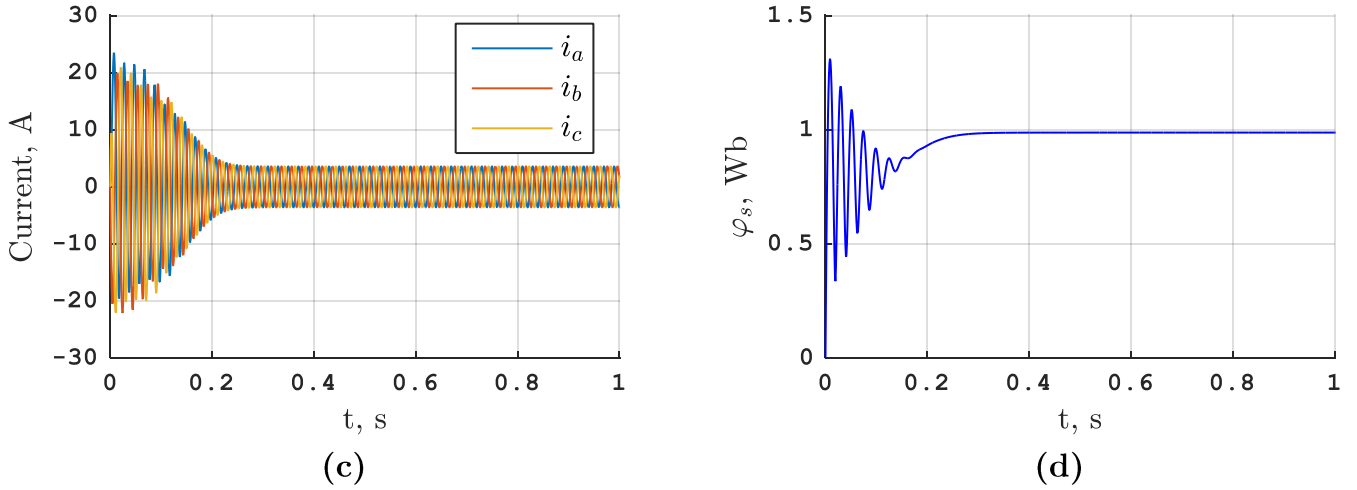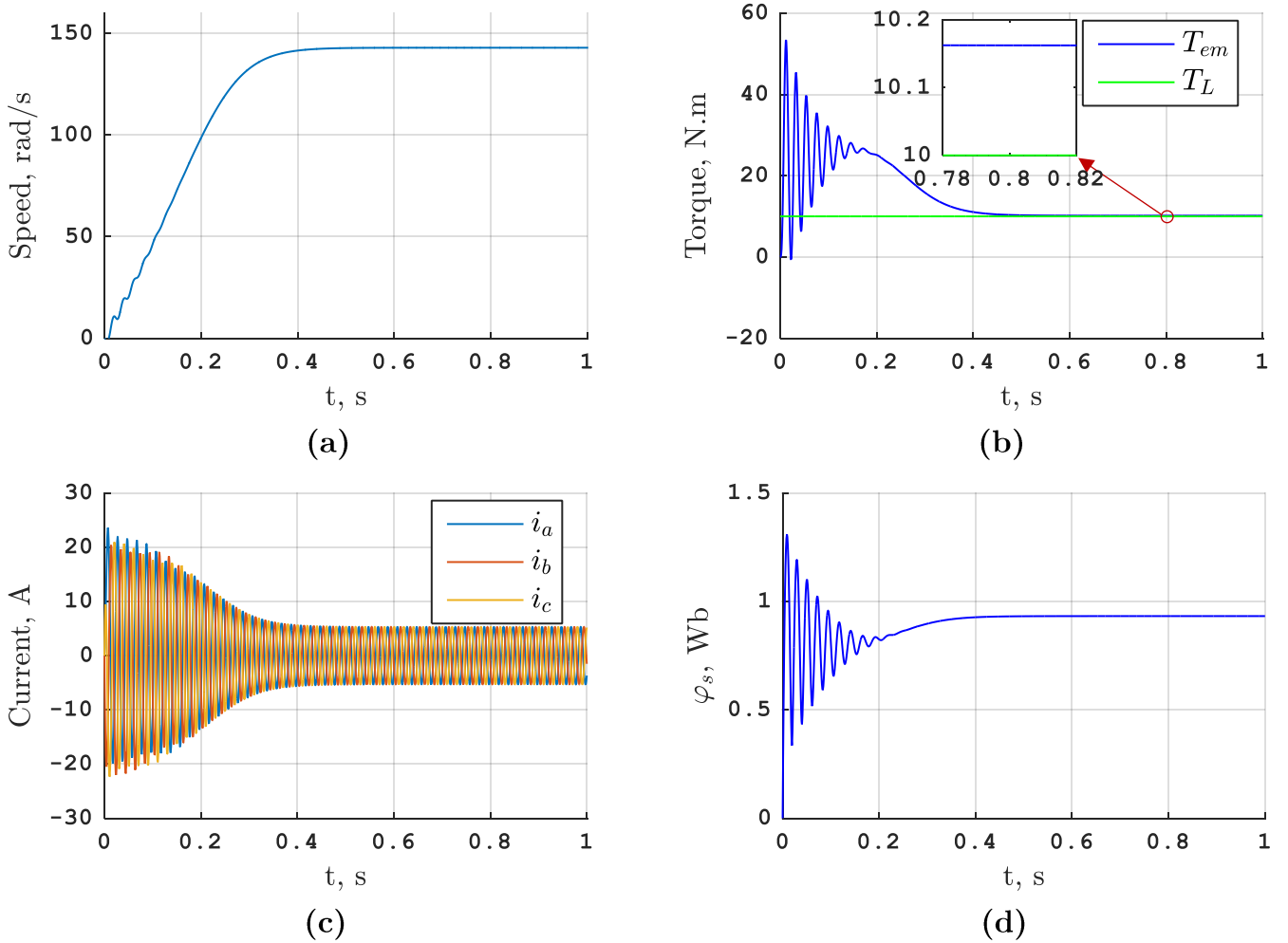
Figure III.4 presents an open-loop, no load simulation results of the induction motor model.

Figure III.4**(a)** shows that the speed at steady state is 156.8634 rad/s which is very close to its nominal value which is 1500 rpm or 157.0792 rad/s. This difference is due to the slip which is essential in an induction machine.

As shown in Figure III.4**(b)**, the load torque is zero and even at steady state, the value of the electromagnetic torque is non-zero, due to the dry friction coefficient k_f. The difference equals the product of the mechanical speed and k_f.

Figure III.5 presents an open-loop, with load simulation results of the induction motor model.

Figure III.5**(a)** shows that the mechanical speed doesn't reach its nominal speed, it stops at 142.9688 rad/s.

Similar to the previous case, the electromagnetic torque is a little bit greater than the load torque due to the dry friction coefficient k_f as shows Figure III.5**(b)**.

Due to the higher value of the electromagnetic torque in the second case, the magnitude of the stator current is higher at steady state (3.6059 A in Figure III.4**(c)** and 5.3368 A in Figure III.5**(c)**).

III.5. Cost function

The goal of this control scheme is to select a voltage vector of the inverter that minimizes the error between the output electromagnetic torque and its reference value and between the magnitude of the stator flux and its reference value, which is normally set to its the nominal value.

Thus, the cost function is expressed as:

$$J = \frac{|T_{em}^p - T^*|}{T_{nom}} + \frac{|\varphi_s^p - \varphi_s^*|}{\varphi_{s\,nom}}$$ (III.17)

Where:

- T_{em}^p : the predicted value of the electromagnetic torque
- T^* : the reference value of the electromagnetic torque
- T_{nom} : the nominal value of the electromagnetic torque
- φ_s^p : the predicted value of the stator flux
- φ_s^* : the reference value of the stator flux
- $\varphi_{s\,nom}$: the nominal value of the stator flux

III.6. Working principle

The working principle of the MPTC is summarized in Figure III.1. At each instant kT_s, the future values of the state variables (the stator current i_s and the rotor flux vectors φ_r) of the system are predicted for the instant $(k+1)T_s$ using the system model, the measurements and necessary estimations. The optimal actuation is selected by the cost function and then applied to the inverter.

The following figure represents a flow diagram of the working principle of the MPTC. It uses finite number of valid switching states of the inverter in order to find the x_{opt} by using the following steps:

Step 1: Measurements of the stator currents and estimation of the stator flux and rotor flux.

Step 2: For each valid switching state, apply the corresponding voltage vector.

Step 3: Predict the values of the electromagnetic torque and stator flux of the next sampling period $k+1$ T_s by applying the voltage vector $v_s[k]$ to the load model.

Step 4: Evaluate the cost function by comparing the predicted values with their respective references and select the switching state that corresponds to the minimum value of the cost function.

Step 5: Apply the optimal switching state x_{opt} to the inverter.

In order to further reduce the computational effort, only one out of two nil vectors of the 2LVSI is considered (the possible switching states of the converter are listed in Table II.1)
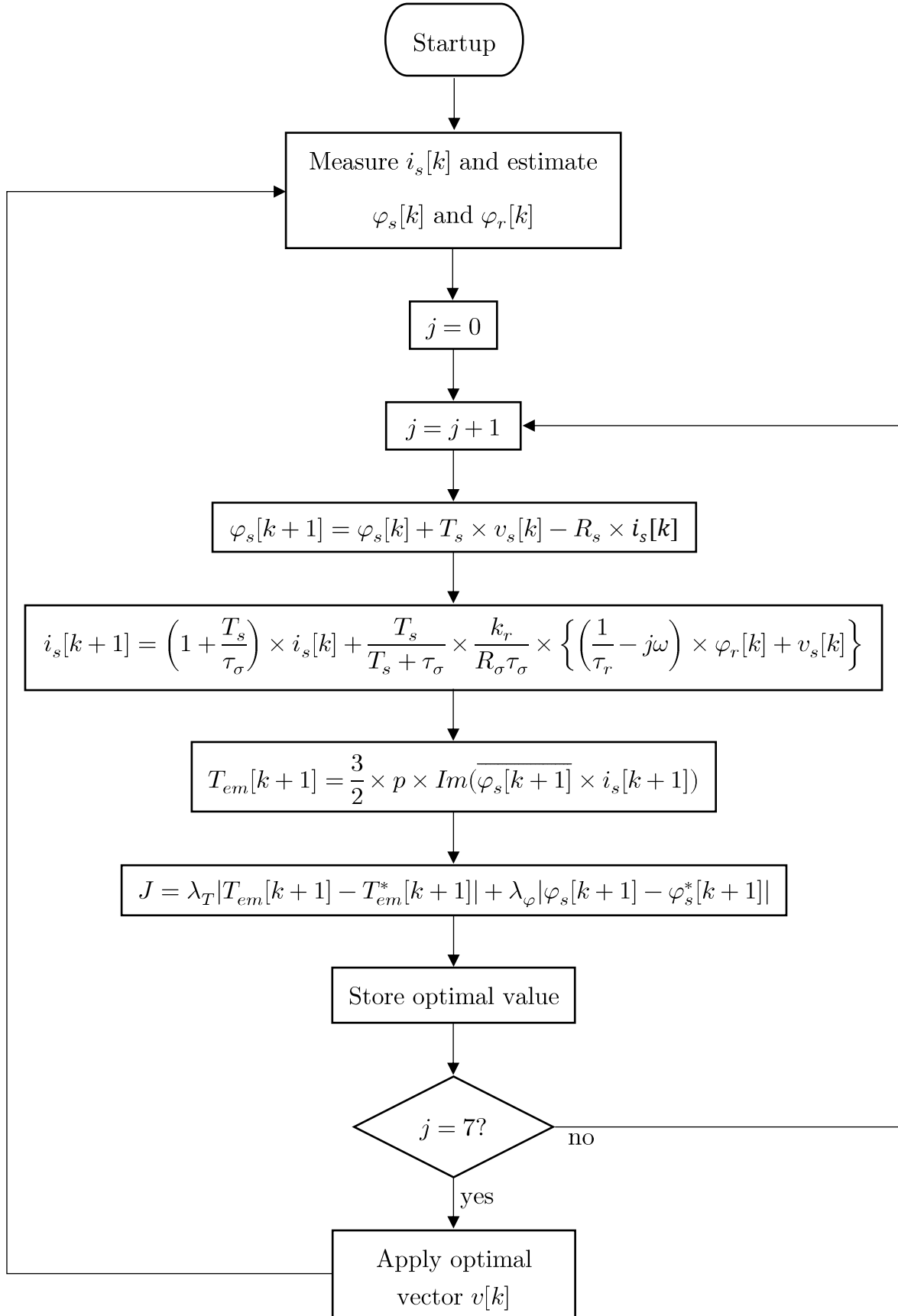
Figure III.6: Flow diagram of the MPTC

III.7. Implementation

Due to the discrete nature of digital controllers, a discretization of the models has to be done. To do so, we use the Euler forward method which is accurate enough when the sampling period T_s is small.

Choosing the stationary reference frame, $\omega_k = 0$, eliminates both multipliers in the internal feedback loops of the rotor winding and the stator winding [45].

After discretization and some arrangements of (III.12), (III.14), (III.15), and (III.16) we get:

$$\varphi_s[k+1] = \varphi_s[k] + T_s \times v_s[k] - R_s \times i_s[k] \qquad \text{(III.18)}$$

$$i_s[k+1] = \left(1 + \frac{T_s}{\tau_\sigma}\right) \times i_s[k]$$
$$+ \frac{T_s}{T_s + \tau_\sigma} \times \frac{k_r}{R_\sigma \tau_\sigma} \times \left\{ \left(\frac{1}{\tau_r} - j\omega\right) \times \varphi_r[k] + v_s[k] \right\} \qquad \text{(III.19)}$$

$$T_{em}[k+1] = \frac{3}{2} \times p \times Im(\overline{\varphi_s[k+1]} \times i_s[k+1]) \qquad \text{(III.20)}$$

We introduce the weighting factors λ_T and λ_φ where: $\lambda_T = \frac{1}{T_{nom}}$ and $\lambda_\varphi = \frac{1}{\varphi_{s\,nom}}$. The cost function, thus, becomes:

$$J = \lambda_T \, T_{em}[k+1] - T_{ref} \, + \lambda_\varphi ||\varphi_s[k+1]| - \varphi_{s\,ref}| \qquad \text{(III.21)}$$

The model used to estimate the stator flux is derived from the equation (III.8), given that the reference frame is stationary we get:

$$\frac{d\varphi_s}{dt} = v_s - R_s i_s \qquad \text{(III.22)}$$

We can estimate the rotor flux φ_r by replacing i_r by its expression from (III.10) in (III.11), we get:

$$\varphi_r = \frac{L_r}{L_m}\varphi_s + \left(L_m - \frac{L_r L_s}{L_m}\right) i_s \qquad \text{(III.23)}$$

As shown in Figure III.1, the Proportional-Integral (PI) controller receives the error signal of the mechanical speed and computes the torque reference for the predictive controller.

By transforming (III.5) to Laplace domain we get:

$$\frac{\Omega}{T_{em} - T_l} = \frac{1}{Js + k_f} \qquad \text{(III.24)}$$
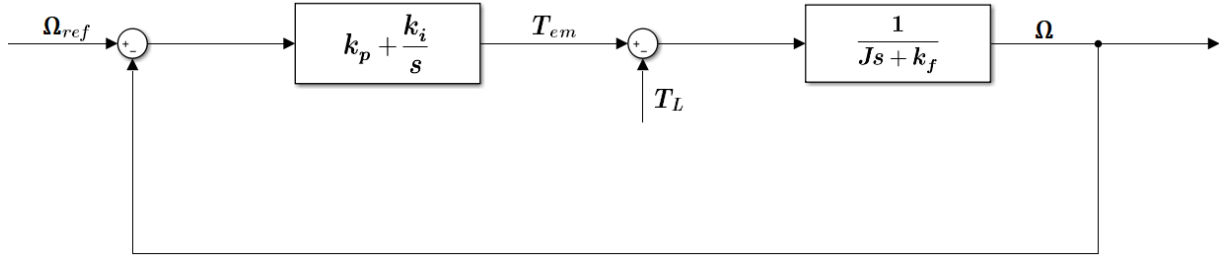
Where s is the Laplace operator.

Figure III.7: PI speed controller

By considering the load torque T_L as a nil disturbance [2], the transfer function (III.24), in closed loop, becomes:

$$\Omega = \frac{k_p}{J} \times \frac{s + \dfrac{k_i}{k_p}}{s^2 + \dfrac{k_p + k_f}{J}s + \dfrac{k_i}{J}} \Omega_{ref} \tag{III.25}$$

The denominator of (III.25) is a second order system of the form:

$$s^2 + 2\xi\omega_n s + \omega_n^2$$

By identification we get:

$$\begin{cases} k_i = J\omega_n^2 \\ k_p = 2\xi\omega_n - k_f \end{cases}$$

Where:

- ξ : damping coefficient
- ω_n : natural circular pulse

III.8. Simulation results and analysis

The MPTC technique was simulated with an Induction Machine fed by a two-level inverter. The MPTC has been simulated in the MATLAB/Simulink environment with different values of the speed reference and the load torque in order to justify the performance of this control scheme in both transient and steady states.

The parameters used in the simulation are given in Table B.1 and Table B.2 in Appendix B. Two cases are analysed. First, the simulation of the control scheme without the constraint of the stator flux. While in the second case, the priority of the control of stator flux over the electromagnetic torque is taken into account in the cost function as a soft constraint.

As for the stator flux reference, it is taken around its nominal value (0.82 Wb). The reference torque is generated from an external PI regulator loop.
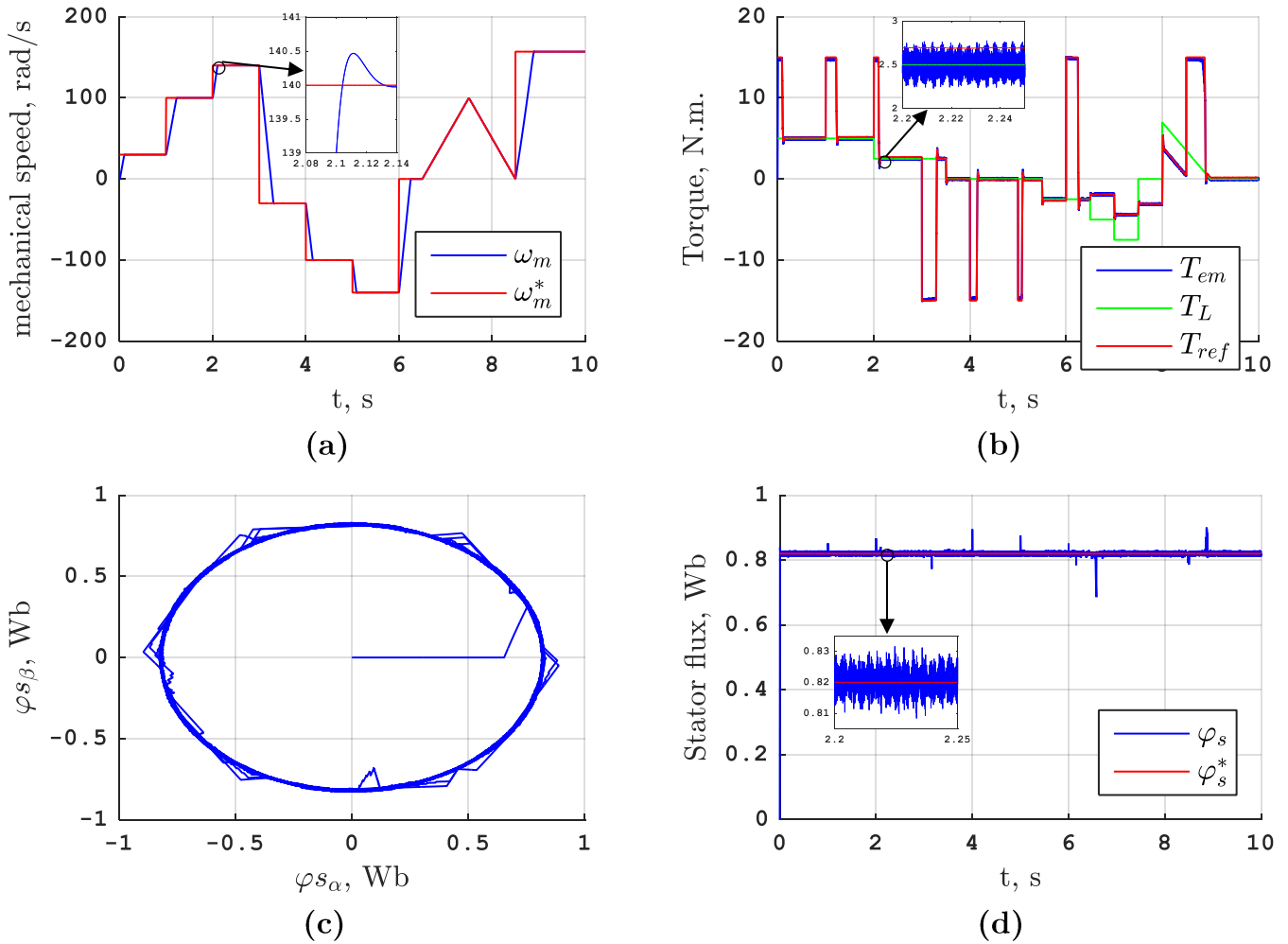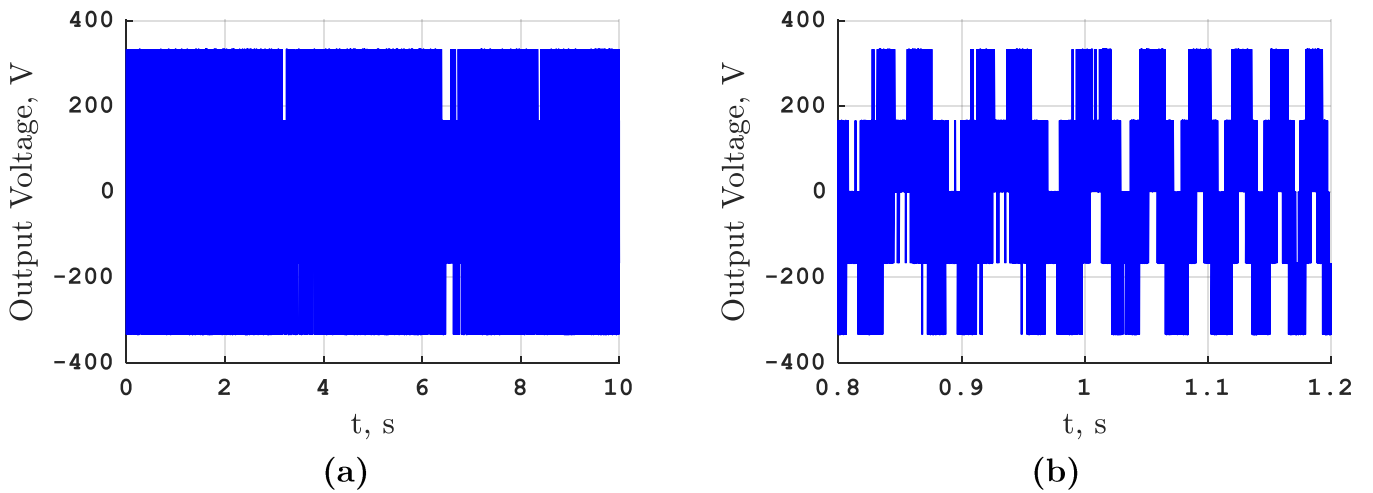
(a)

(b)

(c)

(d)

Figure III.8: Simulation results (mechanic and electromagnetic) of the MPTC of an inverter-fed induction machine without prioritizing the control of the stator flux: (a) rotor speed and its reference, (b) electromagnetic, load and reference torque, (c) stator flux

(a)

(b)

(c)   **(d)**
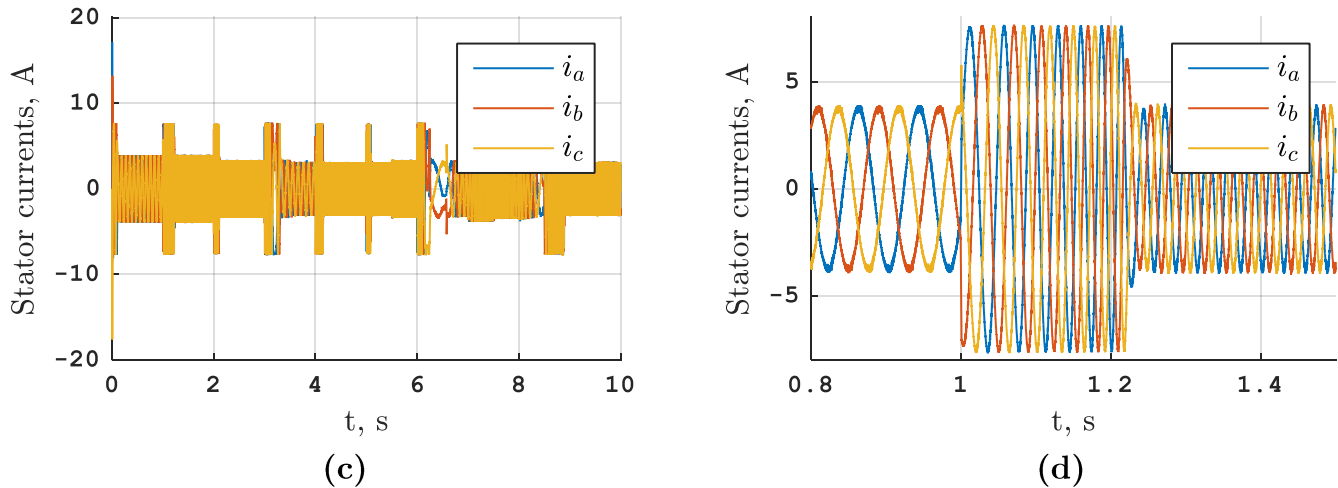
Figure III.9: Simulation results (electrical parameters) without prioritizing the control of the stator flux with a sampling frequency of 50 kHz: (a,b) output voltage of one phase of the inverter and its zoom, (c,d) Stator currents and their zoom

Figure III.8 and Figure III.9 present the results of the simulation of the MPTC of a 1.5 kW squirrel-cage induction machine fed by a two-level inverter without enforcing the priority of the control of the stator flux.

In both cases, the induction motor starts at t = 0.0059 s after a slight inverse response of the speed with a load torque of 5 N.m, which is the cause of that negative value of the speed. The mechanical speed and the electromagnetic torque follow their references:

- At t = 0 s, the speed reference is set to 30 rad/s and it takes the motor 0.0972s to reach that setpoint. This response time could be reduced if the electromagnetic torque hadn't been limited to 15 N.m by the PI controller;
- At t = 1 s, the speed reference is set to 100 rad/s with the same load torque;
- At t = 2 s, although the load torque has decreased, the electromagnetic torque is at its peak value in order to get to rotor speed to 140 rad/s;
- At t = 3 s, the speed reference has been reversed resulting in a negative electromagnetic torque, which is also limited by the PI controller to -15 N.m, until the moment the rotor reaches its reference -30 rad/s;
- At t = 6.5 s, a linear increase in the speed reference is set up to 100 rad/s followed by linear decrease to 0 rad/s at t = 7.5 s;
- The changes in the load torque value affect the speed but the PI controller compensates for that disturbance with a slight overshoot, which is due to the nature of the controller;
- At t = 8.5 s, the speed is set to its nominal value, which is 157 rad/s.

Figure III.8**(a)** shows that the mechanical speed follows its reference despite the variations of the load torque (and thus the reference torque) with a very small overshoot

Figure III.8**(b)** shows that the electromagnetic torque follows its reference and oscillates around the load torque. Same thing for the stator flux magnitude, it follows and oscillates around its reference with certain spikes during the transient states of the electromagnetic torque as shows Figure III.8**(d)**.

Figure III.9 presents the results of the electric variables using MPTC. It shows that the frequency of these variables depends on the rotor speed. It also shows that the variations in the magnitude of the stator currents depend on the electromagnetic torque.
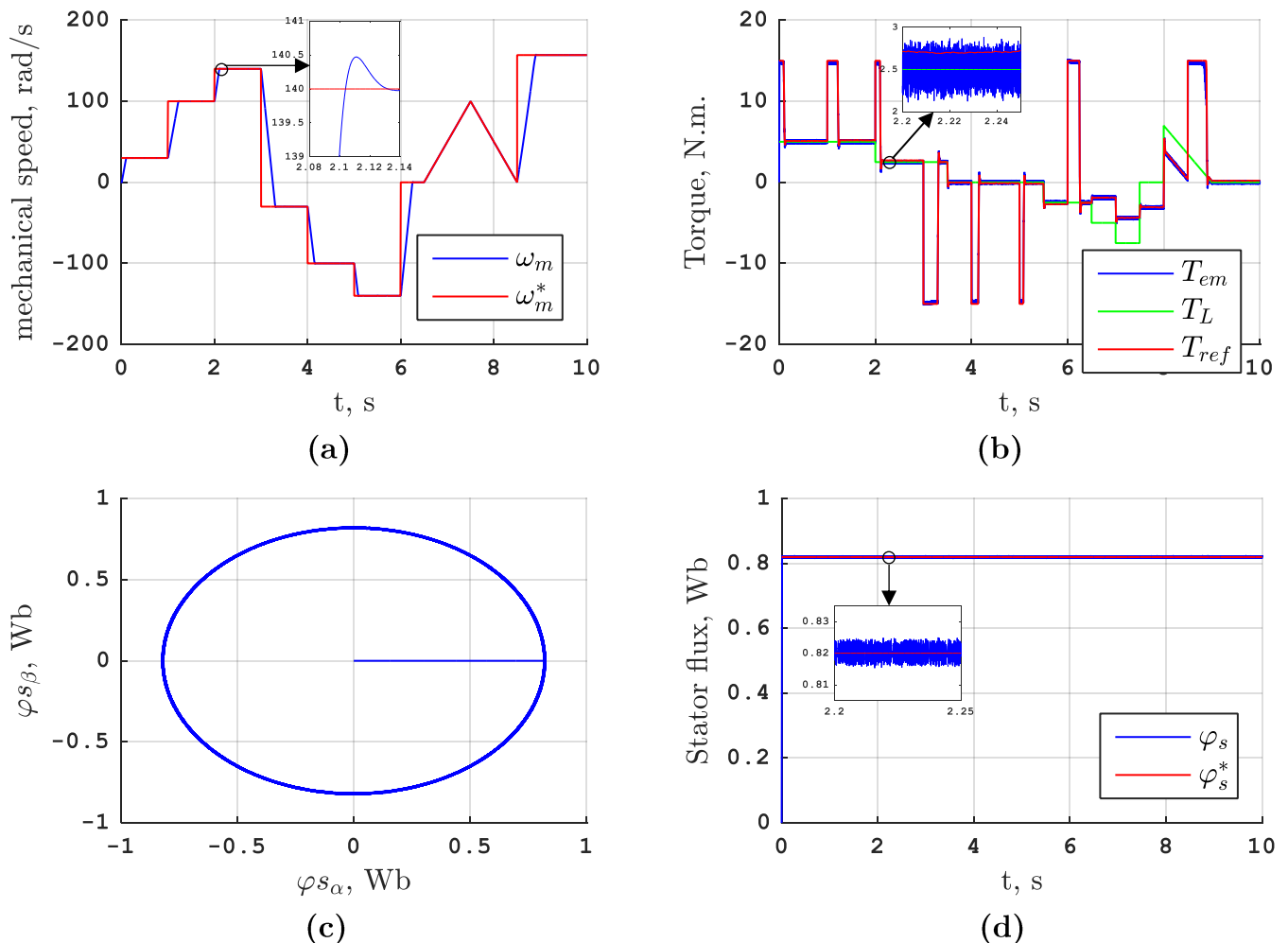

(a)

(b)

(c)

(d)

Figure III.10: Simulation results (mechanic and electromagnetic) of the MPTC of an inverter-fed induction machine with prioritizing the control of the stator flux : (a) rotor speed and its reference, (b) electromagnetic, load and reference torque, (c) stator flux vector, **(d)** stotor flux magnitude and its reference

Figure III.10 represents the results of the simulation of the MPTC of a 1.5 kW squirrel-cage induction machine fed by a two-level inverter with prioritizing the control of the stator flux.

Although there is not a noticeable difference between the two cases in terms of mechanical speed (Figure III.8(a) and Figure III.10(a)), the higher value of λ_φ in the second case has led to better results of the stator flux (Figure III.8(d) and Figure III.10(d)). The flux magnitude oscillates around its reference within a thinner band than that of the first case: In the first case, the max of the error between the reference an the output magnitude of the stator flux in steady-state is 0.0107 Wb whereas in the second case, the max of the error is 0.0056 Wb even at transient-state (except for the start-up transient state).

The algorithm selects the actuation that minimizes the error between the predicted values and the reference values of both the controlled variables. However, by giving a higher weighting factor to the stator flux's error signal in the cost function, the error between the predicted value and the reference value of this controlled variable gets magnified, penalizing the actuation even when the error is small. And the error between the predicted value and the reference value of the electromagnetic torque remains the same. Thus, the selected actuation gets the stator flux closer to its reference.

This improvement of the stator flux comes at the cost of the quality of the electromagnetic torque. As can be observed from Figure III.8(b) and Figure III.10(b), the electromagnetic torque oscillates around its reference within a thicker band than that of the first case. In the first case at steady-state, the max torque ripple is 0.4113 N.m, whereas in the second case, the max ripple is 0.4745 N.m.

In order the evaluate the quality of the stator current with respect to the switching frequency, a simulation has been done where the nominal speed has been set as reference and a load torque of 5 N.m.

Figure III.11 presents the simulation results of the stator currents of an inverter-fed induction machine using MPTC and their spectra with different sampling frequencies.

The quality of the stator currents seems to get better with high sampling frequencies. The machine windings act as filter for high-frequency harmonics.
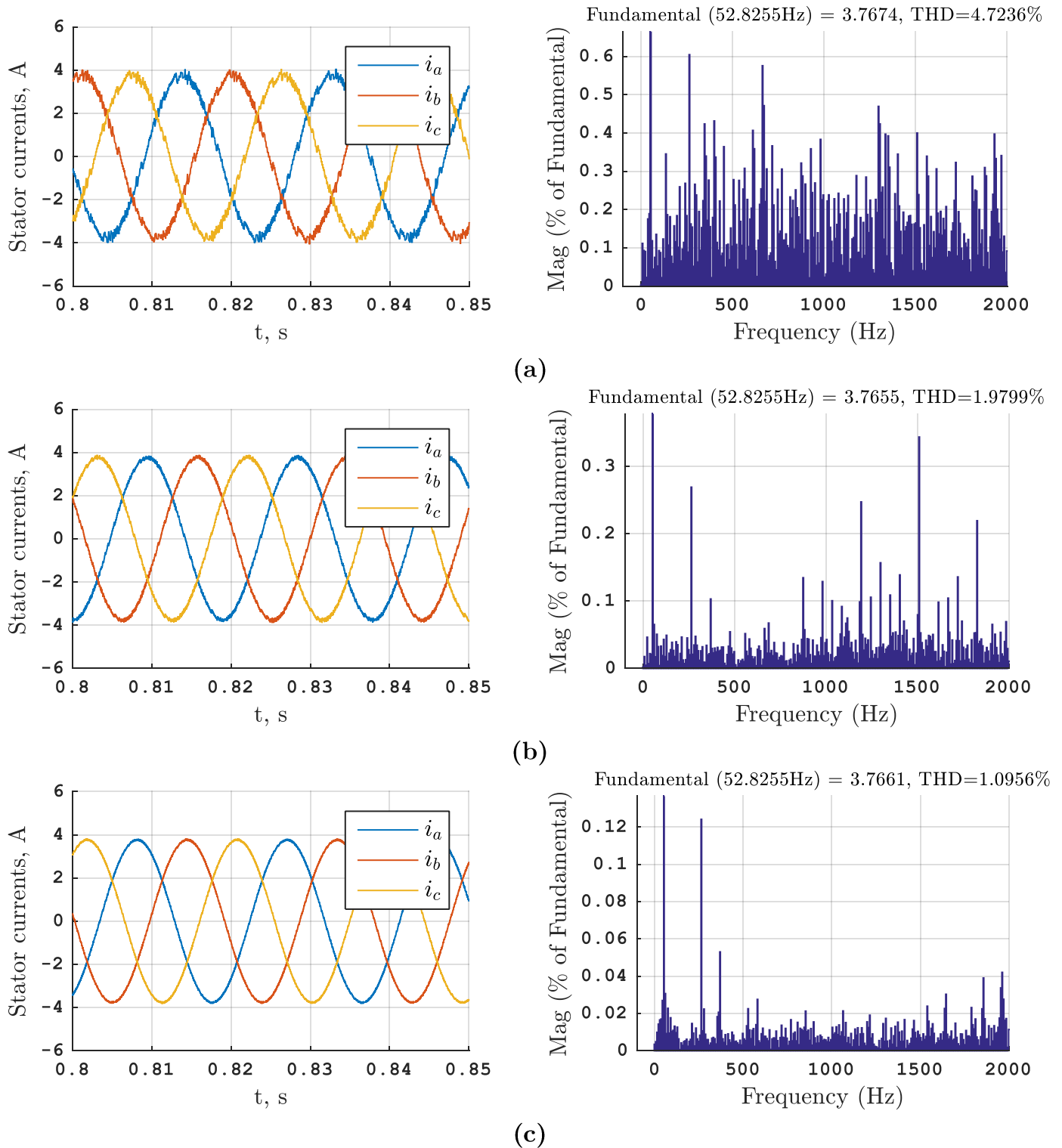
(a)

(b)

(c)

Figure III.11: Simulation results of the stator currents of an inverter-fed induction machine using MPTC and their spectra with a sampling frequency of: **(a)** 20 kHz, **(b)** 50 kHz, **(c)** 100 kHz

III.9. Conclusion

In this chapter, the Model Predictive Torque control applied to an induction motor that is fed by a two-level, three-phase inverter has been introduced, the induction machine has been modelled in a way that suits the control scheme and a cost function has been expressed in order to satisfy the objective of the control. The working principle of the MPTC has been explained in detail.

The control strategy was simulated in MATLAB/Simulink for different values of the weighting factors to demonstrate one of the advantages of Model Predictive Control.

The simulation results show the performance and the fast dynamics of this control strategy, and that it is comparable to the traditional approaches such as DTC.

Using MPTC, a system constraint is easily included in the cost function by tuning the weighting factors. Thus, the different importance of the electromagnetic error signal versus the stator flux error signal can be decided which shows a flexibility in the control strategy.

The converter in these last two chapters is a voltage source inverter. However, in the industry, the consumption of electric energy has leaned towards AC sources. In the following chapters, two topologies of the matrix converter are studied, one of which shares almost 50% of its topology with the inverter.

Chapter IV:

Model Predictive Current Control of a Matrix Converter-Fed RL-load

Chapter IV : Model Predictive Current Control of a Matrix Converter-fed RL-load

IV.1. Introduction

As mentioned in Chapter I, the matrix converter is capable of feeding a three-phase load by a three-phase source directly without the need of a storage capacitor. Which makes it smaller in volume. Furthermore, the MC allows power flowing in both directions, while operating at the same time at unity power factor on the input side [2], [6].

This chapter presents a MPCC scheme of an RL-load fed by a matrix converter with topologies direct and indirect. The modelling of both converters is presented alongside with the modelling of the input filter. The working principle of the MPCC and the load model are explained in detail in Chapter 2.

The control scheme is simulated using the two topologies in MATLAB/Simulink for different references of the output current and reactive power.

IV.2. Modelling of the input filter

Matrix converters produce output voltages and input currents that are very rich in harmonics. These harmonics may have a negative effect on the performance of the system and on the electronic systems [2], [46]. Thus, an input filter must be added between the converter and the supply voltage in order to avoid the generation of overvoltages produced by the short-circuit impedance of the power supply, due to the fast commutation of currents i_e and to eliminate high-frequency harmonics in the input currents [6].

A second-order low-pass filter (Figure IV.1) at the input is considered to avoid over-voltages and harmonics distortions in the source current.
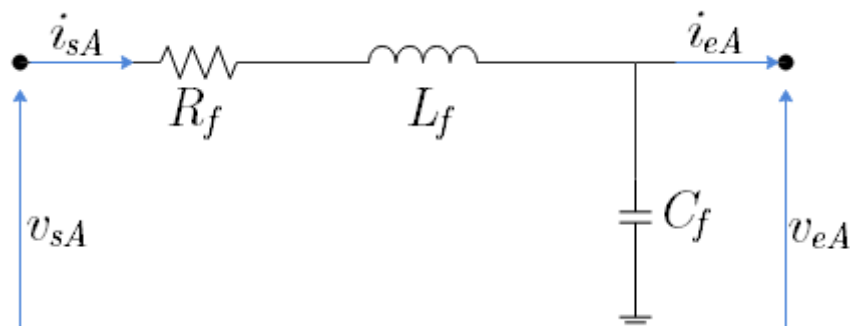

Figure IV.1: Input filter

In order to obtain the dynamic model of the filter, Kirchhoff's first and second law are applied to the power circuit in Figure IV.1, we get:

$$v_s = R_f i_s + L_f \frac{di_s}{dt} + v_e \tag{IV.1}$$

$$i_s = i_e + C_f \frac{dv_e}{dt} \tag{IV.2}$$

With:
$$\begin{cases} v_s = \frac{2}{3}(v_{sA} + a v_{sB} + a^2 v_{sC}) \\ v_e = \frac{2}{3}(v_{eA} + a v_{eB} + a^2 v_{eC}) \\ i_s = \frac{2}{3}(i_{sA} + a i_{sB} + a^2 i_{sC}) \\ i_e = \frac{2}{3}(i_{eA} + a i_{eB} + a^2 i_{eC}) \end{cases}$$

By considering the vector $[v_e \ i_s]^T$ as a state variable and the vector $[v_s \ i_e]^T$ as an input variable, we end up with a continuous-time state space representation of the filter.

$$\underbrace{\begin{bmatrix} v_e \\ i_s \end{bmatrix}}_{X} = \underbrace{\begin{bmatrix} 0 & 1/C_f \\ -1/L_f & -R_f/L_f \end{bmatrix}}_{A_f} \underbrace{\begin{bmatrix} v_e \\ i_s \end{bmatrix}}_{X} + \underbrace{\begin{bmatrix} 0 & -1/C_f \\ 1/L_f & 0 \end{bmatrix}}_{B_f} \underbrace{\begin{bmatrix} v_s \\ i_e \end{bmatrix}}_{U} \tag{IV.3}$$

IV.3. Modelling of the Direct Matrix Converter

The power circuit of the DMC is presented in Figure IV.2. It uses a set of bidirectional switches to directly connect the three-phase power supply to a three-phase load, or in this case, through an input filter.
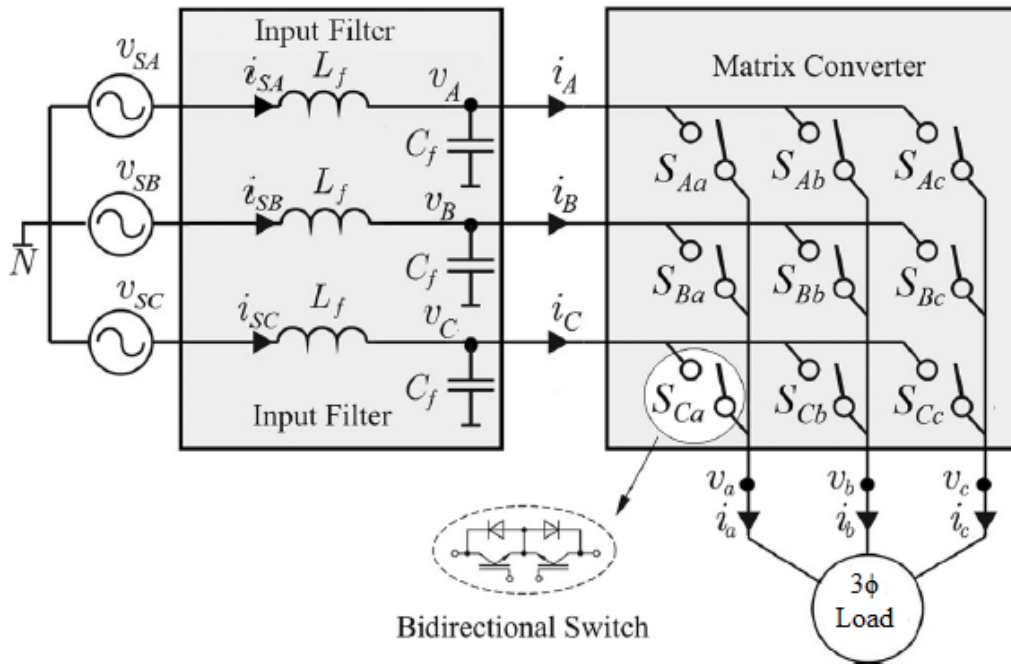

Figure IV.2: 3×3 Direct Matrix Converter

The output voltage is formed from segments of three input voltages. The input current is of three output current segments [2].

It must be mentioned that the load current must not be interrupted abruptly, because the inductive nature of the load will generate an important overvoltage that can destroy the components. In addition, operation of the switches cannot short-circuit two input lines, because this switching state will generate short-circuit currents. These restrictions can be expressed in mathematical form by the following equation [2], [6]. Those are the two conditions of operation of the MC.

$$S_{Ay} + S_{By} + S_{Cy} = 1, \qquad \forall y \in \{a, b, c\} \qquad (IV.4)$$

$$S_{xy} = \begin{cases} 0, \text{if } S_{xy} \text{ is open} \\ 1, \text{if } S_{xy} \text{ is close} \end{cases} \qquad (IV.5)$$

Where:

S_{xy} : The connection function

$y \in \{a, b, c\}$: The phases of the load

$x \in \{A, B, C\}$: The phases of the supply

The two conditions of operation of the MC are translated into equations (IV.4) and (IV.5). Which leads to 27 valid switching states of the 3×3 DMC.

Referenced to the voltage source neutral point N, the instantaneous load voltages can be expressed as the product of the input voltage vector and a matrix, which is called the instantaneous transfer matrix [2], [46].

$$\begin{bmatrix} v_a \\ v_b \\ v_c \end{bmatrix} = \underbrace{\begin{bmatrix} S_{Aa}(t) & S_{Ba}(t) & S_{Ca}(t) \\ S_{Ab}(t) & S_{Bb}(t) & S_{Cb}(t) \\ S_{Ac}(t) & S_{Bc}(t) & S_{Cc}(t) \end{bmatrix}}_{S} \times \begin{bmatrix} v_{eA} \\ v_{eB} \\ v_{eC} \end{bmatrix} \qquad (IV.6)$$

The input current of the DMC is given by:

$$\begin{bmatrix} i_A \\ i_B \\ i_C \end{bmatrix} = \begin{bmatrix} S_{Aa}\ t & S_{Ba}\ t & S_{Ca}\ t \\ S_{Ab}\ t & S_{Bb}\ t & S_{Cb}\ t \\ S_{Ac}\ t & S_{Bc}\ t & S_{Cc}\ t \end{bmatrix}^T \times \begin{bmatrix} i_a \\ i_b \\ i_c \end{bmatrix} \qquad (IV.7)$$

Where:

- v_a, v_b and v_c are the load voltages referenced to the load neutral point;
- v_{eA}, v_{eB} and v_{eC} are the filter capacitor voltages, also input voltages of the DMC;
- i_a, i_b and i_c are the load currents;
- i_A, i_B and i_C are the input currents of the DMC.

IV.4. Modelling of the Indirect Matrix Converter

The power circuit of the IMC is presented in Figure IV.3. The converter can be divided into two stages: the rectifier stage and the inverter stage.
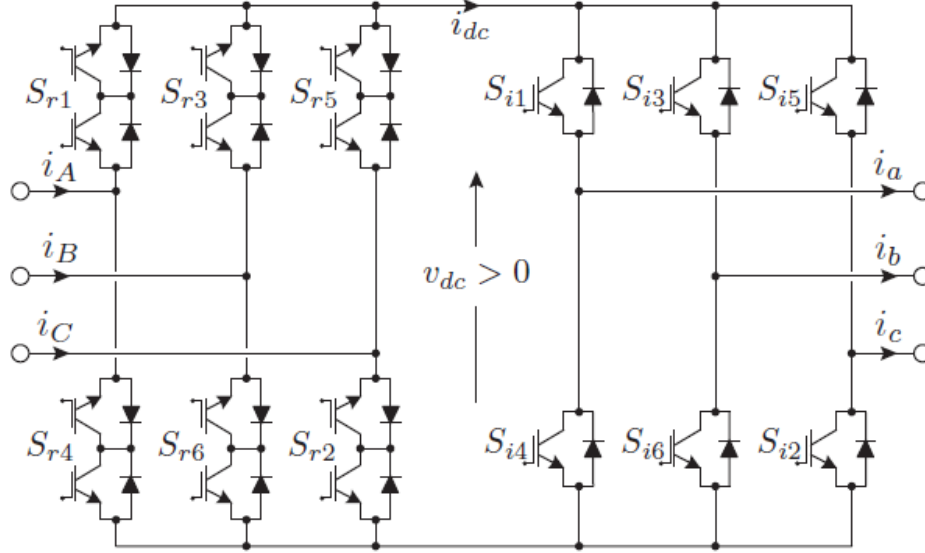

Figure IV.3: 3×3 Indirect Matrix Converter

The rectifier stage is a current source rectifier that consists of six bidirectional switches, which makes it capable of operating in all four quadrants. The inverter stage is a conventional voltage source inverter. This topology helps extend the control technique of the inverter on the previous two chapters.

The model of the converter can be described as the product of two instantaneous transfer matrices of the rectifier and the inverter.

$$
\begin{bmatrix} v_a \\ v_b \\ v_c \end{bmatrix} = \underbrace{\begin{bmatrix} S_{i1}\ t & S_{i4}\ t \\ S_{i3}\ t & S_{i6}\ t \\ S_{i5}\ t & S_{i2}\ t \end{bmatrix}}_{S_{inv}} \times \underbrace{\begin{bmatrix} S_{r1}\ t & S_{r3}\ t & S_{r5}\ t \\ S_{r4}\ t & S_{r6}\ t & S_{r2}\ t \end{bmatrix}}_{S_{rec}} \times \begin{bmatrix} v_{eA} \\ v_{eB} \\ v_{eC} \end{bmatrix} \qquad \text{(IV.8)}
$$

The input current of the IMC is given by:

$$
\begin{bmatrix} i_A \\ i_B \\ i_C \end{bmatrix} = \begin{bmatrix} S_{r1}\ t & S_{r3}\ t & S_{r5}\ t \\ S_{r4}\ t & S_{r6}\ t & S_{r2}\ t \end{bmatrix}^T \times \begin{bmatrix} S_{i1}\ t & S_{i4}\ t \\ S_{i3}\ t & S_{i6}\ t \\ S_{i5}\ t & S_{i2}\ t \end{bmatrix}^T \times \begin{bmatrix} i_a \\ i_b \\ i_c \end{bmatrix} \qquad \text{(IV.9)}
$$

Where:

- v_a, v_b and v_c are the load voltages referenced to the load neutral point;
- v_{eA}, v_{eB} and v_{eC} are the filter capacitor voltages, also input voltages of the IMC;
- i_a, i_b and i_c are the load currents;

- i_A, i_B and i_C are the input currents of the IMC.

The two conditions of operation of the IMC are translated to the following equations:

$$\begin{cases} S_{r1} + S_{r3} + S_{r5} = 1 \\ S_{r2} + S_{r4} + S_{r6} = 1 \end{cases} \tag{IV.10}$$

$$S_{ij} + S_{i(j+3)} = 1, \quad j = \{1,2,3\} \tag{IV.11}$$

According to (IV.10) and (IV.11), there are 72 possible switching states of the 3×3 IMC, 9 for the rectifier and 8 for the inverter.

Table IV.1: Possible switching states for the rectifier stage

	Vectors	S_{r1}	S_{r2}	S_{r3}	S_{r4}	S_{r5}	S_{r6}	i_A	i_B	i_C	v_{dc}
Active	I_1	1	1	0	0	0	0	i_{dc}	0	$-i_{dc}$	v_{AC}
	I_2	0	1	1	0	0	0	0	i_{dc}	$-i_{dc}$	v_{BC}
	I_3	0	0	1	1	0	0	$-i_{dc}$	i_{dc}	0	$-v_{AB}$
	I_4	0	0	0	1	1	0	$-i_{dc}$	0	i_{dc}	$-v_{AC}$
	I_5	0	0	0	0	1	1	0	$-i_{dc}$	i_{dc}	$-v_{BC}$
	I_6	1	0	0	0	0	1	i_{dc}	$-i_{dc}$	0	v_{AB}
Nil		1	0	0	1	0	0	0	0	0	0
	I_0	0	1	0	0	1	0	0	0	0	0
		0	0	1	0	0	1	0	0	0	0

Table IV.2: Possible switching states for the inverter stage

	Vectors	S_{i1}	S_{i2}	S_{i3}	S_{i4}	S_{i5}	S_{i6}	v_{ab}	v_{bc}	v_{ca}	i_{dc}
Active	V_1	1	1	0	0	0	1	v_{dc}	0	$-v_{dc}$	i_a
	V_2	1	1	1	0	0	0	0	v_{dc}	$-v_{dc}$	$i_a + i_b$
	V_3	0	1	1	1	0	0	$-v_{dc}$	v_{dc}	0	i_b
	V_4	0	0	1	1	1	0	$-v_{dc}$	0	v_{dc}	$i_b + i_c$
	V_5	0	0	0	1	1	1	0	$-v_{dc}$	v_{dc}	i_c
	V_6	1	0	0	0	1	1	v_{dc}	$-v_{dc}$	0	$i_a + i_c$
Nil	V_0	1	0	1	0	1	0	0	0	0	0
		0	1	0	1	0	1	0	0	0	0

IV.5. Working principle

The working principle of the MPCC is explained in detail in Chapter 2. As mentioned before, it is possible to operate in unity power factor, which means the

minimization of the instantaneous input reactive power. The reactive power in the $\alpha\beta$ reference frame is given by the following equation.

$$Q = v_{s\alpha}i_{s\beta} - v_{s\beta}i_{s\alpha} \qquad \text{(IV.12)}$$

At each sampling period, the control scheme calculates predictions of the reactive power and selects the actuation that minimizes it. Hence the need of prediction values of supply current. The supply current is predicted using the filter model

For minimizing the reactive power, a term must be added to the cost function in (II.8) to penalize the switching states that produce higher values of reactive power predictions. Since the goal is to control the output current and operate in the input unity factor mode, the cost function then becomes:

$$J = |i_a^* - i_a^p| + |i_b^* - i_b^p| + |i_c^* - i_c^p| + \lambda|Q^p| \qquad \text{(IV.13)}$$

Where:

- i^* : The reference value of the current;
- i^p : The predicted value of the current;
- Q^p : The predicted value of the input reactive power;
- λ : The weighting factor.

IV.6. Implementation of the MPCC

The control scheme has been implemented in MATLAB/Simulink using the models (II.6), (IV.3), (IV.6), (IV.7), (IV.8) and (IV.9). The filter, load and simulation parameters are given in

Table C.2, Table A.1 and Table C.1 respectively.

Although continuous-time models (load and filter) have been used in MATLAB/Simulink, discrete-time models are mandatory because of the discrete nature of microcontrollers.

The discrete-time model of the load is given in equation (II.7) and the discrete-time model of the filter is given as follows [6]:

$$\begin{bmatrix} v_e[k+1] \\ i_s[k+1] \end{bmatrix} = A_{fd} \begin{bmatrix} v_e[k] \\ i_s[k] \end{bmatrix} + B_{fd} \begin{bmatrix} v_s[k] \\ i_e[k] \end{bmatrix} \qquad \text{(IV.14)}$$

Where:

$$A_{fd} = e^{A_f T_s} \quad \text{and} \quad B_{fd} = \int_0^{T_s} e^{A_f(T_s - \tau)} B_f d\tau$$

In order to minimize computation time, only active vectors of the rectifier are used and only one nil vector of the inverter is used, totalling in 42 possible of the IMC instead of 72.

IV.7. Simulation results and analysis

The MPCC technique was simulated with an RL-load fed by a both topologies of the MC. The MPCC has been simulated in the environment MATLAB/Simulink with different values of the output current reference and in order to justify the performance of this control scheme in both transient and permanent states.

The parameters used in the simulations are given in Table C.1 and Table C.2 in Appendix C. Two cases are analysed. First, the validation of the control scheme without the control of the reactive power. While in the second case, the control of the reactive power is taken into account in order to operate with a unity power factor.
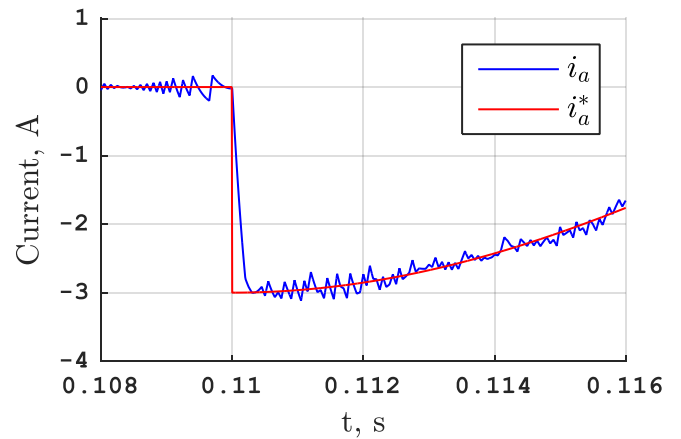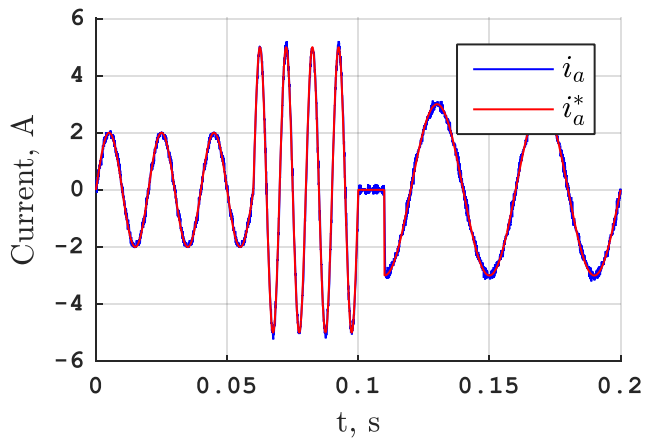
(a)
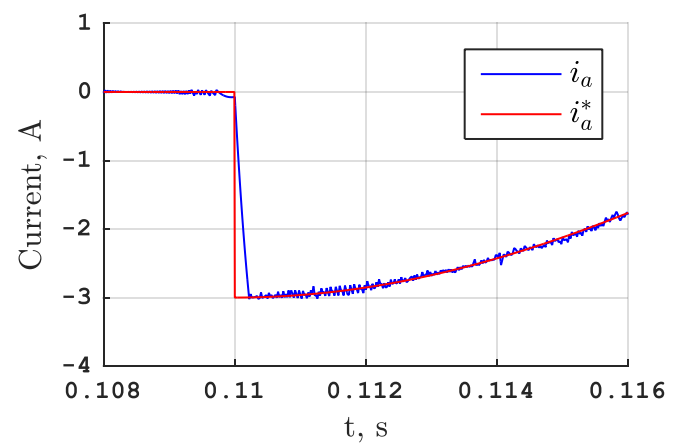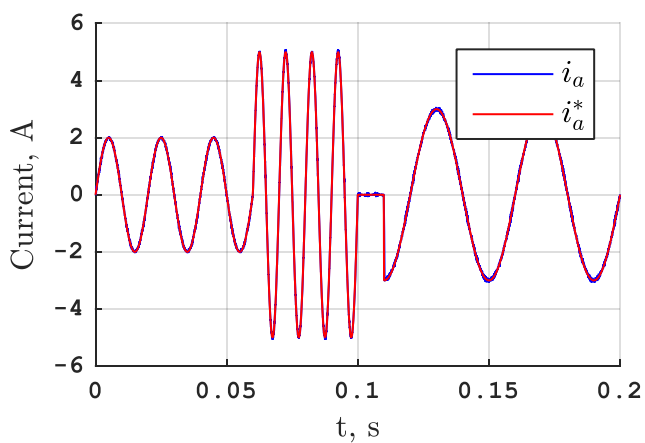
(b)
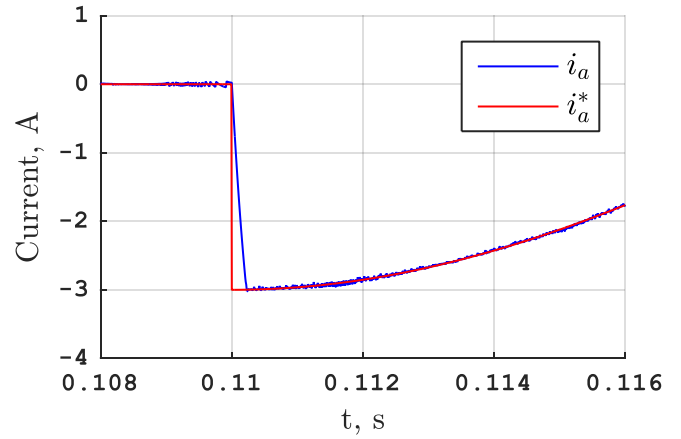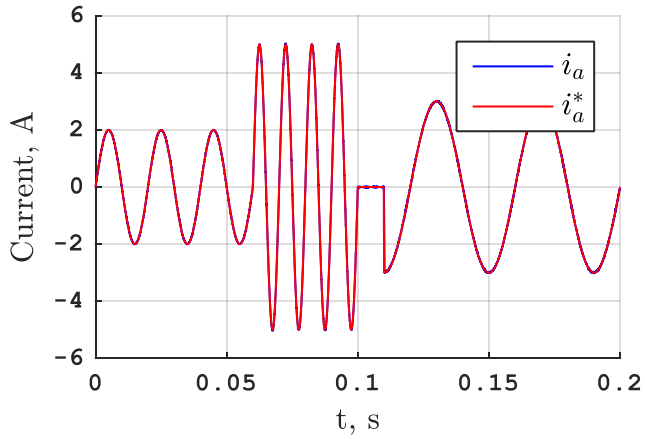
(c)

Figure IV.4: Simulation results of MPCC of a DMC-fed RL-load: Reference and output current of phase A and their zoom with a sampling frequency of: (a) 20 kHz, (b) 50 kHz, (c) 100 kHz
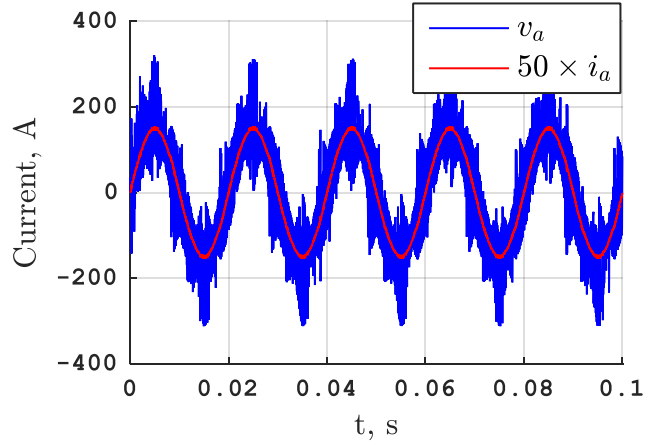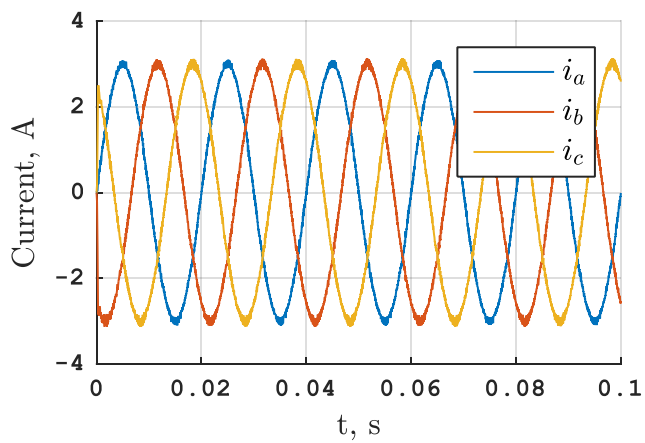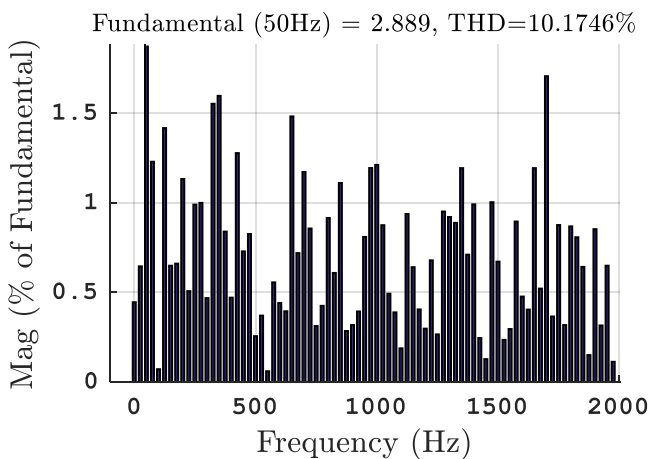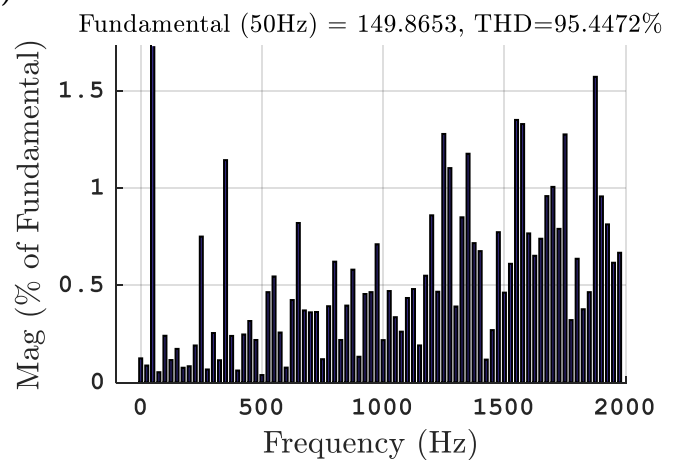

(a)
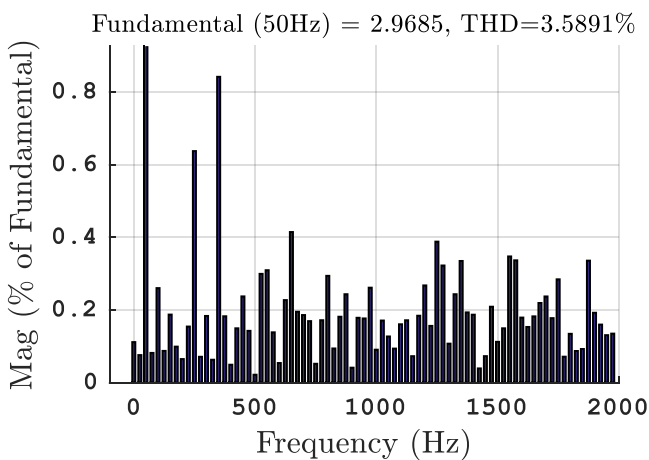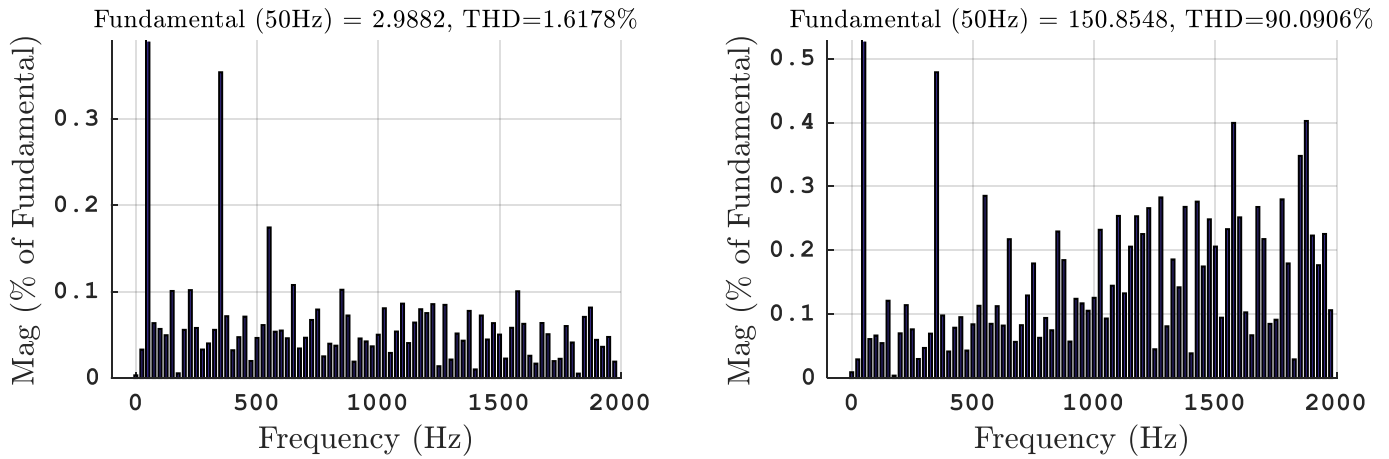

(b)
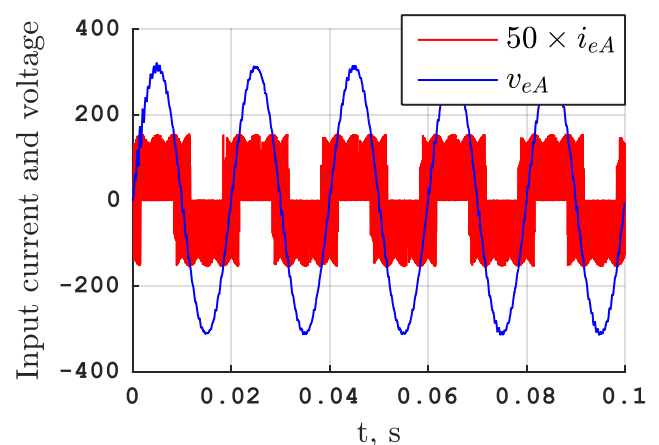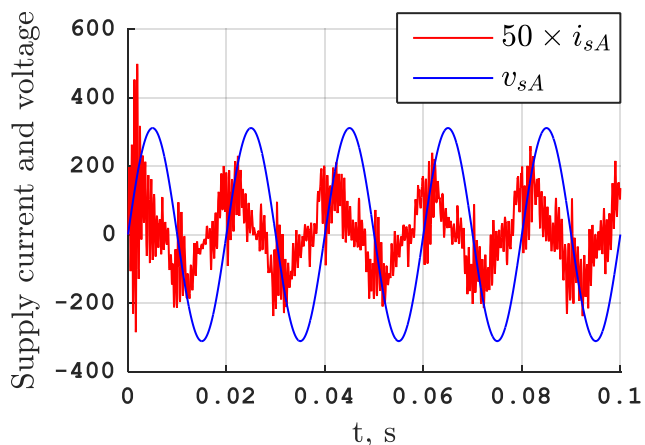
(c)

(d)
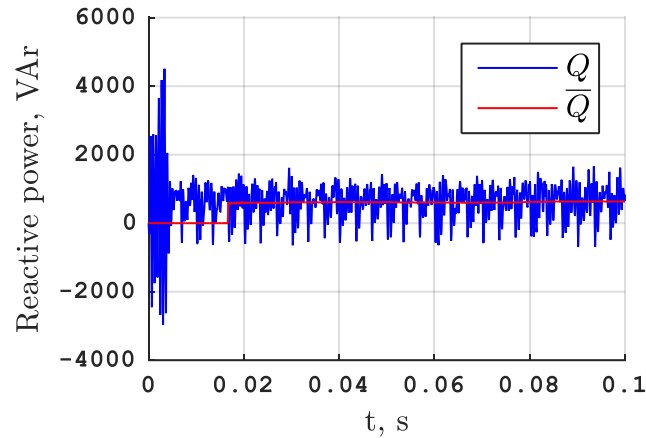
(e)

Figure IV.5: Simulation results of MPCC of a DMC-fed RL-load without input reactive power minimization with a sampling frequency of 50 kHz: steady-state analysis of: **(a)** load currents, **(b)** load voltage and current, **(c)** supply current and voltage, **(d)** input current and voltage of DMC, **(e)** input reactive power and its moving average value
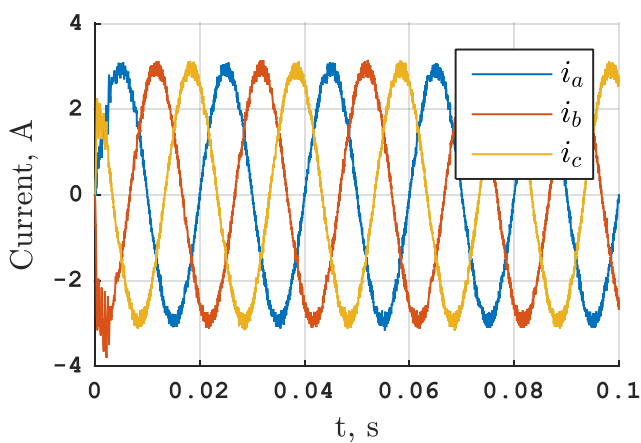
(a)
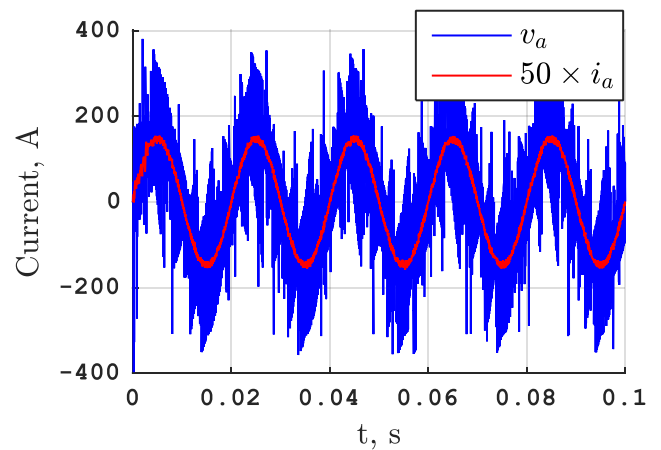
(b)
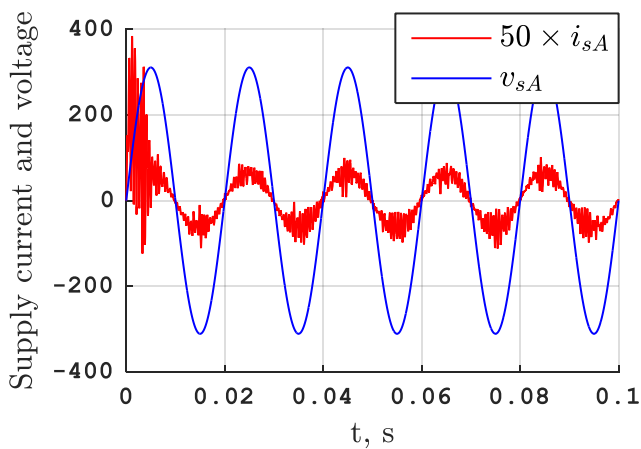
(c)
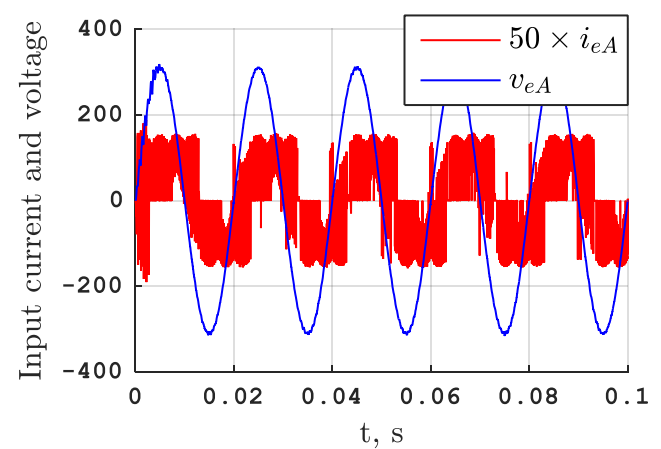
(d)
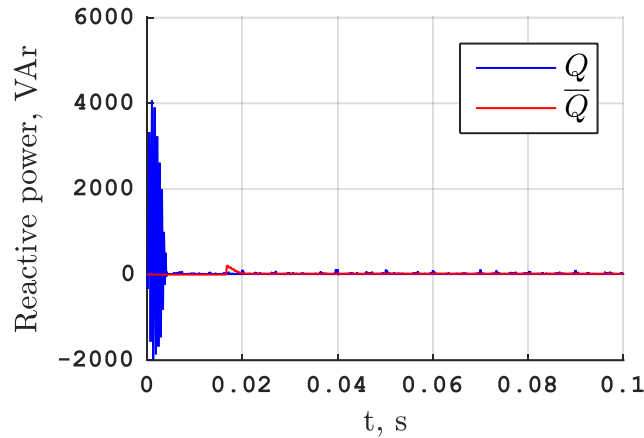
(e)

Figure IV.6: Simulation results of MPCC of a DMC-fed RL-load with input reactive power minimization with a sampling frequency of 50 kHz: steady-state analysis of: **(a)** load currents, **(b)** load voltage and current, **(c)** supply current and voltage, **(d)** input current and voltage of DMC, **(e)** input reactive power and its moving average value
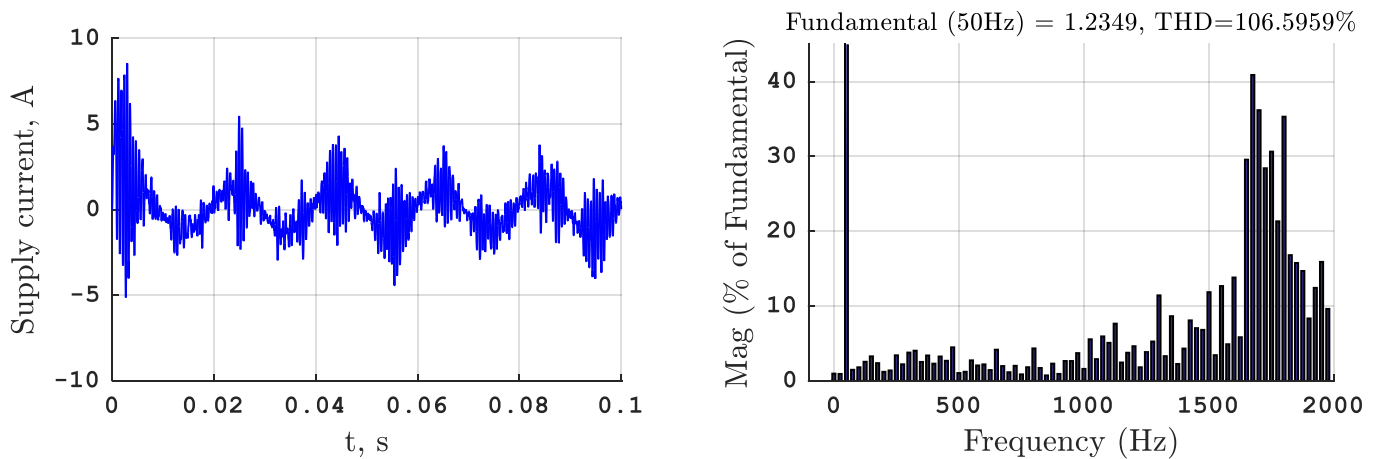

(a)

(b)

Fundamental (50Hz) = 2.9882, THD=1.6178%
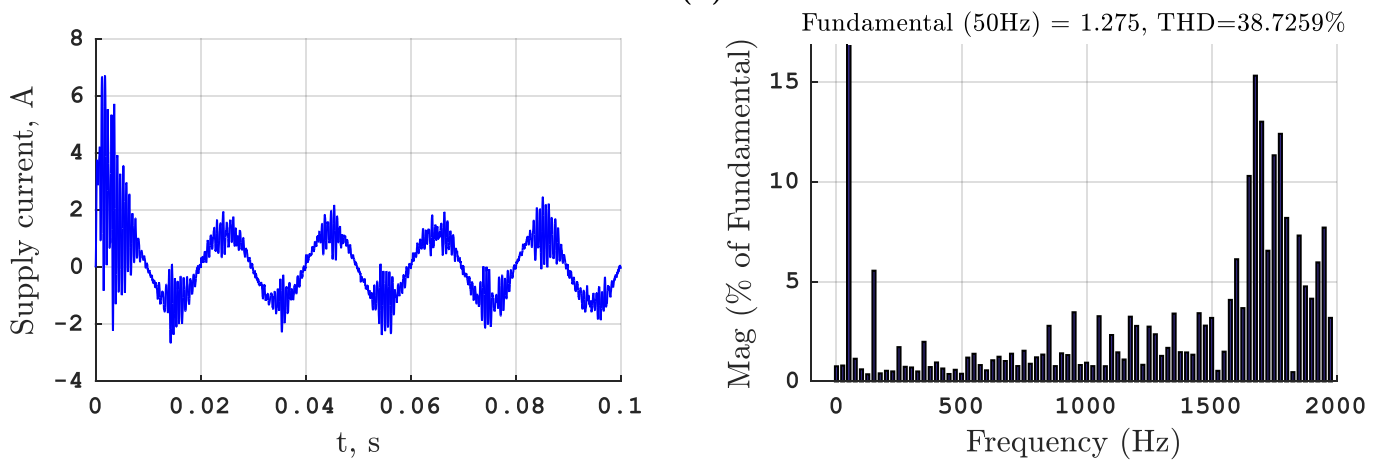
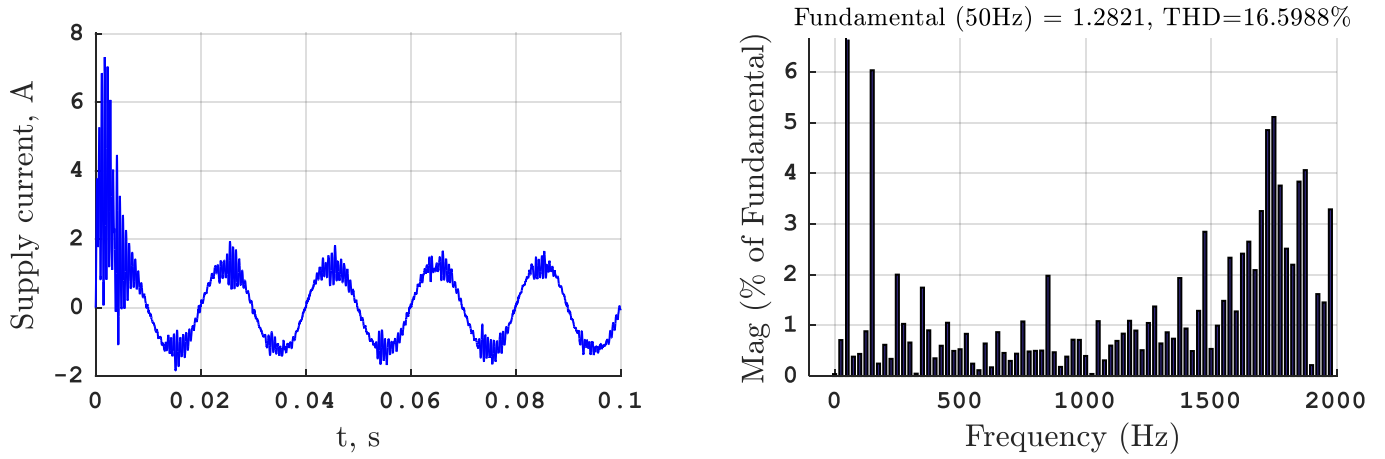Fundamental (50Hz) = 150.8548, THD=90.0906%
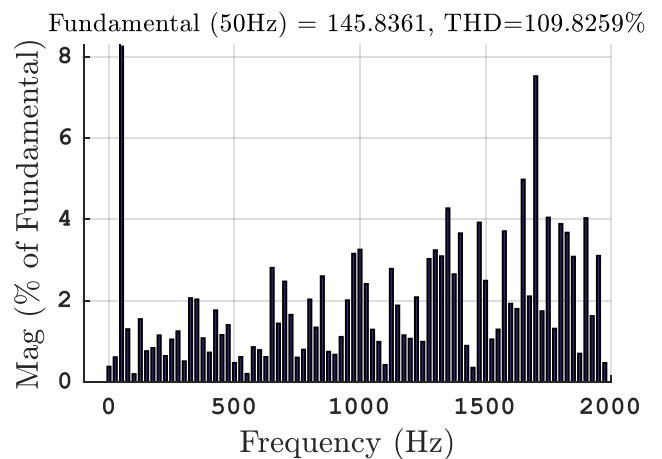
(c)

Figure IV.7: Simulation results of MPCC of an DMC-fed RL-load with input reactive power minimization: Output current and output voltage spectra expressed as percentages of fundamental magnitude with a sampling frequency of: (a) 20 kHz, (b) 50 kHz, (a) 100 kHz
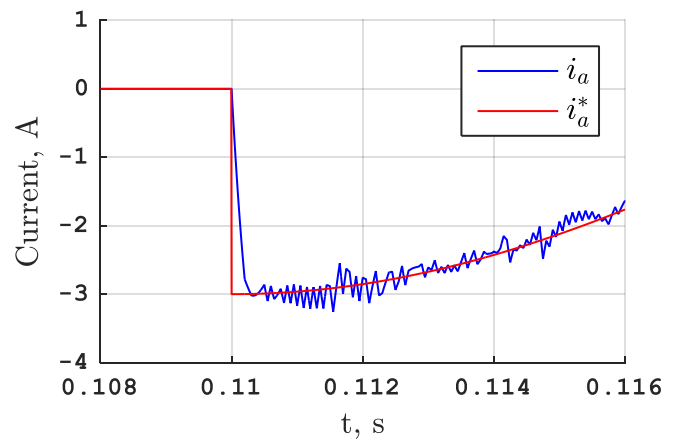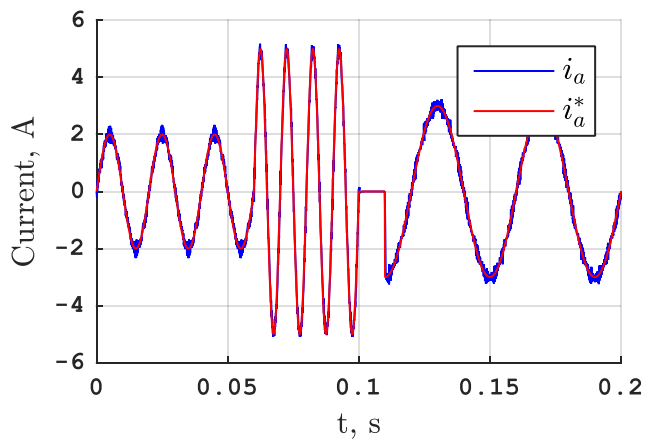
Fundamental (50Hz) = 1.2349, THD=106.5959%

(a)
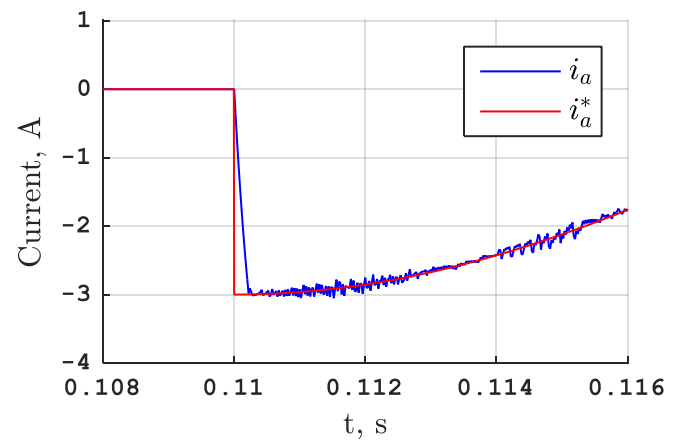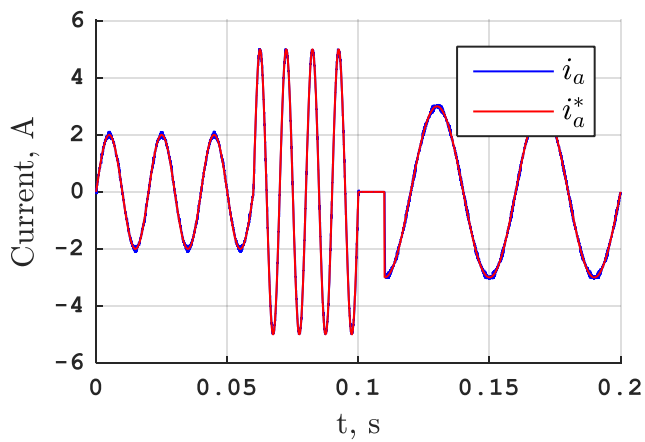
Fundamental (50Hz) = 1.275, THD=38.7259%
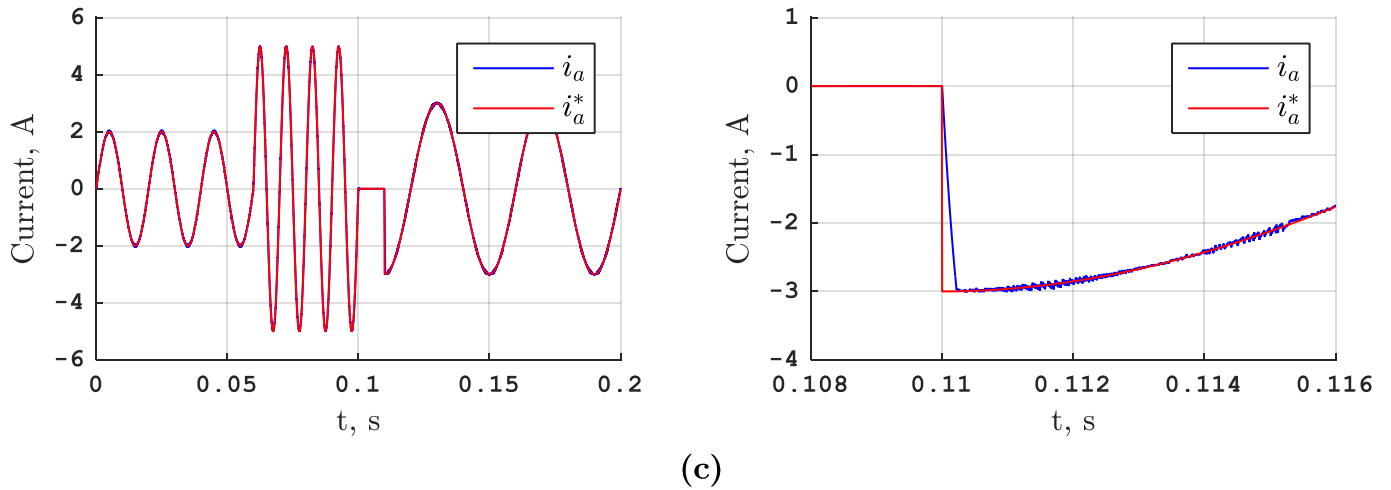
(b)

(c)

Figure IV.8: Simulation results of MPCC of an DMC-fed RL-load with input reactive power minimization: Supply current and its spectra expressed as percentages of fundamental magnitude with a sampling frequency of: (a) 20 kHz, (b) 50 kHz, (a) 100 kHz
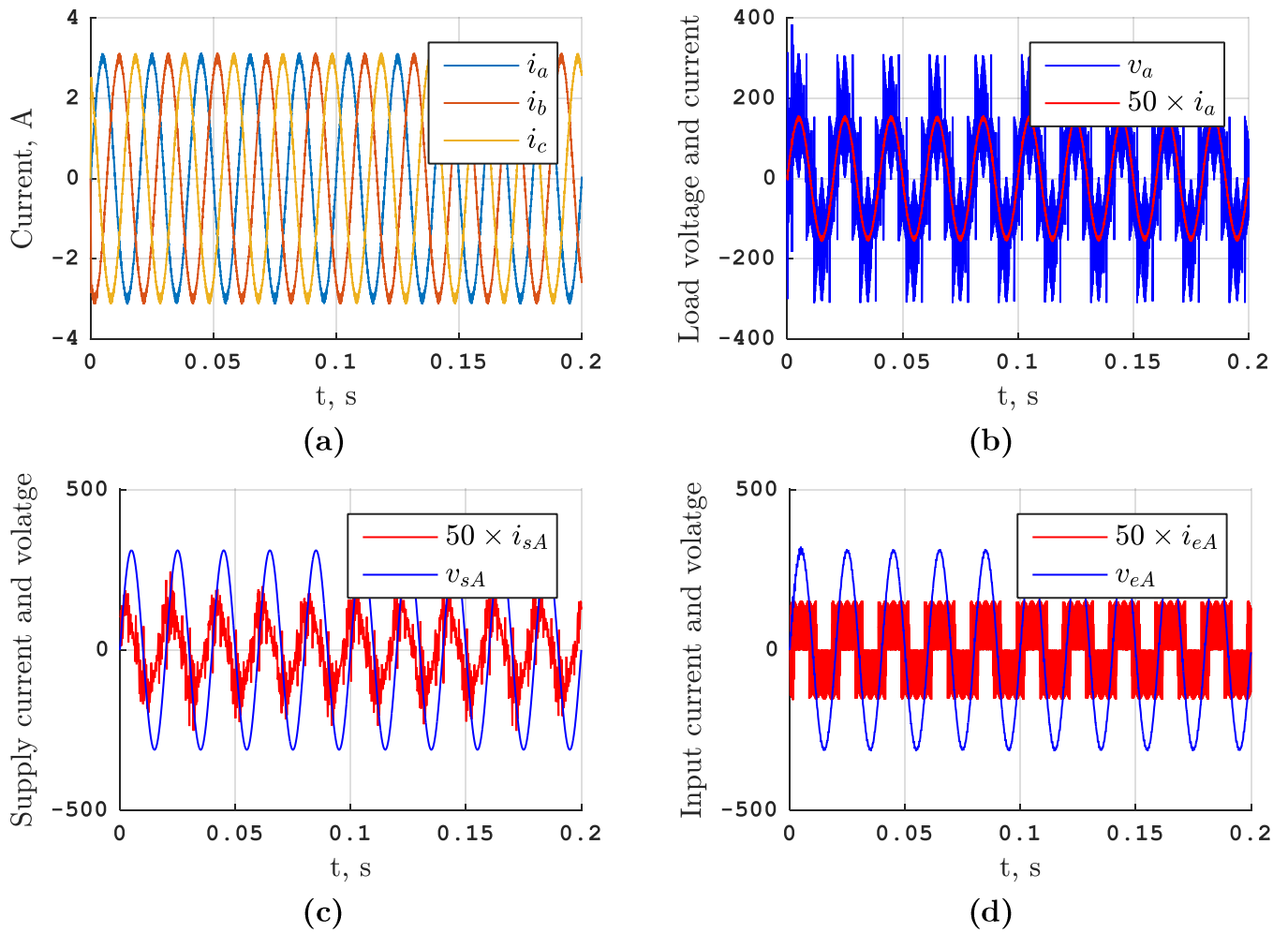

(a)

(b)

(c)

Figure IV.9: Simulation results of MPCC of an IMC-fed RL-load: Reference and output current of phase A and their zoom with a sampling frequency of: **(a)** 20 kHz, **(b)** 50 kHz, **(c)** 100 kHz

(a)

(b)

(c)

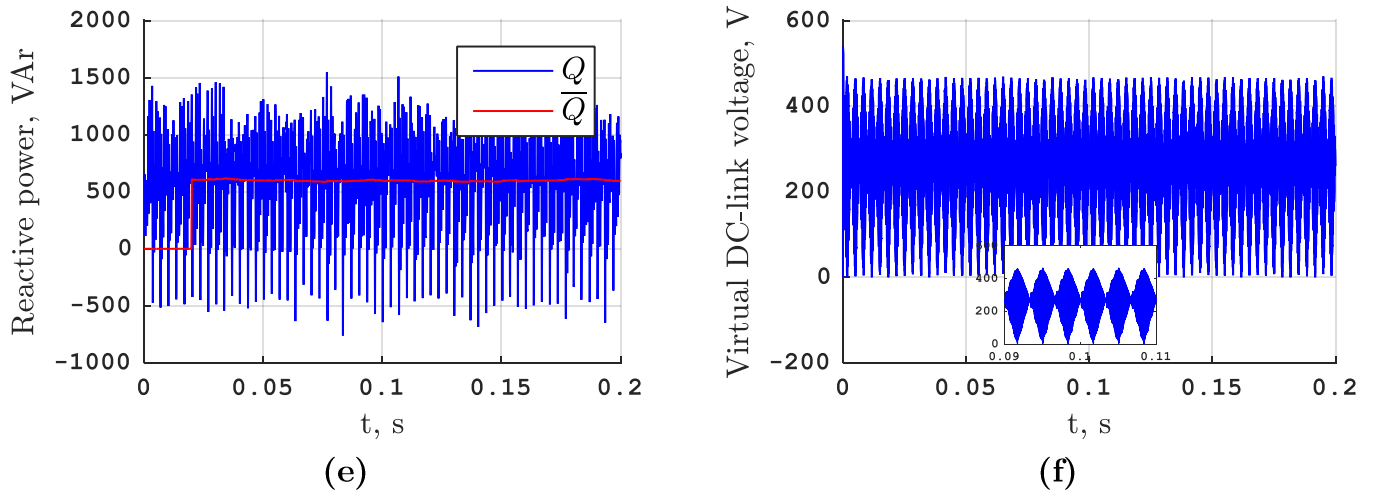(d)

Figure IV.10: Simulation results of MPCC of an IMC-fed RL-load without input reactive power minimization with a sampling frequency of 50 kHz: steady-state analysis of: **(a)** load currents, **(b)** load voltage and current, **(c)** supply current and voltage, **(d)** input current and voltage of DMC, **(e)** input reactive power and its moving average value, **(f)** virtual DC-link voltage

(e)

(f)
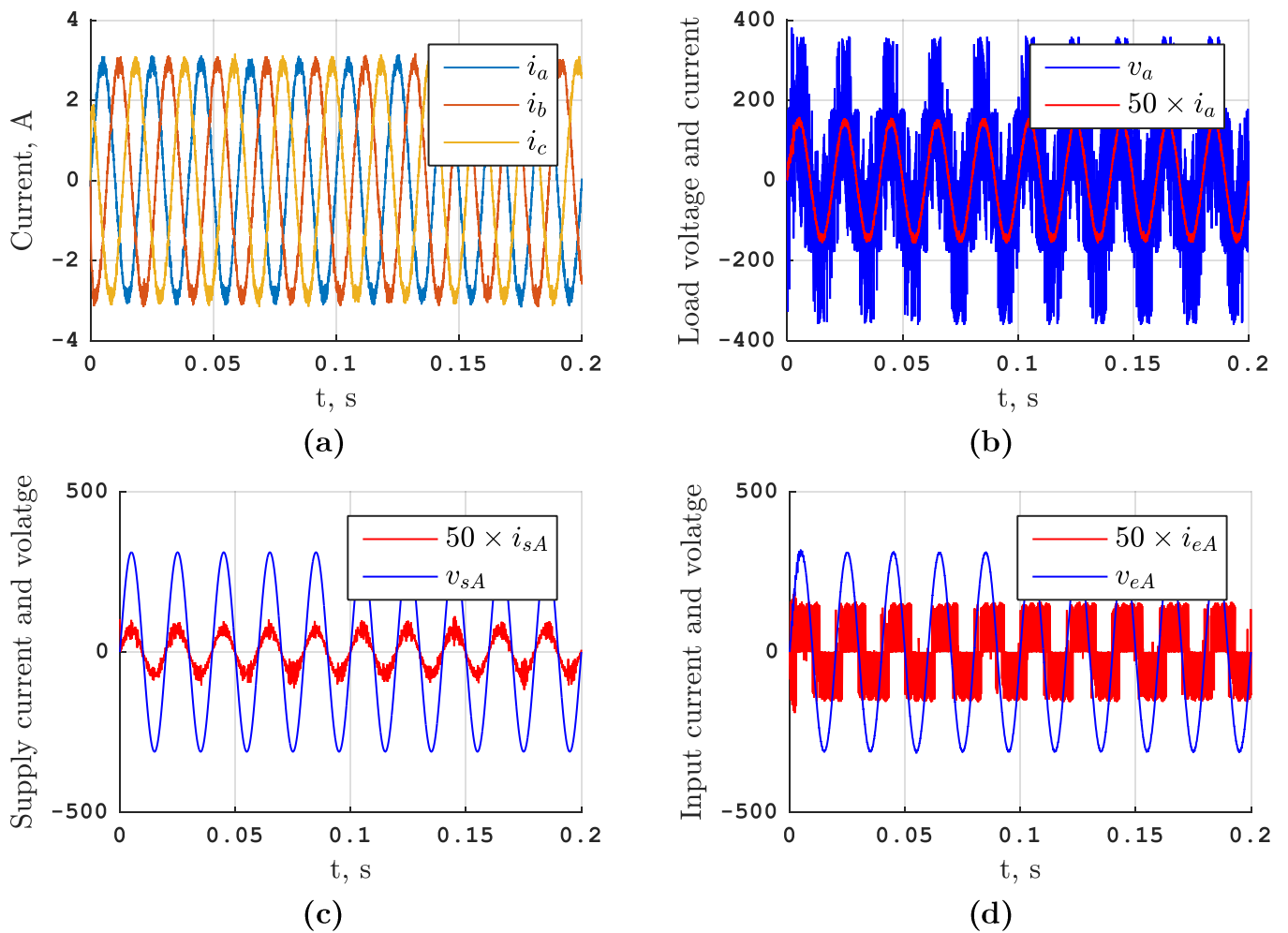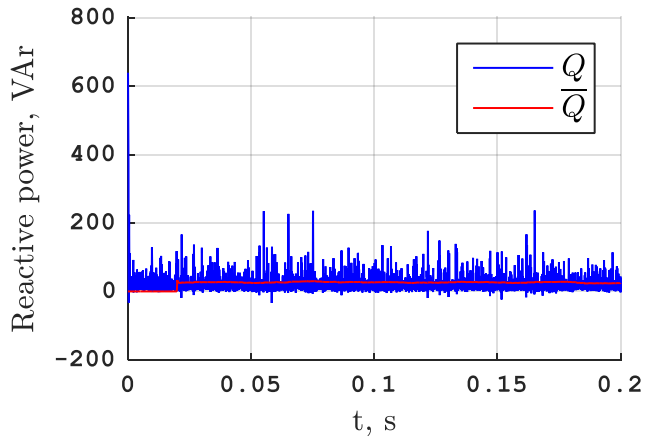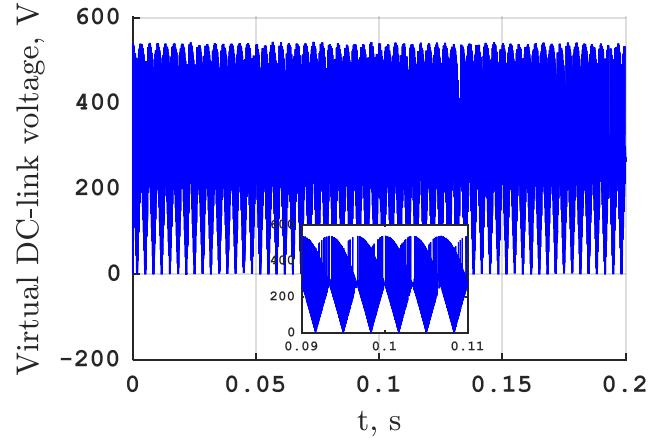
Figure IV.11: Simulation results of MPCC of an IMC-fed RL-load with input reactive power minimization with a sampling frequency of 50 kHz: steady-state analysis of: **(a)** load currents, **(b)** load voltage and current, **(c)** supply current and voltage, **(d)** input current and voltage of DMC, **(e)** input reactive power and its moving average value, **(f)** virtual DC-link voltage

Fundamental (50Hz) = 2.7262, THD=14.4777%

Fundamental (50Hz) = 137.677, THD=114.4063%

(a)

Fundamental (50Hz) = 2.9309, THD=4.1873%

Fundamental (50Hz) = 147.9841, THD=101.5714%

(b)

Fundamental (50Hz) = 2.9766, THD=1.8223%

Fundamental (50Hz) = 150.2878, THD=98.74%

(c)
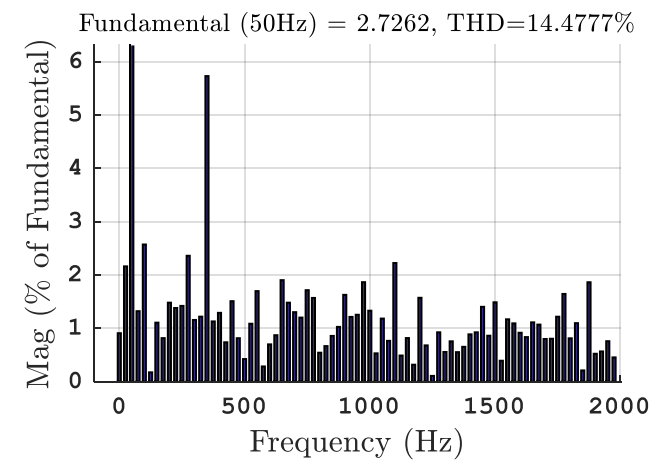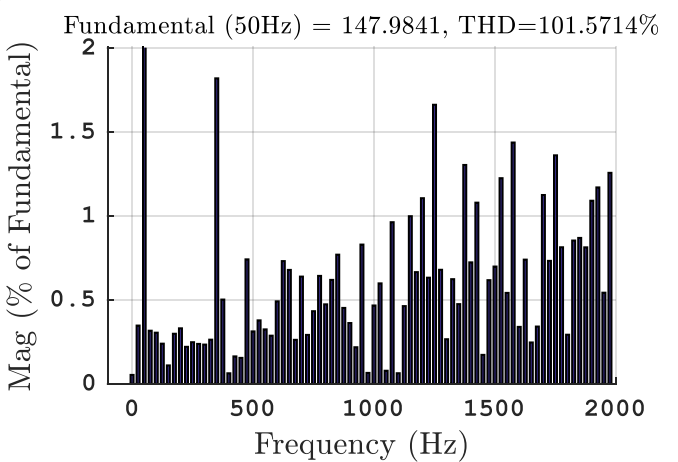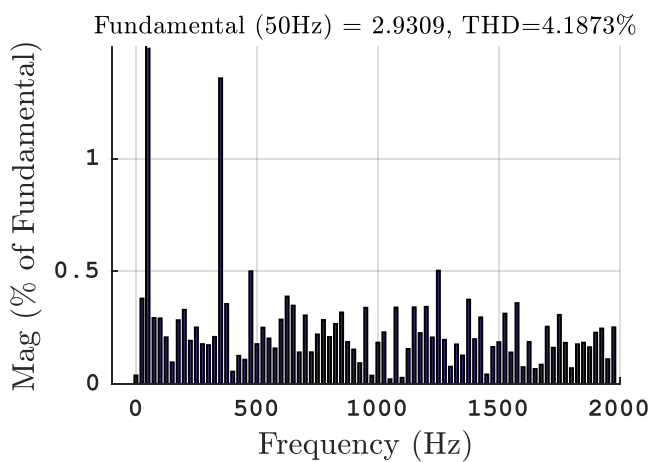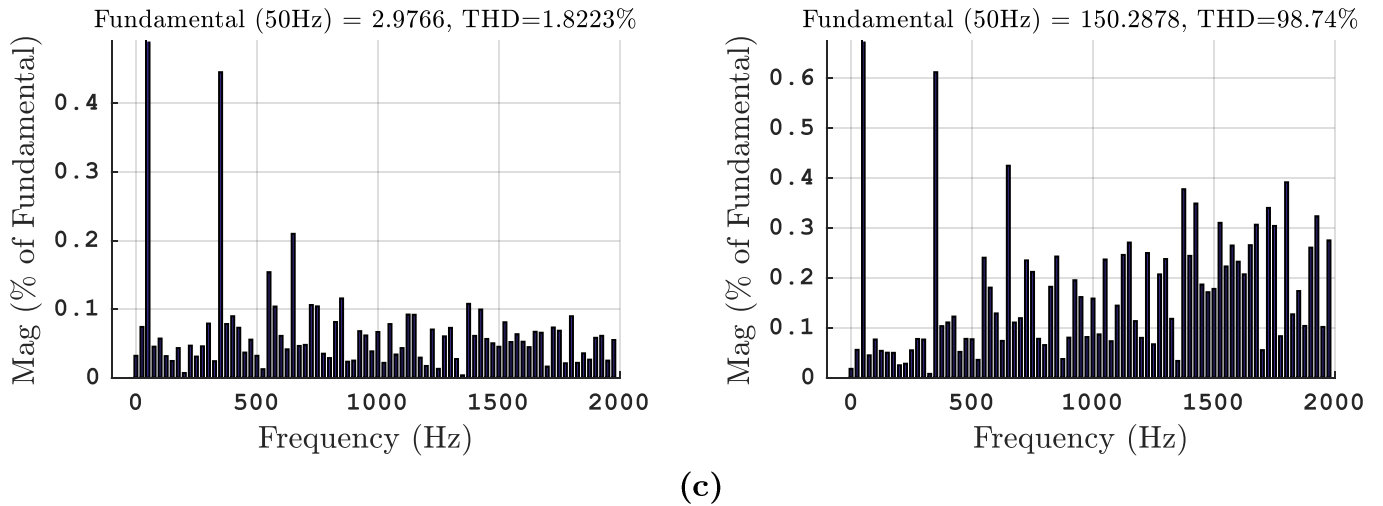
Figure IV.12: Simulation results of MPCC of an IMC-fed RL-load with input reactive power minimization: Output current and output voltage spectra expressed as percentages of fundamental magnitude with a sampling frequency of: **(a)** 20 kHz, **(b)** 50 kHz, **(a)** 100 kHz

Fundamental (50Hz) = 1.2886, THD=93.2305%
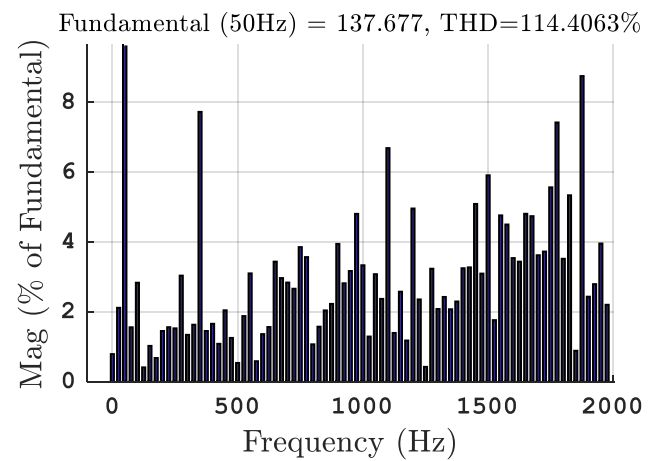
(a)

Fundamental (50Hz) = 1.3864, THD=19.6855%

(b)

(c)
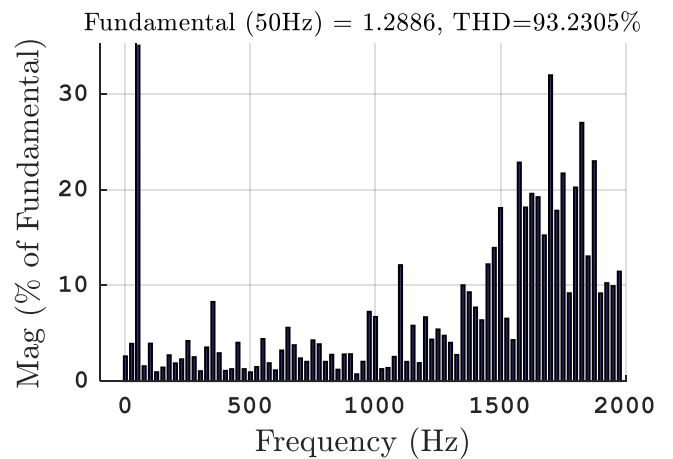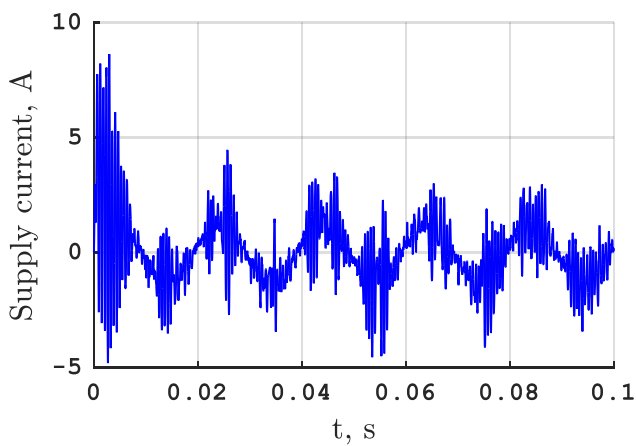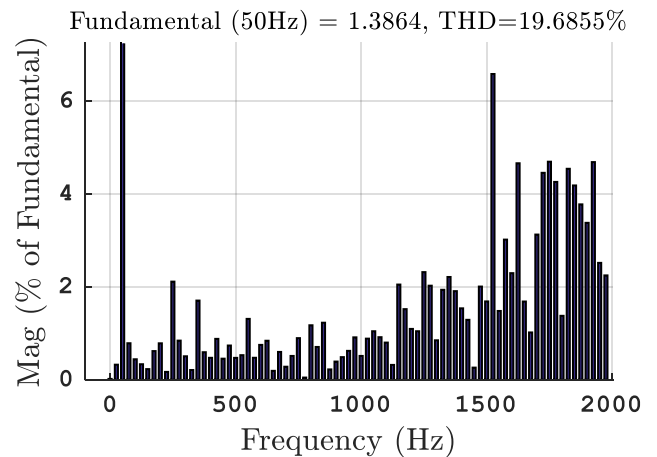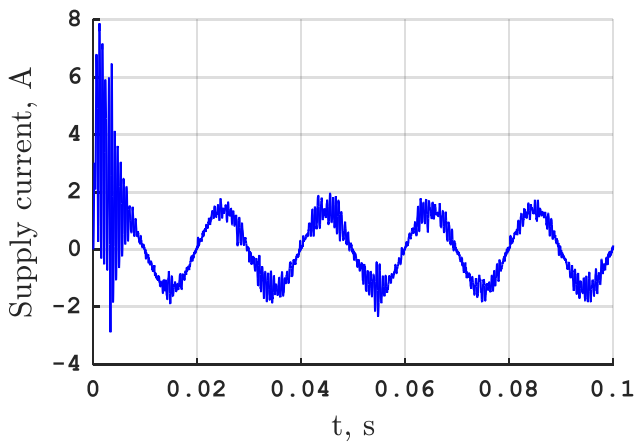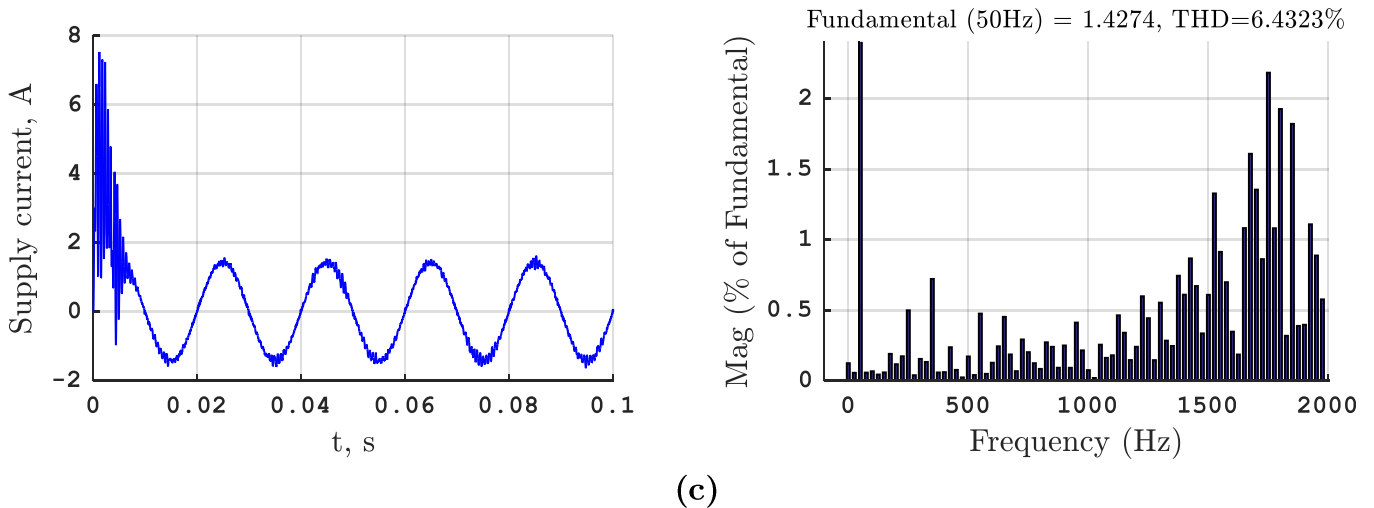
Figure IV.13: Simulation results of MPCC of an IMC-fed RL-load with reactive power minimization: Supply current and its spectra expressed as percentages of fundamental magnitude with a sampling frequency of: (a) 20 kHz, (b) 50 kHz, (a) 100 kHz

Figures from Figure IV.4 to Figure IV.8 present the simulation results of MPCC of a DMC-fed RL-load and from Figure IV.9 to Figure IV.13 present the simulation results of the same control strategy of the same load that is fed by an IMC with the same simulation parameters.

Figure IV.4 and Figure IV.9 show that the output current tracks its reference in magnitude and frequency within a short response time using both topologies. The output current oscillates around its reference forming a ripple around the reference. These oscillations were reduced when high sampling frequencies are applied.

It can be observed that the oscillations of the output current are more important with the indirect topology. However, the direct topology when the reference is zero, the output current oscillates around it. Whereas with the indirect topology, the output current is precisely zero when the reference is zero.

Figure IV.5 and Figure IV.10 present the behaviour of the system with the control of the input reactive power of both converters. A phase shift between the supply voltage and current plus an almost chaotic behaviour of the supply current and the input reactive power.

The noticeable difference in the supply current and in the input reactive power at transient state is due the different simulation components. In the DMC topology, the models (II.6), (IV.4) and (IV.6) have been used. Whereas in the IMC topology, components from the *SimPowerSystems* library in Simulink, which are more reliable because they take into account phenomena that have been neglected in this thesis such

as the magnetic saturation of the power switches and diode forward voltage drop, which gives more reliable results. In the reactive power figure, the mean value is nil at first because it is calculated by a moving average.

Figure IV.6 and Figure IV.11 present steady state analysis of the simulation results of the MPCC of both topologies with a sampling frequency 50 kHz with the control of the input reactive power. It can be observed the good quality of the output variables is maintained, while the waveform of the supply current is greatly improved, it is in phase with the grid voltage and has much less distortion. A shift in the input current of the converters is also observed and much lower values of the reactive power in the second case (input reactive power minimization). An improvement in the waveform of the virtual DC-link voltage of the IMC is observed as well. The virtual DC-link voltage varies with six-pulse per period of the supply in accordance to the six sextants of the rectifier.

Figure IV.7 and Figure IV.12 present the output current and voltage spectra expressed as percentages of the fundamental magnitude. As expected, the THD of both variables decreases as the sampling frequency increases.

Figure IV.8 and Figure IV.13 present the supply current and its spectra expressed as percentages of the fundamental magnitude. The supply current is rich in harmonics and its THD is greater than that of the output current.

IV.8. Comparison between the three converters

The following table presents a comparison between the simulation results of the MPCC of a RL-load that is fed by the three converters studied in this thesis with the same simulation parameters previously used.

Table IV.3: Comparison between the simulation results of the MPCC using the three converters

Feature	2LVSI	DMC	IMC
THD of output current	1.32%	0.95%	01.09%
THD of output voltage	105.53%	63.56%	78.06%
THD of supply current	-	69.95%	49.01%
Complexity of the algorithm	Low	Medium	High
Input reactive power controllability	-	Yes	Yes (best)
Output voltage waveform	Good	Good	Good

The MPCC was simulated without the control of the input reactive power. The indirect topology of the MC presents the best performance in the supply current quality and in the control of the reactive power.

The direct topology generates better quality of the output variables, whereas the indirect topology generates better quality of the input variables.

The IMC presents the highest complexity of the control algorithm as in this case, 48 possible switching states are taken into account. Followed by the DMC with 27 possible switching states and the 2LVSI with 7 switching states.

The number of switching states of both topologies of the MC can be further reduced. In the DMC, the rotating-vector states (which are six) are not usually used, since their angular positions always change together with the input voltage making it difficult to create a repetitive pattern [47], reducing the count to 21 switching states. And in the IMC, 21 switching states suffice, 3 from the rectifier stage and 7 from the inverter stage, to ensure a positive voltage in the fictitious DC-link that guarantees a proper firing of power switches. However, reducing the number of switching states may lead to slightly inferior quality of the results. especially in the input current and the input reactive power.

IV.9. Conclusion

This chapter presents a predictive control scheme for two topologies of the matrix converter, namely the direct topology and the indirect topology, that effectively controls the output currents and the reactive input power. The strategy presented allows the input power factor to be controlled by means of a simple and straightforward technique, controlling the phase of the input current in such a way that the converter can work with unity or inductive power factor, according to the requirements of the application.

In order to ensure minimum instantaneous reactive power, dedicated cost function has been designed by adding a weighted error signal of the reactive power to the previous cost function of the MPCC in Chapter II.

The mean value of the fictitious DC-link voltage increases when operating with a unity input power factor.

This method can be easily implemented by taking advantage of the present technologies available in digital signal processors. The high sampling frequency required should not be a problem nowadays and even less in years to come thanks to technological advancement.

Chapter V:

Model Predictive Torque Control of a Matrix Converter-Fed Induction Machine

Chapter V : Model Predictive Torque Control of Matrix Converter-fed Induction Machine

V.1. Introduction

Over recent decades, control of electrical drives has been widely studied. Linear methods like PI controllers using PWM and non-linear methods such as hysteresis control have been fully documented in the literature and dominate high-performance industrial applications [6]. The most widely used linear strategy in high performance electrical drives is field oriented control (FOC) [48],[4], in which a decoupled torque and flux control is performed by considering an appropriate coordinate frame. A non-linear hysteresis-based strategy such as direct torque control (DTC) appears to be a solution for high performance applications [49].

Due to the rapid development of microprocessors, the MPC was considered to improve the dynamic behaviour, thanks to its non-cascaded structure. Furthermore, the increasing number of drive applications, in which fast dynamic response, low parameter sensitivity, and algorithm simplicity are required, has motivated the development of new control strategies capable of improving the performance. The first ideas on MPC applied to power converters and drives originated in the 1980s [6].

In this chapter, a MPTC has been applied to an induction machine fed by two topologies of the MC, namely the DMC and the IMC.

The parameter sensitivity of this control strategy is analysed and simulated by making an unforeseen (to the controller) increase in the value of the stator resistance.

The control scheme is simulated using both topologies in the MATLAB/Simulink environment.

V.2. Simulation results and analysis

The models used in these simulations have been presented in the two previous chapters. The working principle and the implementation have been explained in detail.

Two cases are analysed. First, the simulation of the control scheme without the control of the input reactive power. While in the second case, the control of the reactive power is taken into account in order to operate with a unity power factor.

In order to control the input reactive power, its weighted error signal must be added to the cost function, thus (III.21) becomes:

$$J = \lambda_T \left| T_{em}[k+1] - T_{ref} \right| + \lambda_\varphi \left| |\varphi_s[k+1]| - \varphi_{s\,ref} \right| + \lambda_Q \left| Q[k+1] - Q_{ref} \right| \quad \text{(V.1)}$$
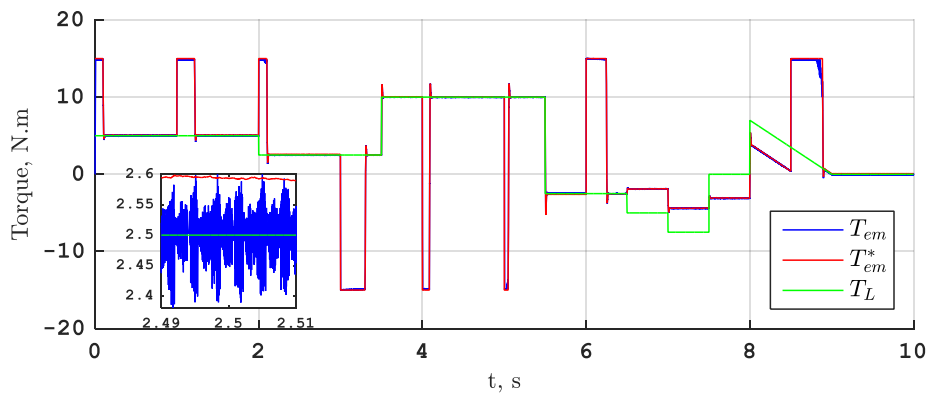
Where:

- $Q[k+1]$: the predicted value of the reactive power
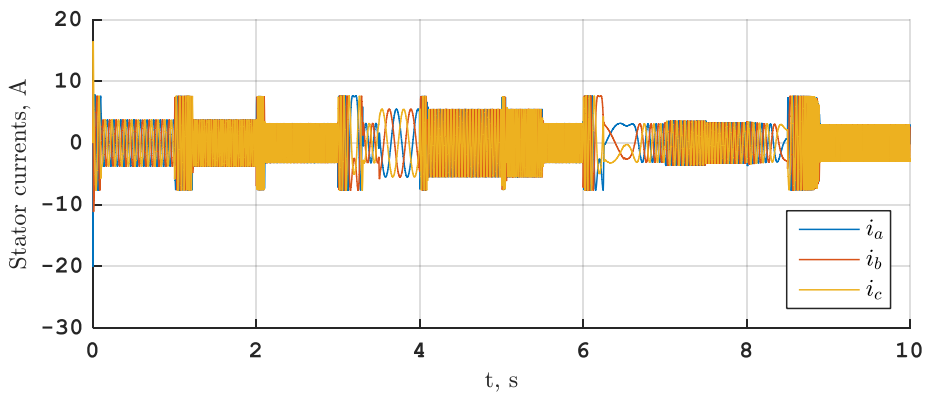- Q_{ref} : the reference value of the reactive power

The MPTC was simulated with different speed set points and load torque to verify its performances in both transient and steady states. The filter, machine and simulation parameters are given in the appendices.
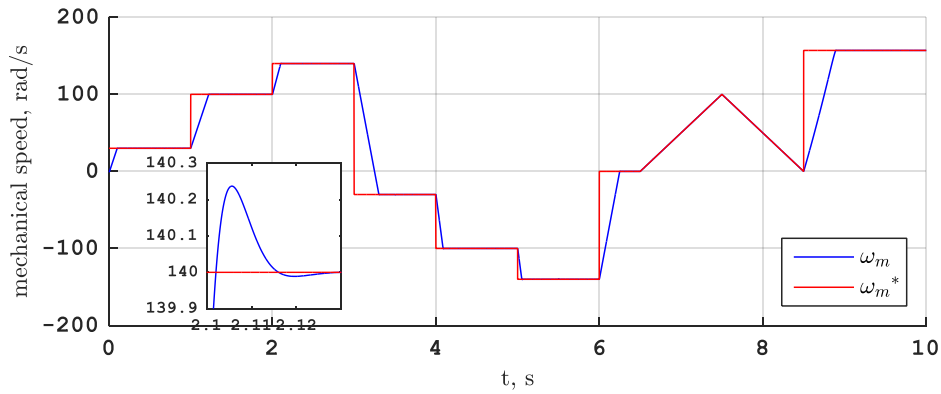
(a)

(b)

(c)

(d)

Figure V.1: Simulation results of the MPTC of a DMC-fed induction machine without the control of input reactive power: **(a)** rotor speed and its reference, **(b)** electromagnetic, load and reference torque, **(c)** stator currents, **(d)** stator flux
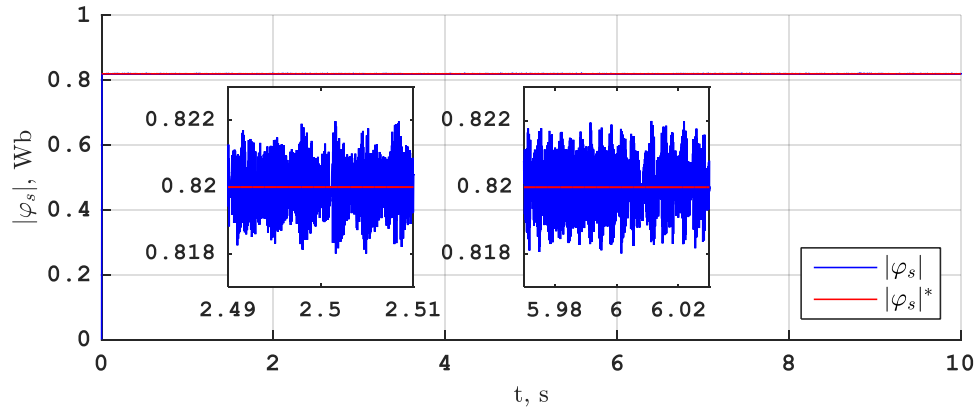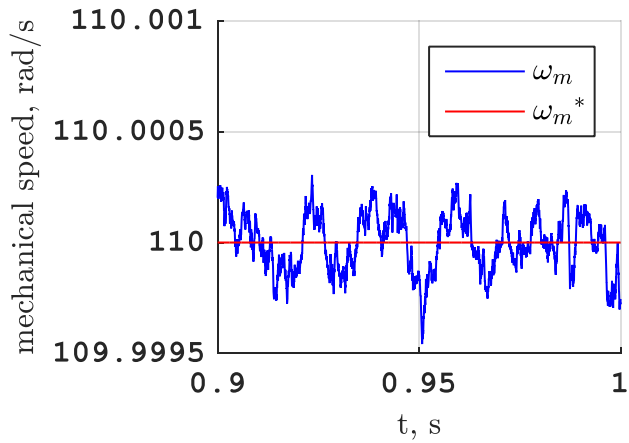

(a)

(a)

(c)

(d)

(e)

(f)

(g)

(h)

Figure V.2: Simulation results of the MPTC of a DMC-fed induction machine without the control of input reactive power: steady state of **(a)** mechanical speed, **(b)** electromagnetic torque, **(c)** 50×supply current and voltage, **(d)** 50×input current and voltage, **(e)** stator voltage, **(f)** stator currents, **(g)** stator flux, **(h)** input reactive power

(a)

(b)
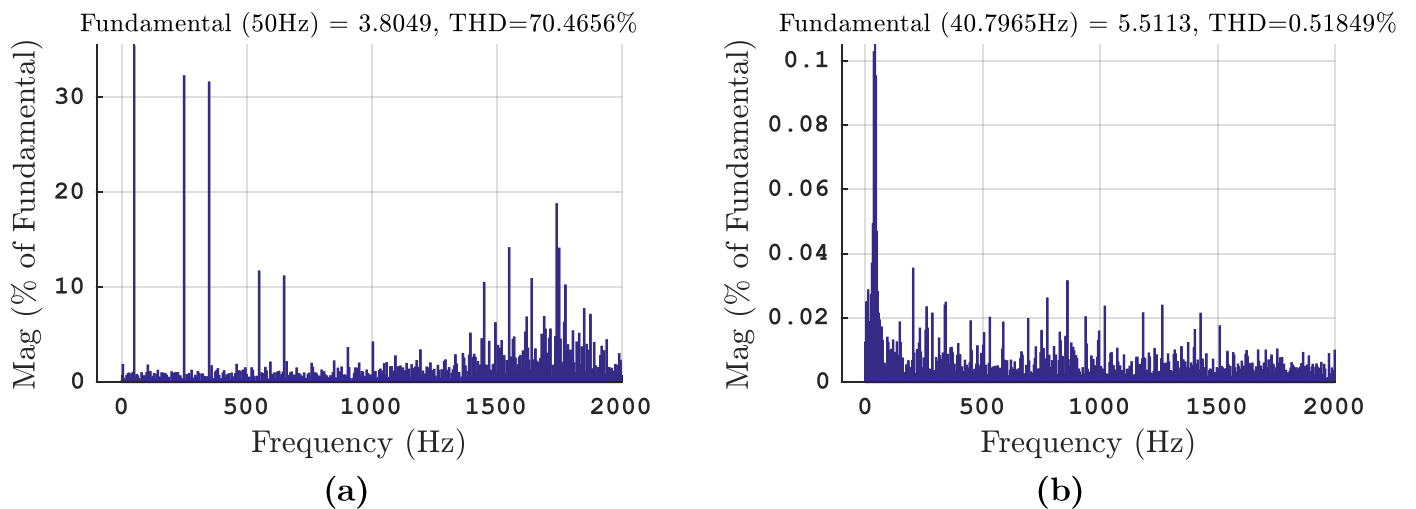
Figure V.3: Harmonic spectrum of **(a)** supply current, **(b)** stator current

(a)

(a)

(c)

(d)

(e)

(f)

(g)

(h)
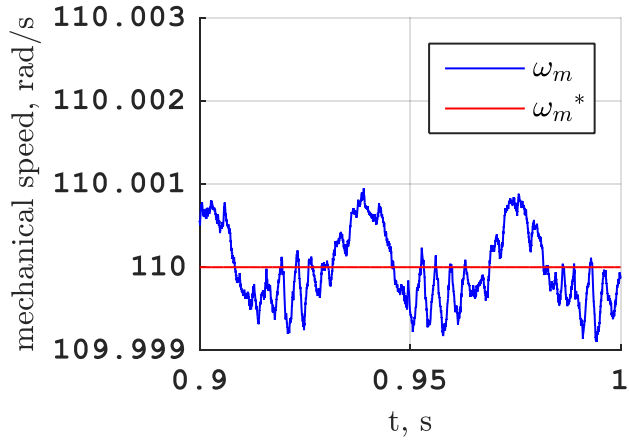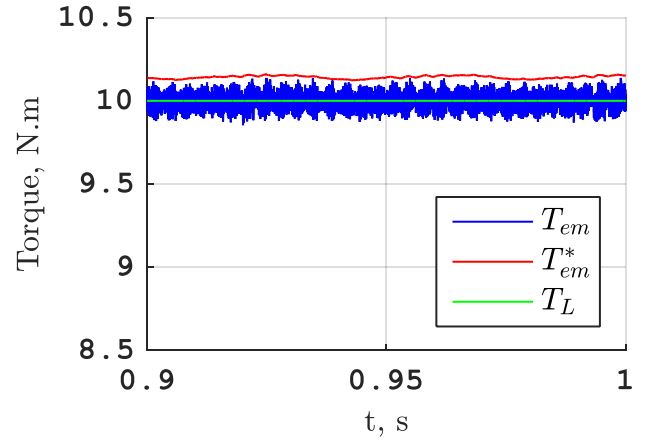
Figure V.4: Simulation results of the MPTC of a DMC-fed induction machine with the control of input reactive power: steady state of **(a)** mechanical speed, **(b)** electromagnetic torque, **(c)** 50×supply current and voltage, **(d)** 50×input current and voltage, **(e)** stator voltage, **(f)** stator currents, **(g)** stator flux vector, **(h)** input reactive power

(a)

(b)

Figure V.5: Simulation results of the MPTC of a DMC-fed induction machine with the control of input reactive power: harmonic spectrum of (a) supply current, (b) stator current
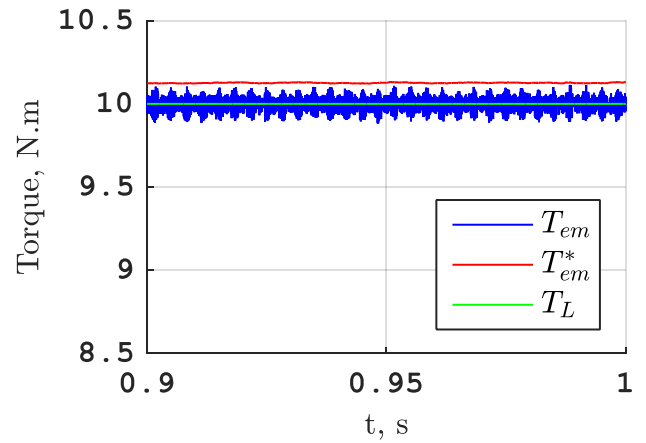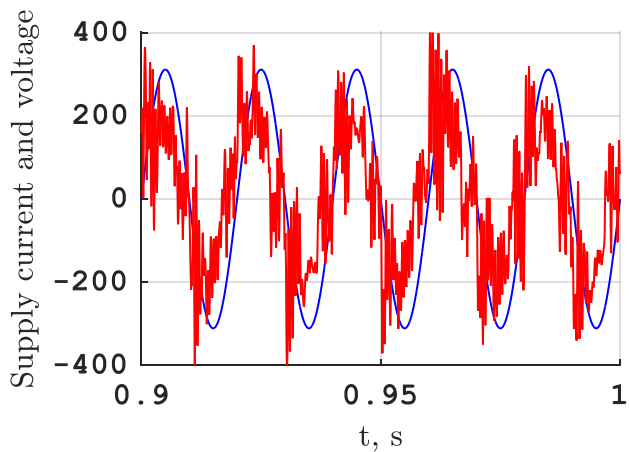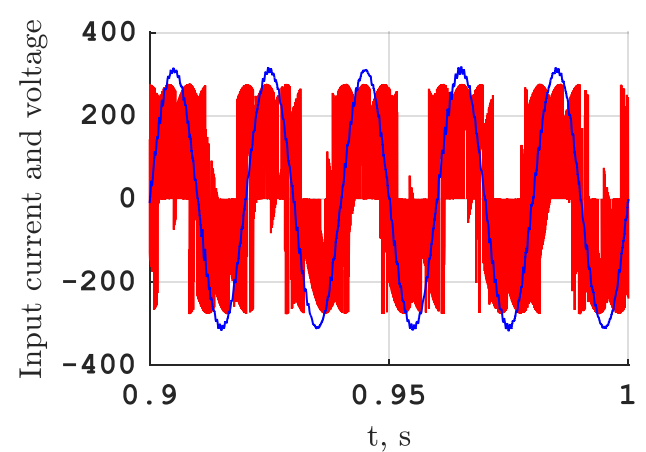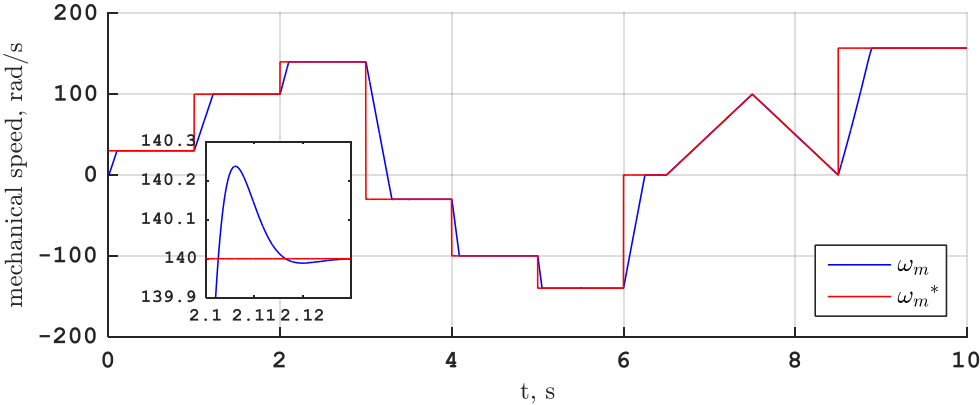
(a)
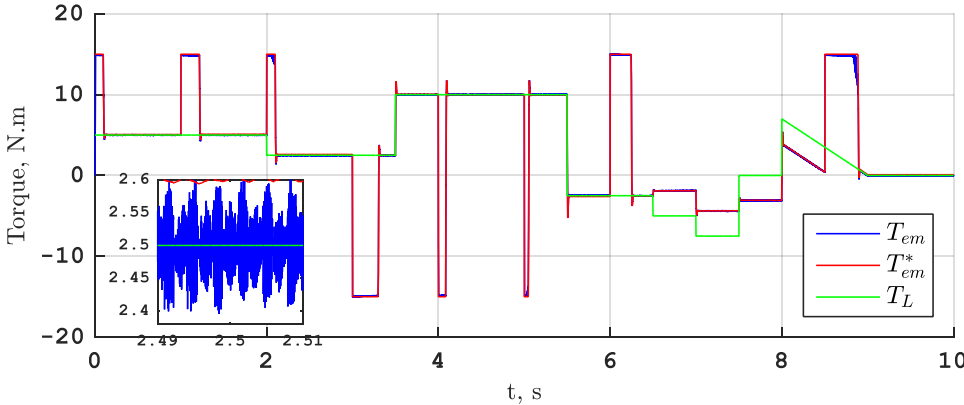
(b)
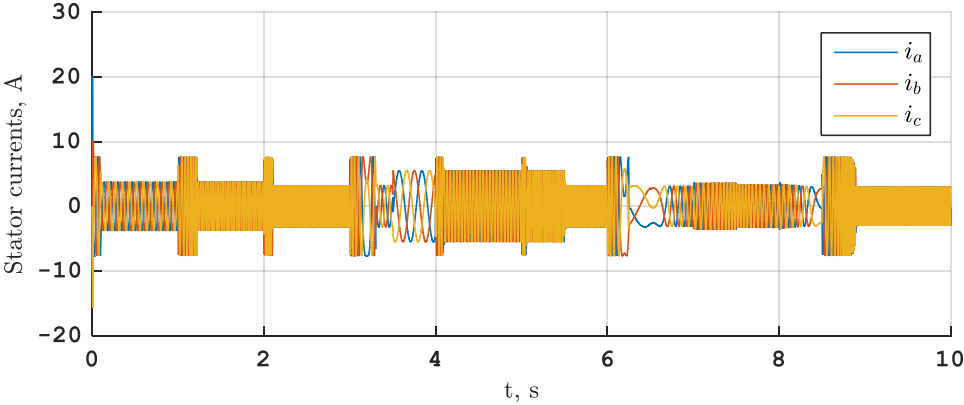
(c)
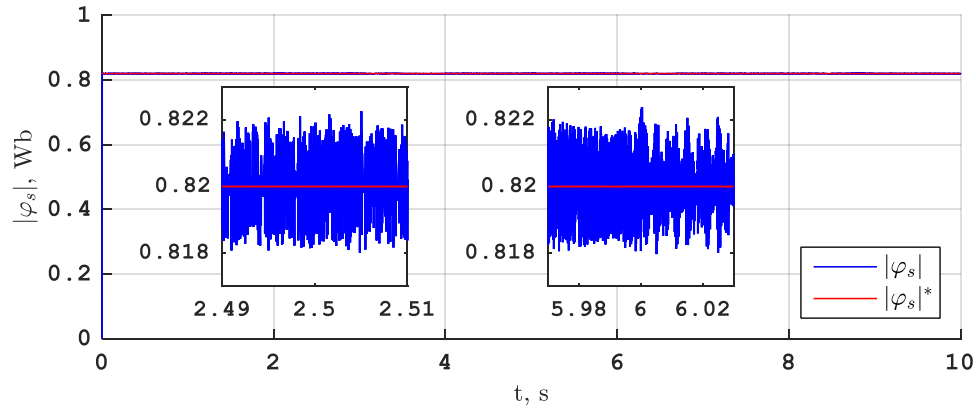
(d)

Figure V.6: Simulation results of the MPTC of an IMC-fed induction machine without the control of input reactive power: **(a)** rotor speed and its reference, **(b)** electromagnetic, load and reference torque, **(c)** stator currents, **(d)** stator flux
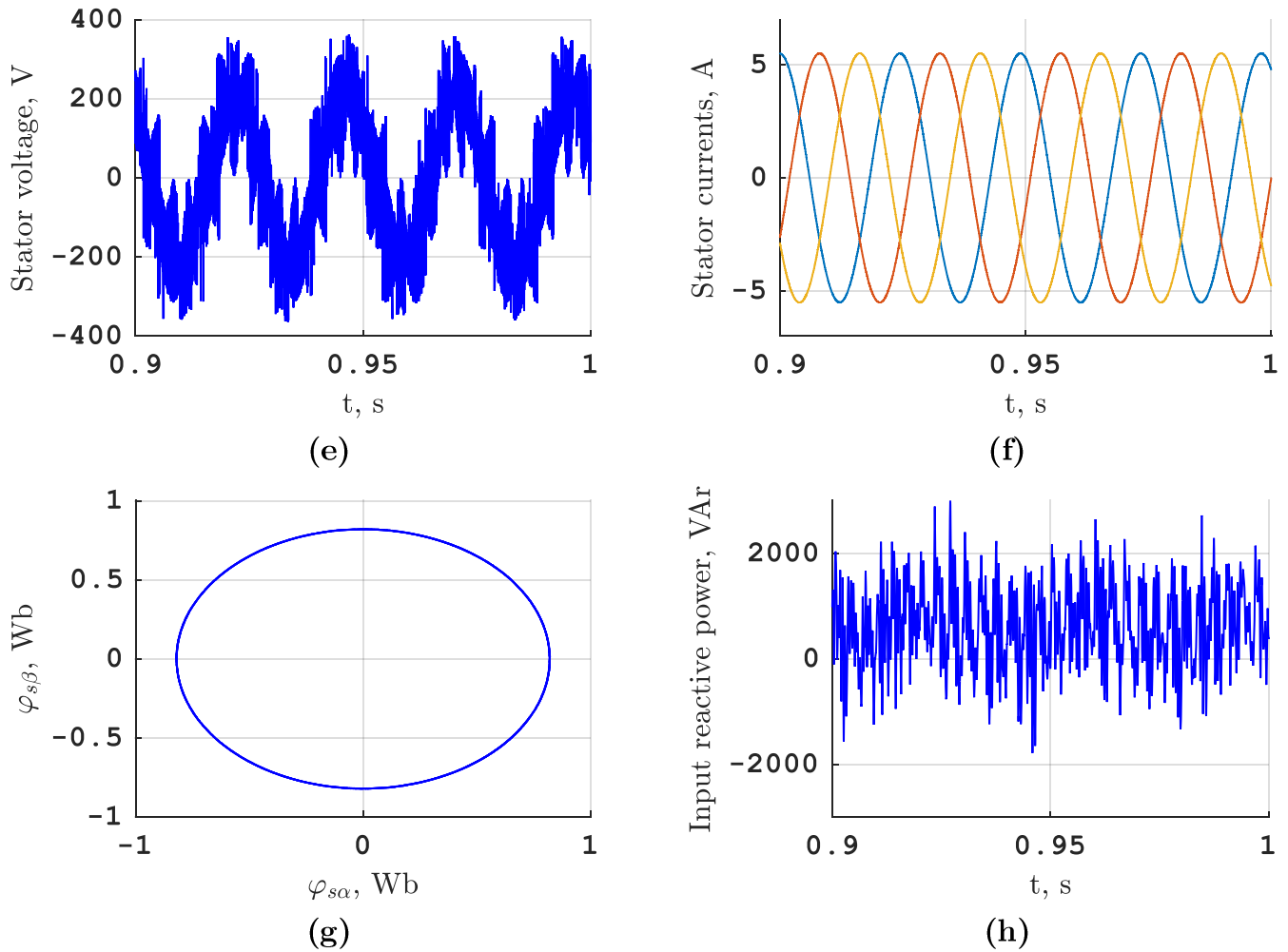

(a)

(a)

(c)

(d)

(e)

(f)

(g)

(h)
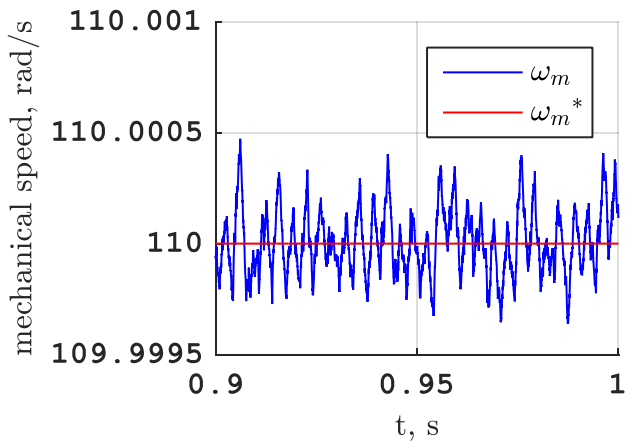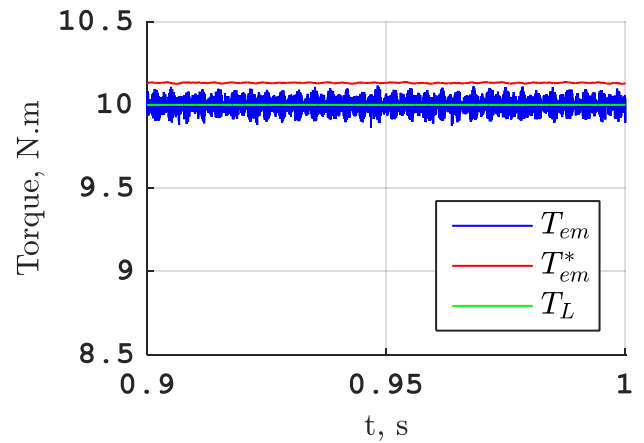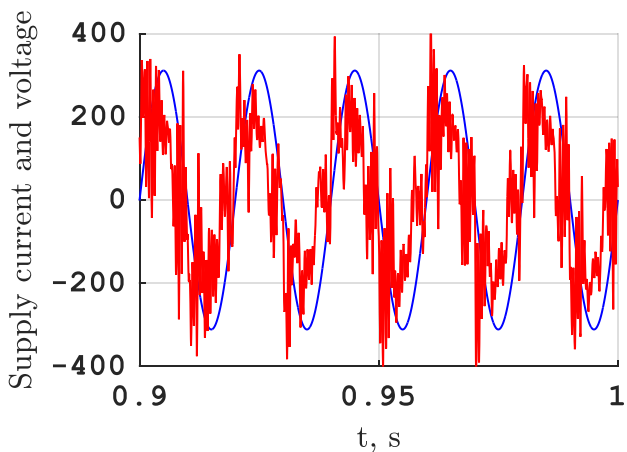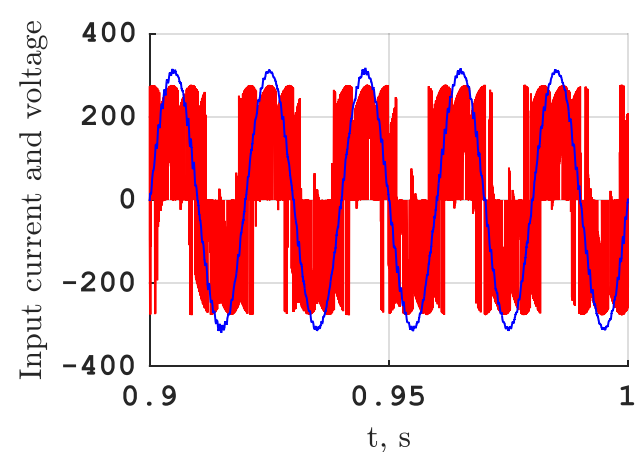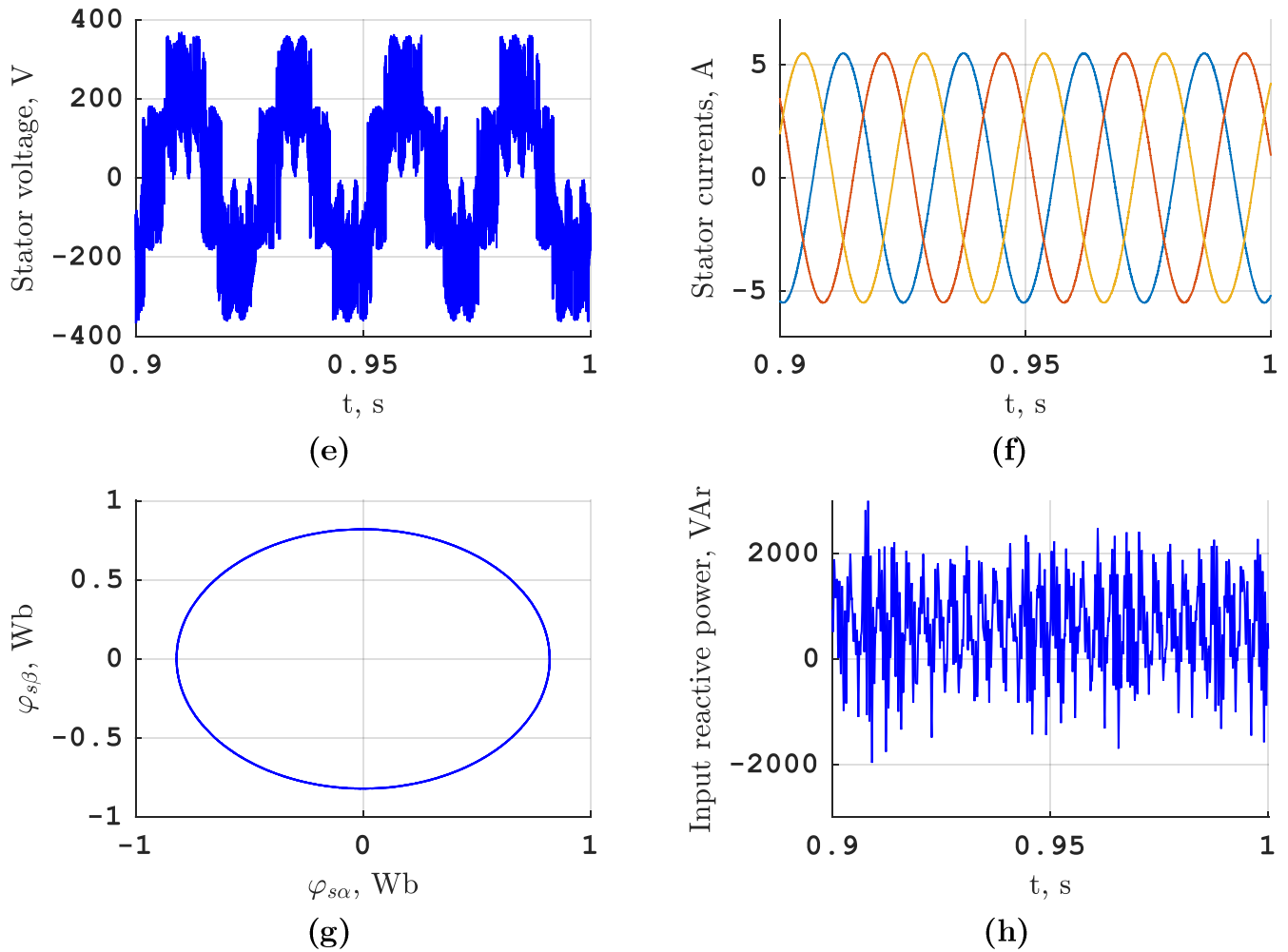
Figure V.7: Simulation results of the MPTC of an IMC-fed IM without the control of input reactive power: steady state of **(a)** mechanical speed, **(b)** electromagnetic torque, **(c)** 50×supply current and voltage, **(d)** 50×input current and voltage, **(e)** stator voltage, **(f)** stator currents, **(g)** stator flux vector, **(h)** input reactive power

Fundamental (50Hz) = 3.8049, THD=70.4656%

Fundamental (40.7965Hz) = 5.5113, THD=0.51849%

(a)

(b)
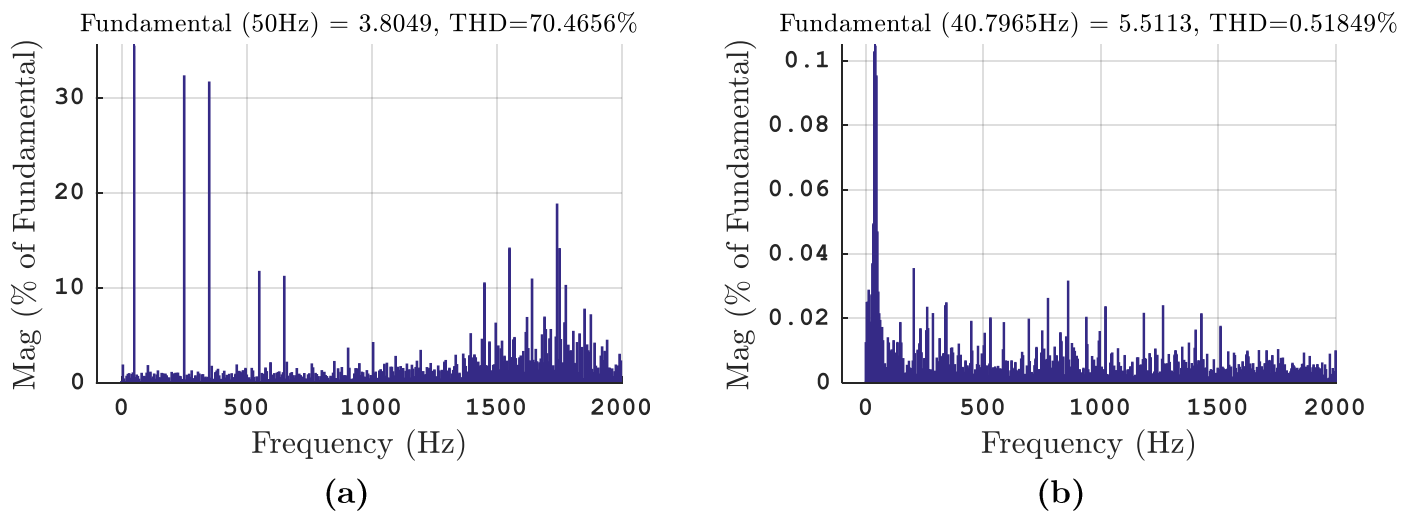
Figure V.8: Harmonic spectrum of: **(a)** supply current, **(b)** stator current

(a)

(b)

(c)

(d)

(e)

(f)

(g)   (h)
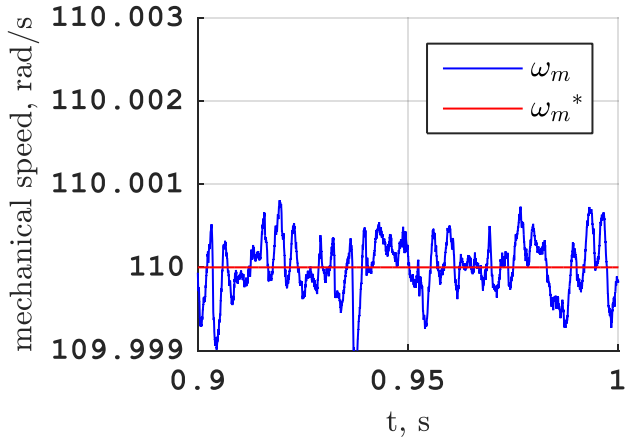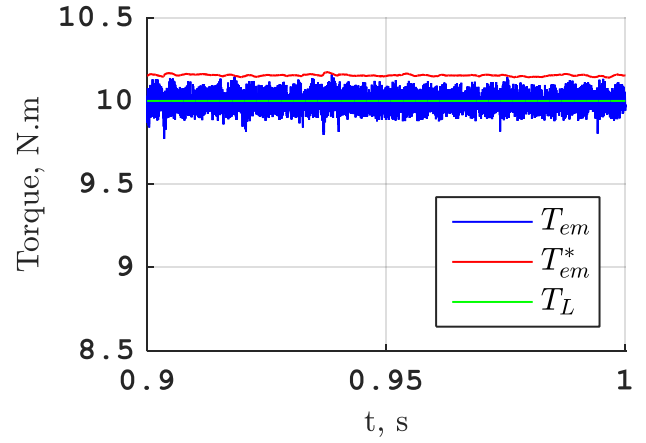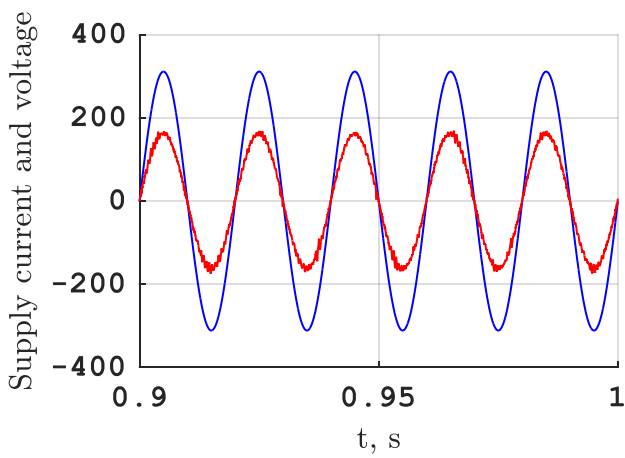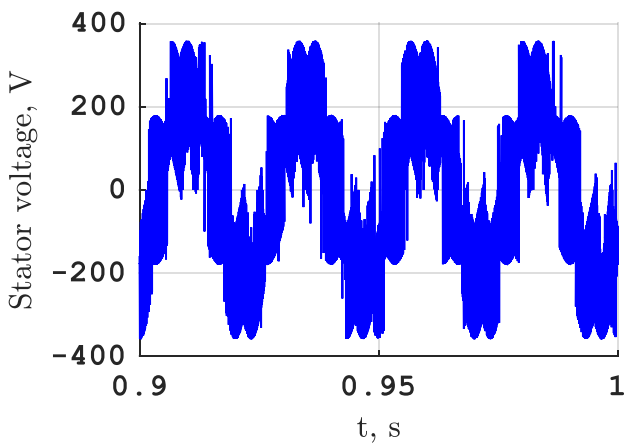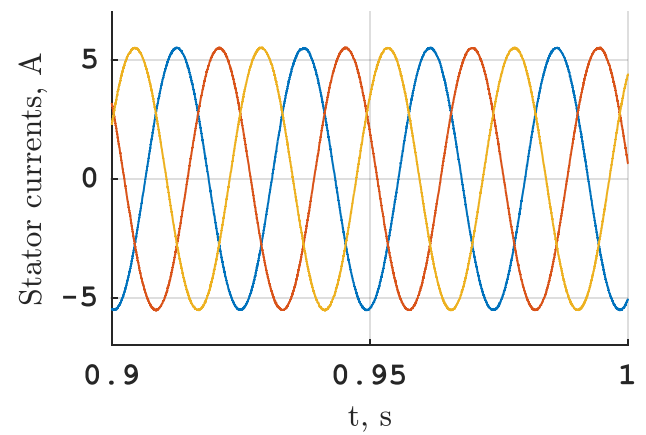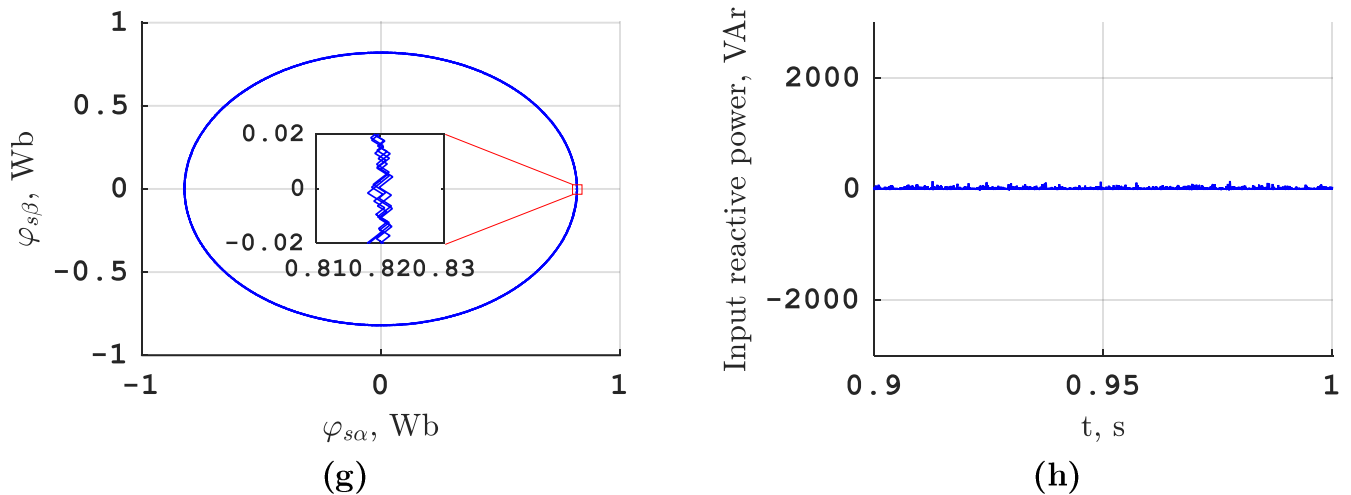
Figure V.9: Simulation results of the MPTC of an IMC-fed induction machine with the control of input reactive power: steady state of **(a)** mechanical speed, **(b)** electromagnetic torque, **(c)** 50×supply current and voltage, **(d)** 50×input current and voltage, **(e)** stator voltage, **(f)** stator currents, **(g)** stator flux, **(h)** input reactive power
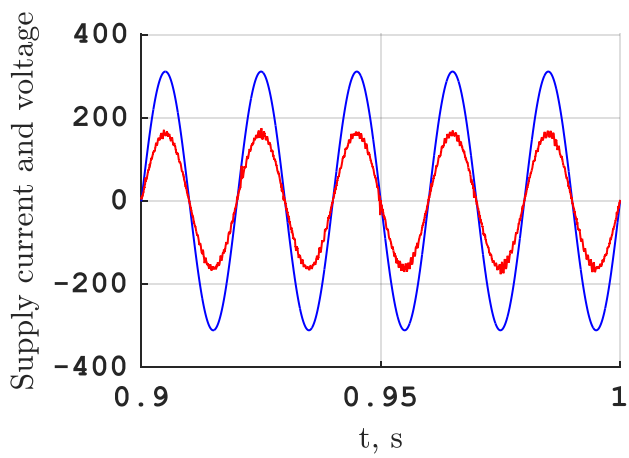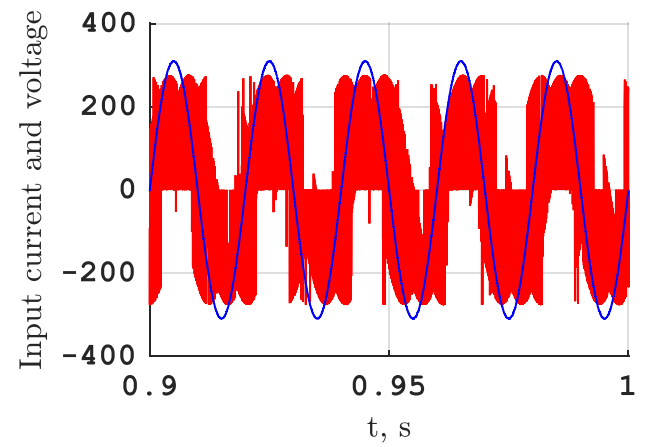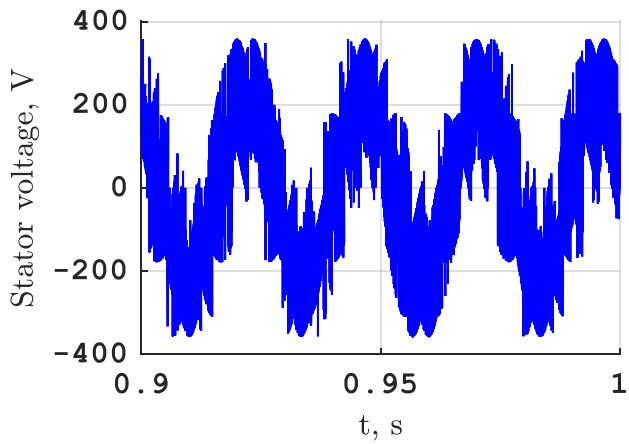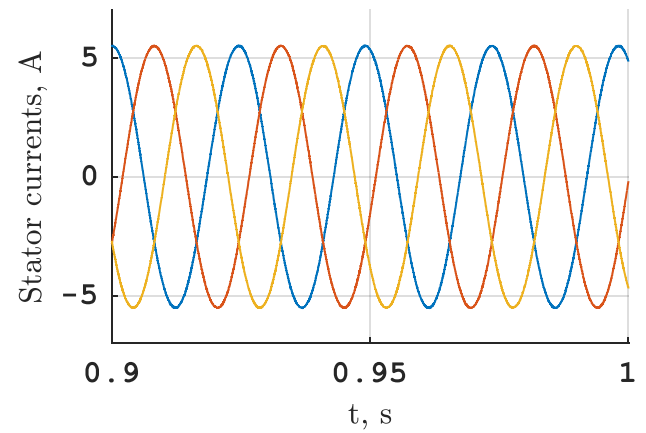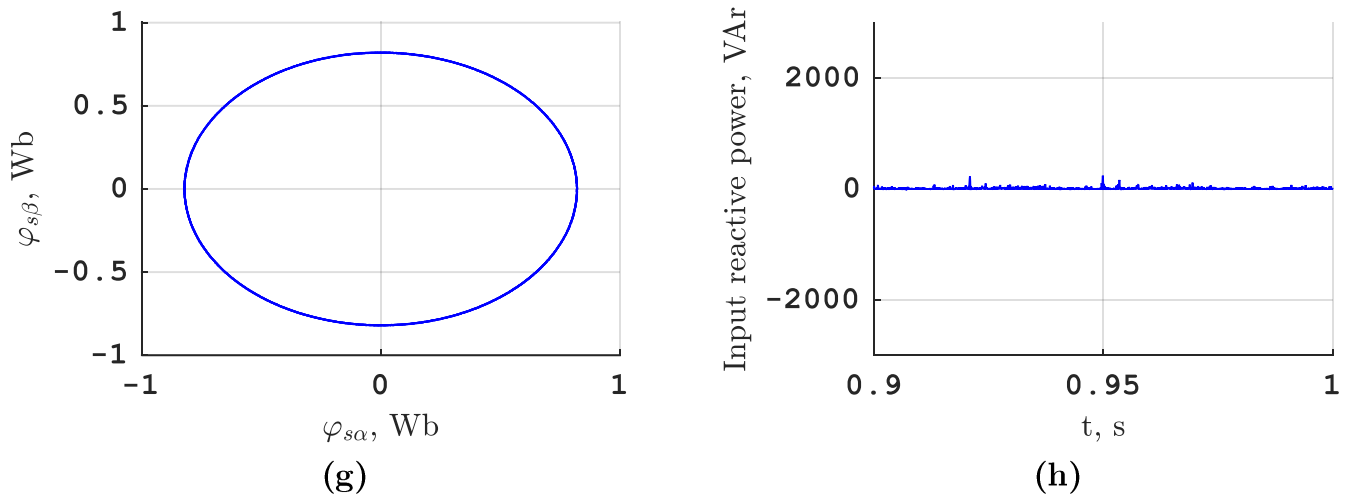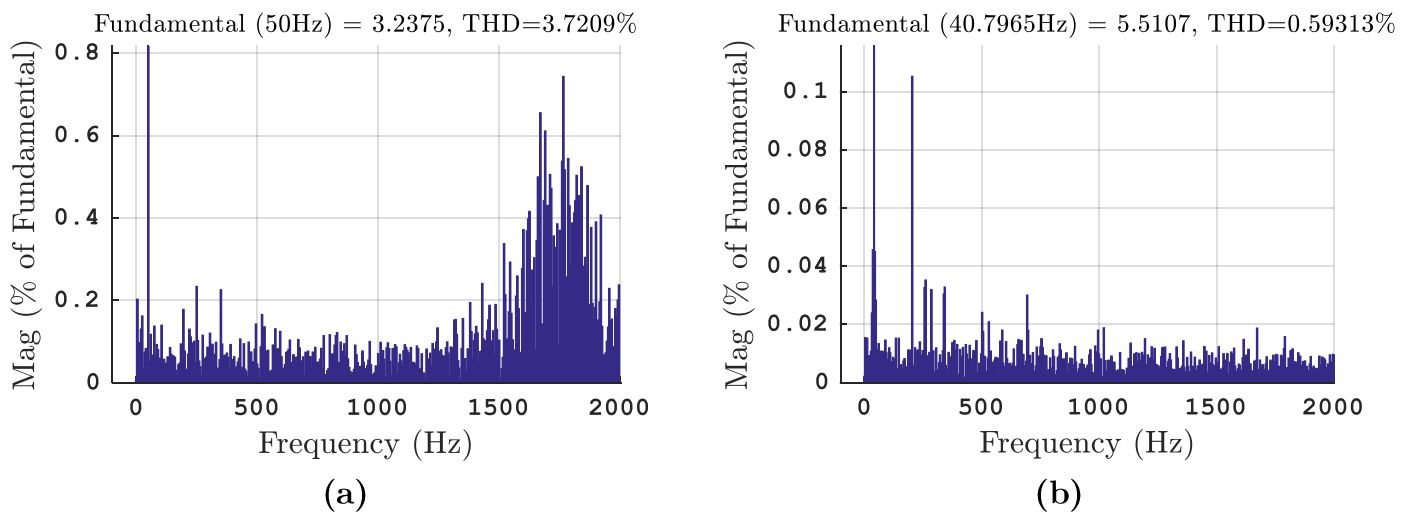

(a)   (b)
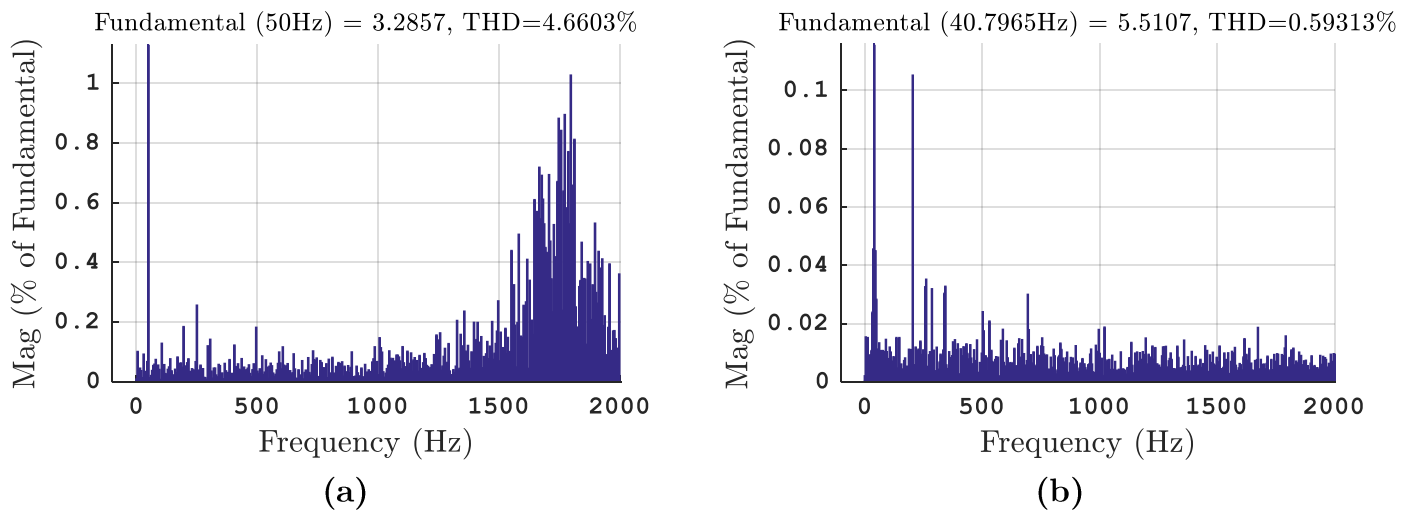
Figure V.10: Simulation results of the MPTC of an IMC-fed induction machine with the control of input reactive power: harmonic spectrum of **(a)** supply current, **(b)** stator current

The figures from Figure V.1 to Figure V.5 present the simulation results of MPTC of a DMC-fed induction machine and the figures from Figure V.6 to Figure V.10 present the simulation results of the same control strategy of the same induction machine using the same simulation parameters using an IMC.

According to Figure V.1 and Figure V.6,

- The speed tracks its reference in spite of the changes in the load torque, which are considered as a disturbance, to which it reacts with slight overshoots;

- At transient state, the electromagnetic torque reference is limited to 15 N.m by the PI controller and at steady state, the electromagnetic torque oscillates around the load torque;
- The magnitude of the stator current depend on the electromagnetic torque and its frequency depends on the mechanical speed;
- Despite the disturbance and the changes in mechanical speed (value and sign), the magnitude of the stator flux remains oscillating around its reference within an error of less than 0.003 Wb using both converters, which shows the performance of this control strategy.

Figure V.2 and Figure V.7 (resp. Figure V.4 and Figure V.9) present the steady state of the simulation results of the MPTC of an MC-fed induction machine without (resp. with) the control of input reactive power. The results show that:

- The mechanical speed and the electromagnetic torque fluctuate around their references with a bigger difference in the second case, and that is because the algorithm penalizes the states that generate high values of the reactive power even if they produce more accurate values of the said variables;
- In the first case, the supply current has a chaotic behavior and is shifted from the supply voltage. Whereas in the second case, the waveform of the supply current is greatly improved while the quality of other variables is maintained;
- The quality of the stator voltage is better in the indirect topology and is less affected by the control of the reactive power;
- The reactive power is minimized in the second case and less spikes are observed when using the indirect topology.

Figure V.3 and Figure V.8 (resp. Figure V.5 and Figure V.10) show the harmonic spectra of the supply and output currents without (resp. with) the control of input reactive power. The results show that in the first case, the supply current is rich in harmonics, as a result it is distorted. With the minimization of the reactive power, the magnitude of the harmonics of the supply current are considerably reduced which results in a better waveform. Some harmonics are observed around the cut-off frequency of the filter in both cases using both converters.

The stator current has a low THD in both cases using both converters, which reflects the good waveform. However, the THD is lower in the first case for the same reason: the electromagnetic torque is better in the first case as mentioned above.

V.3. The effect of the variation of stator resistance

The MPC schemes presented up to now are based on the assumption that the actual system is identical to the model used for prediction, *i.e.*, no model mismatch or unknown disturbances are present. Clearly, this is very unrealistic for practical applications.

The last test is performed to verify the robustness of this MPTC method. The resistance of the stator windings is subject to change during the operation of the machine due to the temperature of the conductors.

The variation of the resistance as a function of the temperature of a conductor can be characterized by the following empirical relation:

$$R = R_{ref}(1 + \alpha(T_{ref} - T)) \tag{V.2}$$

Where:

- R is the resistance of the conductor at the temperature T;
- R_{ref} is the resistance of the conductor at the reference temperature T_{ref} (generally 20 °C) [2];
- α is the temperature coefficient ($\alpha = 0.004041$ for copper).

In order to see the effect of variation of stator resistance, a permanent 400% increase in R_s, which corresponds to a 742.39 °C increase in the temperature of the conductors (extreme overheating of the machine, which could possibly influence the stability of the system), has been simulated at t=0.5 s with the three converters; the inverter, the DMC and the IMC (same simulation parameters and weighting factors).

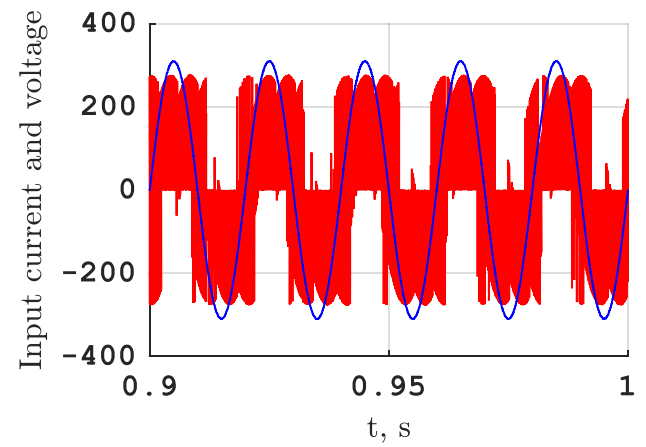(a)   (b)

(c)

(d)
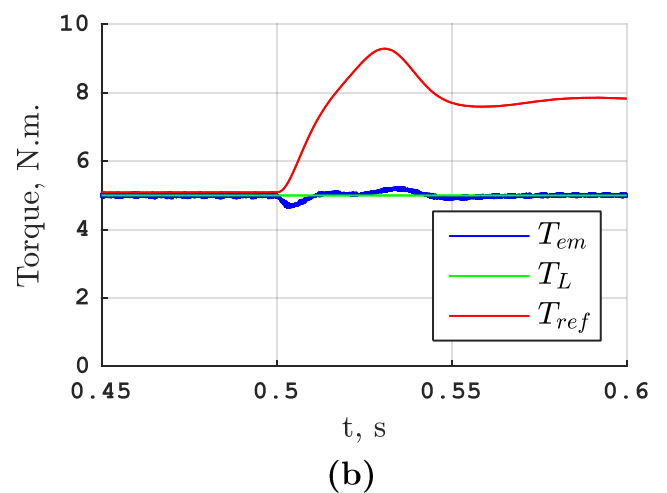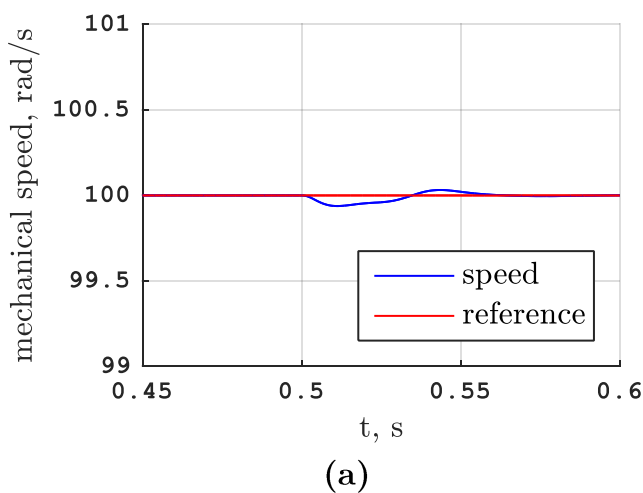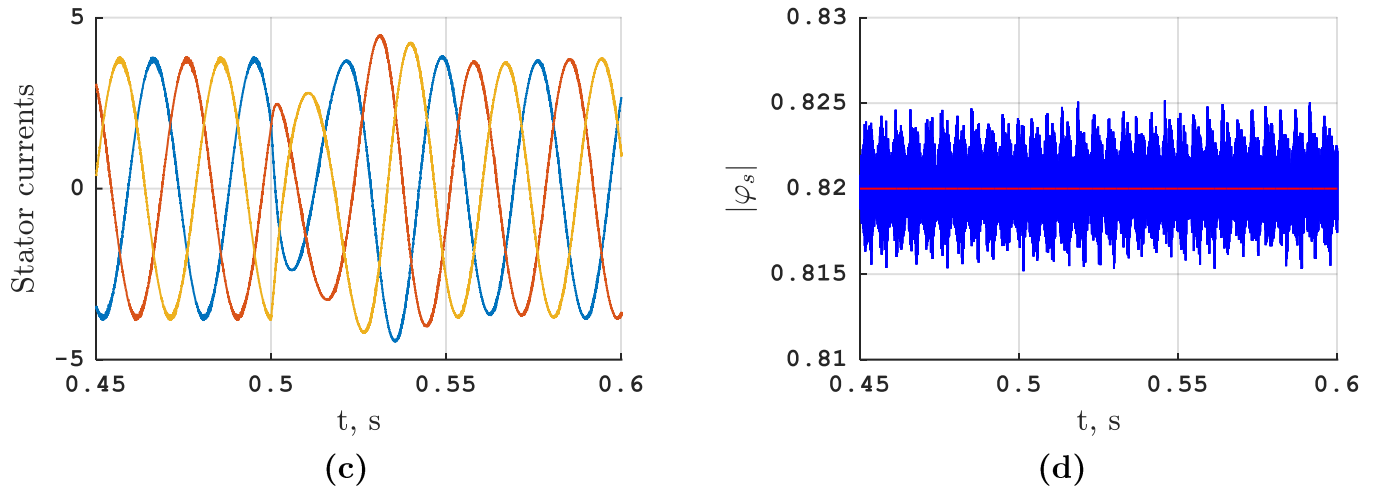
Figure V.11: Simulation results of an 400% increase in stator resistance of an inverter-fed induction machine: (a) rotor speed and its reference, (b) electromagnetic, load and reference torque, (c) stator currents, (d) stator flux

(a)

(b)

(c)

(d)
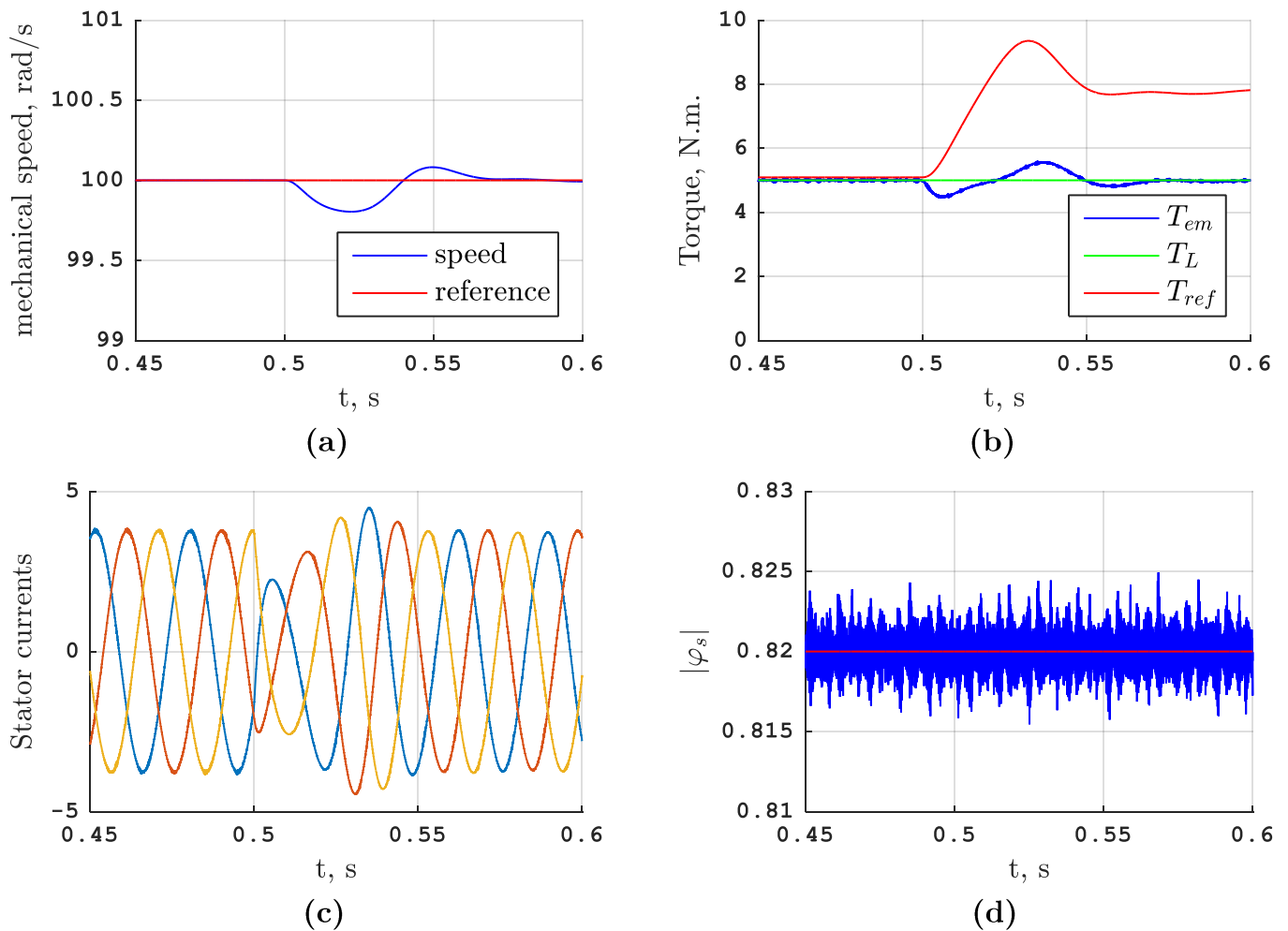
Figure V.12: Simulation results of an 400% increase in stator resistance of a DMC-fed induction machine: (a) rotor speed and its reference, (b) electromagnetic, load and reference torque, (c) stator currents, (d) stator flux
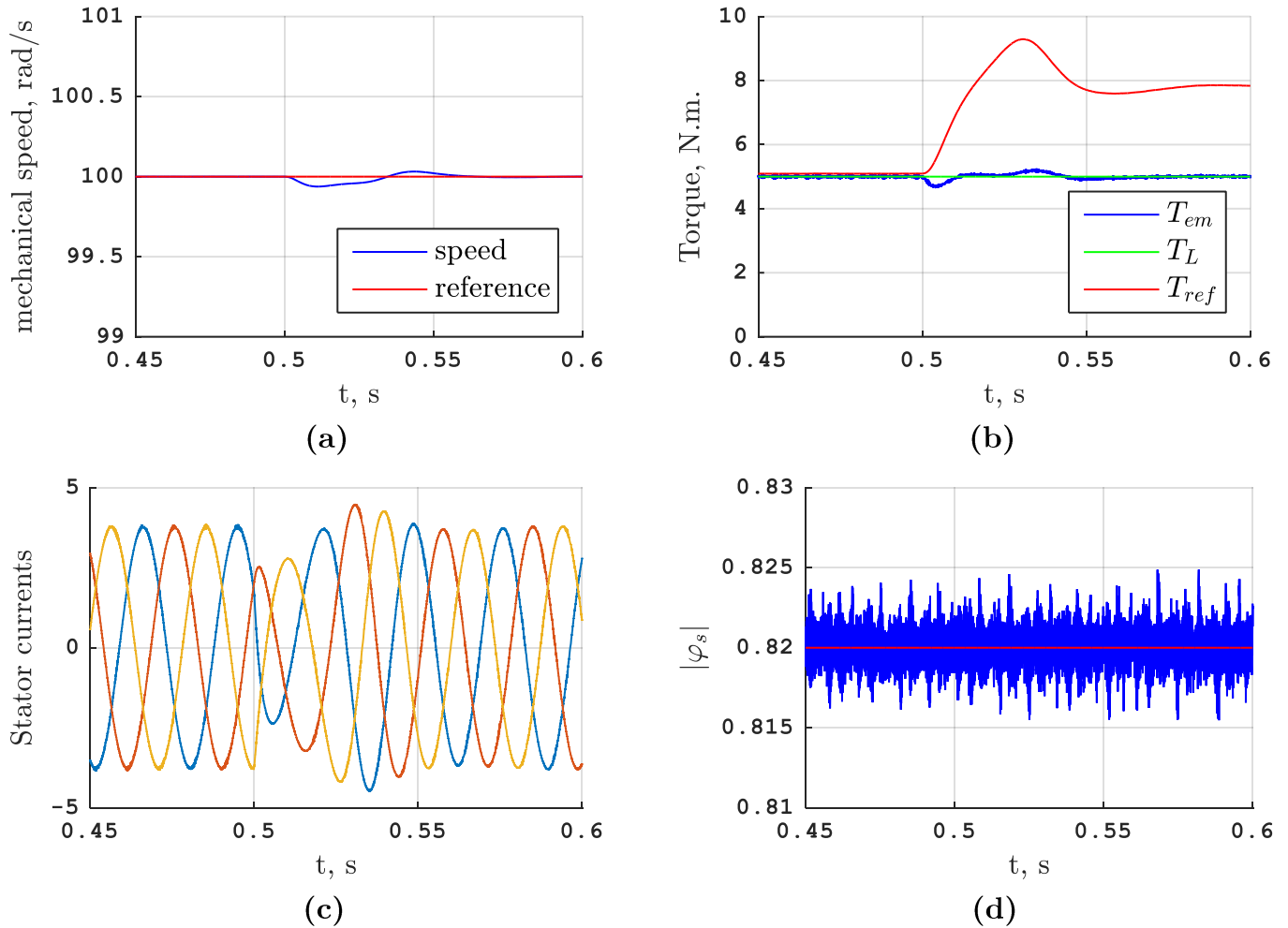
Figure V.13: Simulation results of an 400% increase in stator resistance of an IMC-fed induction machine: (a) rotor speed and its reference, (b) electromagnetic, load and reference torque, (c) stator currents, (d) stator flux

The simulation results show that the increase in value of R_s entails an error in the torque reference when using the three converters, which is caused by the variation of the stator current. As a result, a significant variation is observable in the mechanical speed as well, but the effect on the stator flux is not observable.

There is a static error between the reference and the electromagnetic torque after the increase of R_s, the latter follows the load torque. The algorithm can compensate this variation thanks to the measurements at each instant.

The biggest variation in the mechanical speed and in the electromagnetic torque was observed in the DMC.

V.4. Comparison between the three converters

The following table presents a comparison between the simulation results of the MPTC of an induction machine that is fed by the three converters studied in this thesis with the same simulation parameters previously used and (100 rad/s, 10Nm) as set point.

Both topologies of the MC present similar performance but overall, the indirect topology is better. The MPTC was simulated without the control of the reactive power to make the results as comparable as possible.

Table V.1: Comparison between the simulation results of the MPTC using the three converters

Feature	2LVSI	DMC	IMC
Max torque ripple	0.11 N.m	0.09 N.m	0.09 N.m
Max flux ripple	0.0075 Wb	0.0024 Wb	0.0024 Wb
THD of stator current (with Q minimization)	0.95% (-)	0.43% (0.52%)	0.50% (0.61%)
THD of stator voltage (with Q minimization)	111.40% (-)	58.72% (64.41%)	61.77% (67.55%)
THD of supply current (with Q minimization)	- (-)	74.41% (4.56%)	66.81% (3.73%)
Complexity of the algorithm	Low	Medium	High
Input reactive power controllability	-	Yes	Yes (best)
Stator voltage waveform	Good	Good	Good (best)
Compensation of R_s variation	Yes	Yes	Yes (best)

V.5. Comparison between MPTC and DTC

The direct torque control (DTC) for induction machines was proposed in the middle of 1980s [50]. its control algorithm is simple because of the absence of pulse width modulation (PWM), of Current Controllers and Park Transformations [51]. It does not use PI regulation loops, which should improve its dynamic skills a priori and eliminate the problems related to the saturation of PI regulators

A non-linear hysteresis-based strategy such as DTC appears to be a solution for high performance applications [44], [51]. DTC is based on two basic principles.

V.5.1. Working principle of DTC

The principle of DTC is based on the direct application of a control sequence to the switches [2]. The choice of this sequence is made by the use of a switching table

and two hysteresis regulators whose role is to control and regulate the electromagnetic torque and the flux of the machine in a decoupled manner [50].

$$\frac{d\varphi_s}{dt} = v_s - R_s i_s \qquad (V.3)$$

From (V.3), it can be deduced that the stator flux can be changed by the application of a given stator voltage vector during a time T_s. This allows control of the stator flux vector, making it able to follow a given trajectory.

The torque is estimated as a cross-product of estimated stator flux vector and measured motor current vector as presented in the below equation

$$T_{em} = p(\varphi_{s\alpha} i_{s\beta} - \varphi_{s\beta} i_{s\alpha}) \qquad (V.4)$$

Then, the estimated values of the electromagnetic torque T_{em} and the stator flux φ_s (from (V.3) and (V.4)) are compared respectively to their reference values T_{em}^* and φ_s^*, the results of the comparison form the inputs of the hysteresis comparators [44] as shown in the following figure. The selection of the appropriate voltage vector is based on a predefined control table [50]. The inputs of this table are the flux sector number and the outputs of the two hysteresis comparators.
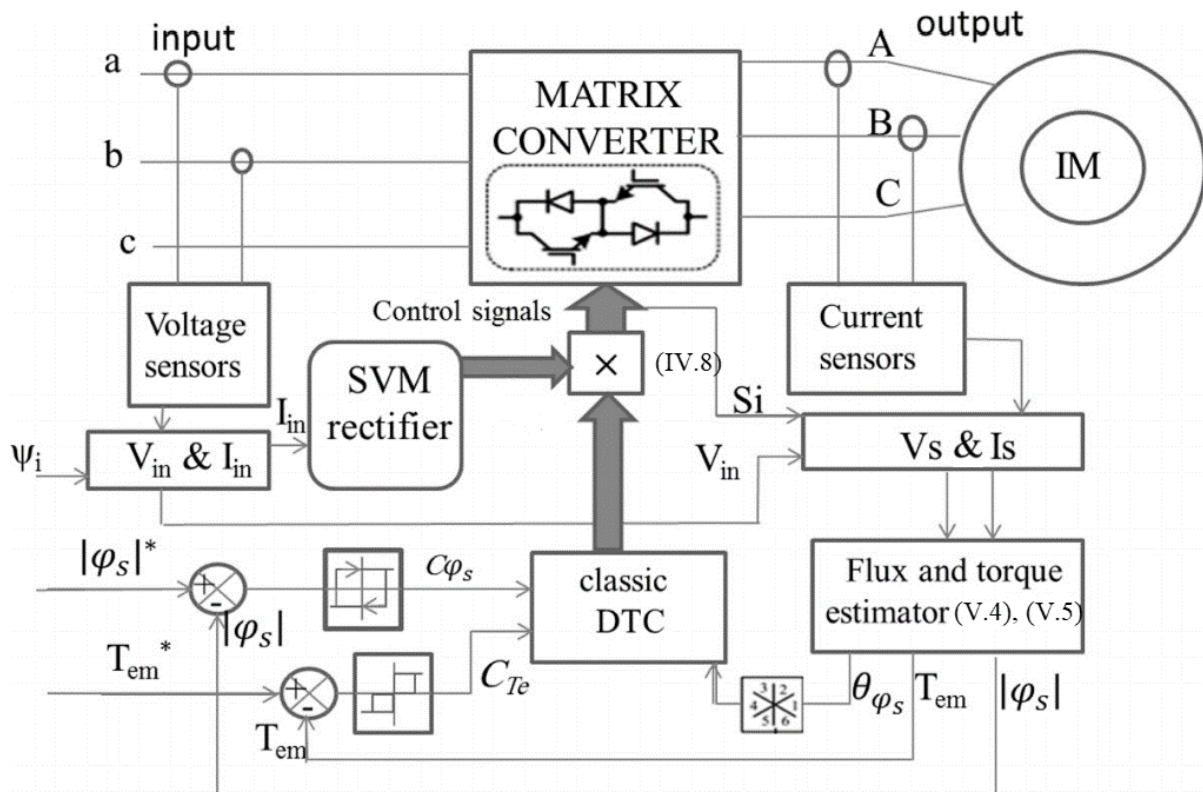
Figure V.14: Block diagram of DTC using IMC

Where:

- $\theta_{\varphi_s} = \arctan(\frac{\varphi_{s\beta}}{\varphi_{s\alpha}})$: angle of the stator flux
- Ψ_i : The input displacement angle
- C_{φ_s}: output of the hysteresis flux comparator
- C_{T_e}: output of the hysteresis flux comparator

V.5.2. Simulation results of DTC and comparison

The DTC of an IMC-fed induction machine is simulated in MATLAB/Simulink environment with the minimization of the input reactive power. The simulation parameters are the same as those applied previously.

(a)

(b)

(c)

(d)
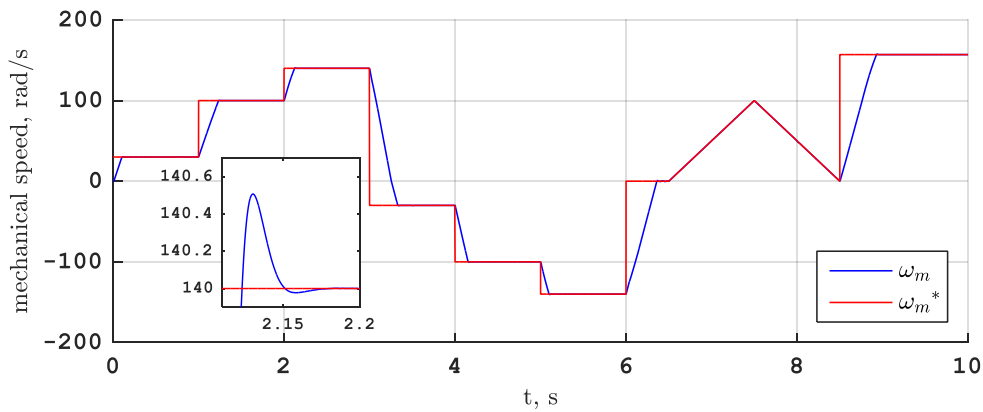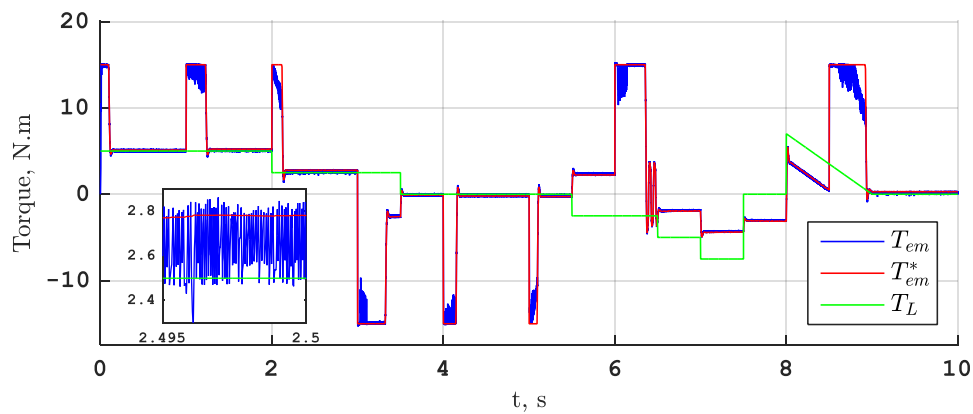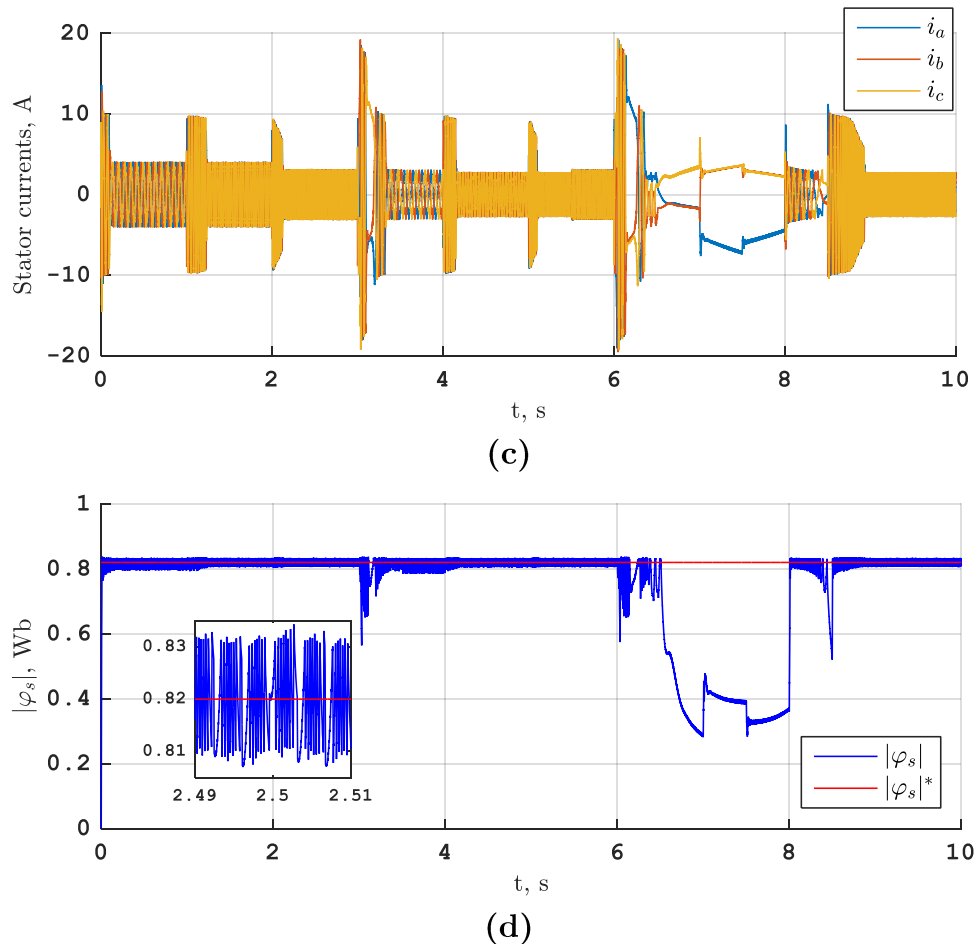
Figure V.15: Simulation results of the DTC of an IMC-fed induction machine without the control of input reactive power: **(a)** rotor speed and its reference, **(b)** electromagnetic, load and reference torque, **(c)** stator currents, **(d)** stator flux

Figure V.15 presents mechanical, electromagnetic and electrical results of DTC with PI speed regulation, applied to an IMC-fed induction machine.

The speed follows its reference well. The reference is chosen so as to have all the possibilities (constant reference, low, medium and high speed, inversion of speed and speed in the form of a ramp). The response time is slightly longer than that of MPTC (by about 50 ms).

The electromagnetic torque follows the load torque in steady state. However, the oscillations are bigger and the transient state lasts longer comparing to the MPTC.

The stator flux follows its reference, yet again with bigger oscillations. When speed is in the form of a ramp, the stator flux and stator current diverge a little.

Both electromagnetic torque and stator flux respect their respective hysteresis bands in steady state

Contrary to MPTC, when the speed is reversed, spikes in the current and stator flux are observed.

(a)

(a)

(c)

(d)

(e)

(f)

(g)

(h)
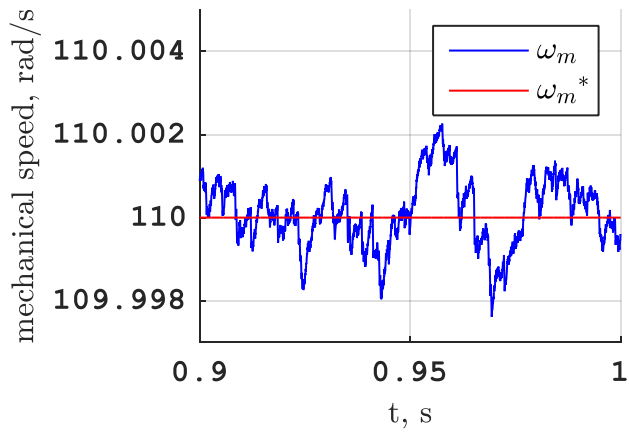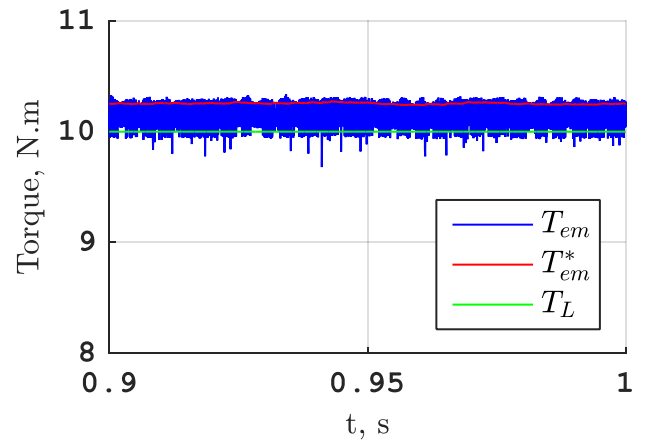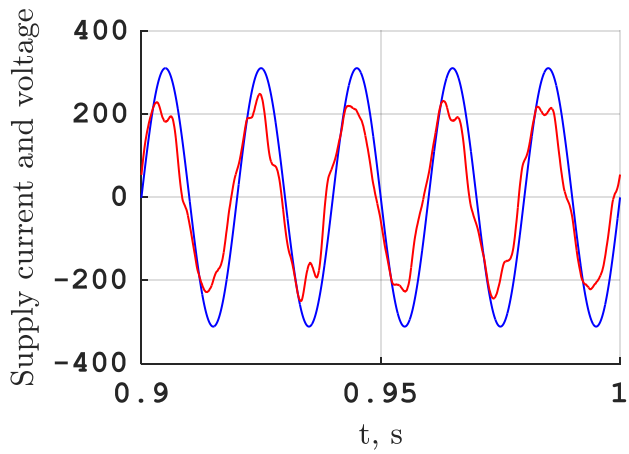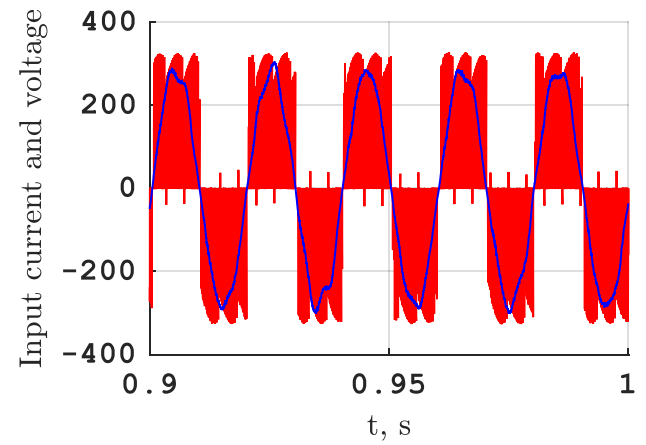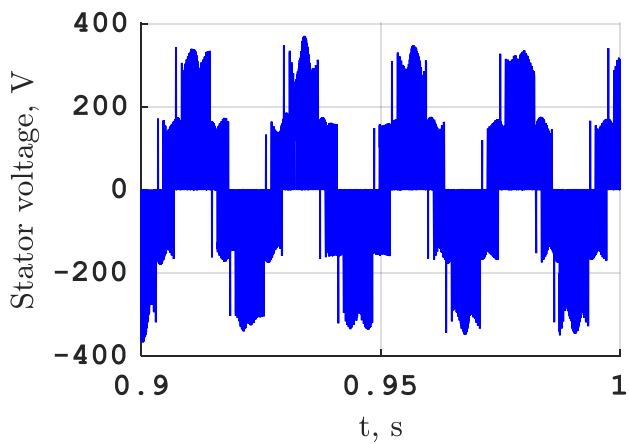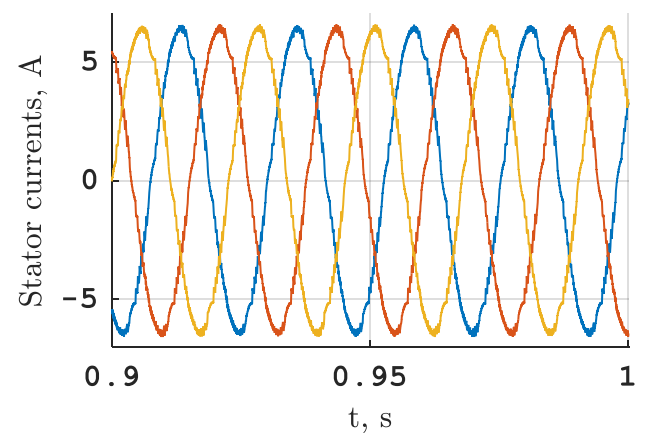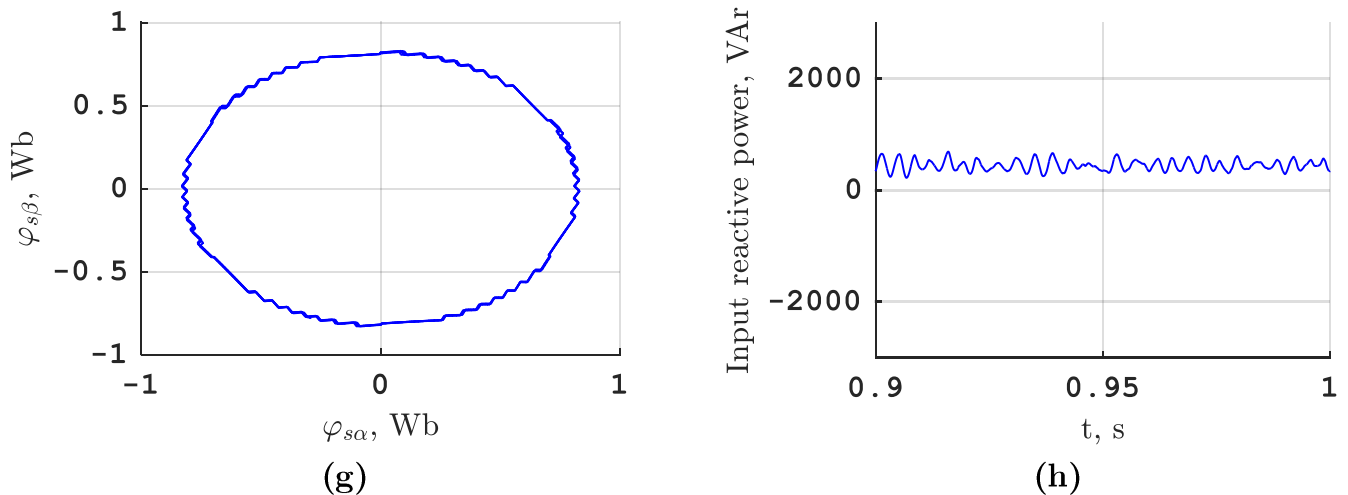
Figure V.16: Simulation results of the DTC of an IMC-fed induction machine with the control of input reactive power: steady state of **(a)** mechanical speed, **(b)** electromagnetic torque, **(c)** 50×supply current and voltage, **(d)** 50×input current and voltage, **(e)** stator voltage, **(f)** stator currents, **(g)** stator flux, **(h)** input reactive power

Figure V.16 shows the steady state of different variables with the set point (110 rad/s, 10 N.m).

The mechanical speed, the electromagnetic torque and the stator flux oscillate further around their respective references using DTC and the stator current is a little distorted compared to MPTC.

However, the DTC offers better waveforms of the stator voltage, supply and input current. Even without the control of the input reactive power, the supply current is not that much shifted from the supply voltage and it is not as distorted when using MPTC.

(a)

(b)
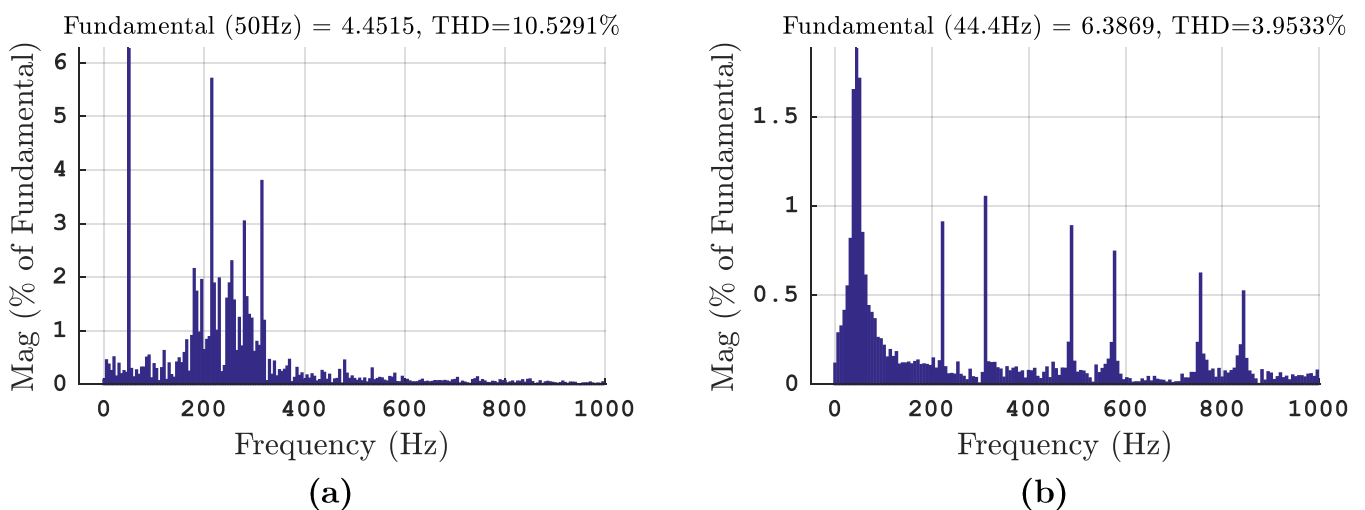
Figure V.17: Harmonic spectrum of **(a)** supply current, **(b)** stator current

Figure V.17 presents the harmonic spectrum of the supply and stator current. The better quality of the supply current by applying is reflected by the lower THD.

The following table presents a steady state comparison between the simulation results of the MPTC and the DTC of an IMC-fed induction machine with (110 rad/s, 10 Nm) as a set point with the control of reactive power.

Table V.2: Comparison between MPTC and DTC

Feature	DTC	MPTC
Max torque ripple	0.48 N.m	0.09 N.m
Max flux ripple	0.0210 Wb	0.0024 Wb
THD of stator current	03.95%	00.59%
THD of supply current	10.53%	04.66%
Switching frequency	Variable	Variable
Conceptual complexity	High	Low
Dynamics	Fast	Fast
Inner control loops[1]	Yes (hysteresis)	No
Calculation effort	Medium	High
Robustness[2]	Yes [2]	Yes (best)
Inclusion of constraints[3]	Hard [51]	Easy
Stator voltage waveform	Good (best)	Good

Both DTC and MPTC methods need the same estimated variable: the stator flux. However, MPTC needs no estimation of the angle of the stator flux which is necessary in DTC method.

In DTC method, both torque and flux hysteresis controllers are necessary. To achieve better results, it is necessary to tune the hysteresis bands. Therefore, there are two necessary parameters [51]. In MPTC there are two weighting factors of the cost function, which makes MPTC more flexible in handling constraints such as importance of electromagnetic torque versus flux control.

Since the same speed PI-controllers are used, there is no difference of the transient response. However, during the transient state, torque ripples are observed, the ripple of PTC is much lower than that of DTC method.

---

[1] The PI speed controller is not considered
[2] To disturbance and parameter variation
[3] Constraints like minimization of input reactive power, current limitation... etc.

V.6. Conclusion

The application of MPC for the control of induction machines is presented in this chapter. The MPTC is based on the idea of the direct torque control.

Both topologies are capable of generating an almost sinusoidal input currents when filtered and controlling their phase shift which gives them the possibility of operating with a unity input power factor.

The control strategy is presented for two topologies of the MC. Good performance of the system is obtained using both topologies due to the fast dynamic response thanks to the lack of external control loops, excepts for the PI speed controller.

The average of the electromagnetic torque in steady state follows the load torque and the mechanical speed follows its reference very well even when the load torque varies with both topologies of the MC.

From a performance of electrical variables point of view, the two converters generate an almost sinusoidal input and output currents with low THD.

It can be concluded that the system has good robustness with respect to the stator resistance variation and changes in the load torque thanks to inherent robustness of closed-loop control strategies for all converters.

Out of the three converters studies thus far, the IMC shows the better overall performance. The control algorithm of this converter can be expanded from a control algorithm of a 2LVSI.

Model predictive torque control achieves high-performance results which are better than the traditional approaches like DTC.

A comparative study between MPTC and DTC has been done. Both DTC and PTC methods need the same estimated variable: the stator flux. However, MPTC doesn't need an estimation of the angle of the stator flux which is necessary in DTC method [2], [51].

Compared with DTC, MPTC is more flexible to handle system constraints *e.g.:* the same importance of electromagnetic torque versus flux control or the minimization of input reactive power.

General Conclusion

General conclusion

With ongoing research efforts, the matrix converter technology is developing as a promising solution for direct AC–AC power conversion. As discussed in Chapter I, the matrix converter topology has the following features that are desirable in a range of applications [2]:

- adjustable input displacement factor, irrespective of the load (controllable power factor);
- the capability of regeneration (Four-quadrant operation, bidirectional energy flow capability [10]);
- high quality input and output waveforms;
- the lack of bulky and limited lifetime energy storage components.

In this work, Model Predictive Control schemes have been applied to power converters associated with a RL-load and with an induction machine, namely the 2LVSI, the DMC and the IMC. The study was done by simulation in the MATLAB/Simulink environment.

The work began with a general description of power converters, followed by a description of the most famous topologies of matrix converters, including a presentation of their state of the art. The first chapter ended with a brief description of the MPC, working principle and its applications. This bibliographic study has shown that this topic is contemporary and promising, attracting the attention of researchers around the world.

In the second chapter, the predictive current control strategy was introduced. Both the converter and the load have been modelled and a cost function has been expressed. The MPCC working principle was explained in detail. The load current manages to track its reference and its quality gets better with high sampling frequencies (low THD). The inverter allows, thanks to the MPCC, to control the output current in magnitude and frequency.

The low complexity of a 2LVSI and the prediction horizon of one step make the MPCC of a 2LVSI-fed RL-load one of the simplest predictive control schemes of predictive control, in terms of conceptional complexity and of calculation effort.

In the third chapter, the MPTC applied to an induction motor that is fed by a 2LVSI has been introduced, the induction machine has been modelled in a way that suits the control scheme and a cost function has been expressed in order to satisfy the

objective of the control. The mechanical speed tracks its reference perfectly even with the variation of the load torque, which is considered as a disturbance. The average value of the electromagnetic torque follows the load torque in steady state and the same goes for the flux. Furthermore, the proposed control strategy shows a good flexibility by adding a soft constraint by means of tuning the weighting factors. The stator current has a low THD and therefore a good waveform.

Chapter four presents a MPCC scheme of an RL-load fed by a matrix converter with both topologies direct and indirect. The modelling of both converters is presented alongside with the modelling of the input filter. The phase shift at the input of the converter between the current and the voltage is also controllable for the both topologies. Operation with a unity power factor is possible in this case. One of the advantages of the operation with a unity power factor is the significant improvement in the supply current waveform.

In the last chapter, MPTC was applied to two topologies of the MC, namely the DMC and the IMC. The mechanical speed tracks its reference perfectly and reacts to load torque variations even better than when the machine is fed by a 2LVSI, same thing for the electromagnetic torque and stator flux. The indirect topology shows better performances of controlling the input variables whereas the direct topology shows better performances of controlling the output variables.

Furthermore, both topologies allow the control of the input reactive power, hence the operation with a unity power factor is possible. And with the predictive control scheme, achieving such objective and adding other constraints is quite easy, only a simple weighted error signal is added to the cost function.

The robustness of the predictive control strategy for all three converters studied in this thesis is tested through simulations without any online parameter identification. The simulation results show that the predictive control, being a feedback control strategy, has an inherited robustness to parametric variation or disturbances. The IMC presents the best results in terms of compensation the stator resistance variation.

A major benefit of using MPC is that it is intuitive and unlike conventional methods, its implementation complexity will not increase for an advanced topology like MC or foe a complex load like the induction machine.

The last part of this thesis is dedicated to showcase the performance of the MPTC compared to the DTC. Even though the MPC has the disadvantage of needing high computational power, it gives better results overall.

The name MPC, in general, stems from the idea of employing an explicit model of the system to be controlled which is used to predict the future output behavior of the controlled variables. According to the studies conducted in this thesis, the predictive control has the following advantages:

- very simple and intuitive concepts;
- multivariable case can be easily considered;
- easy inclusion of constraints and non-linearities;
- fast dynamics;
- robustness.

It can be concluded that the matrix converter is an important alternative for AC-AC conversion thanks to the advantages it offers over other options and that model predictive control emerges as a possible alternative in the field of power converters and electrical drives.

As a perspective to this work, we plan to:

- IMPLEMENT the control strategy on a Field-Programmable Gate Array (FPGA) card to control an induction machine for the EXPERIMENTAL VALIDATION;
- implement other predictive control schemes such as MMPC and MPC with extended prediction horizon;
- study other MC topologies; multilevel IMC, sparse IMC and polyphase MC in particular.

References

References

[1] A. Schuster, "Commande, réglage et optimisation d'un convertisseur matriciel pour entraînements par moteur asynchrone," EPFL, 1998.

[2] A. Benachour, "Commande sans capteur basée sur DTC d'une machine asynchrone alimentée par Convertisseur Matriciel," PhD, ENP, Algiers, 2017.

[3] L. Empringham, J. W. Kolar, J. Rodriguez, P. W. Wheeler, and J. C. Clare, "Technological issues and industrial application of matrix converters: A review," *IEEE Transactions on Industrial Electronics*, vol. 60, no. 10, pp. 4260–4271, 2012.

[4] J. Holtz, "Pulsewidth modulation for electronic power conversion," *Proceedings of the IEEE*, vol. 82, no. 8, pp. 1194–1214, 1994.

[5] Q. Lei, F. Z. Peng, and B. Ge, "Pulse-width-amplitude-modulated voltage-fed quasi-Z-source direct matrix converter with maximum constant boost," 2012, pp. 641–646.

[6] J. Rodriguez and P. Cortes, *Predictive control of power converters and electrical drives*, vol. 40. John Wiley & Sons, 2012.

[7] A. M. Dadu, S. Mekhilef, and T. K. Soon, "Lyapunov model predictive control to optimise computational burden, reference tracking and THD of three-phase four-leg inverter," *IET Power Electronics*, vol. 12, no. 5, pp. 1061–1070, 2019.

[8] M. Abdelrahem, Z. Zhang, R. Kennel, H. Eldeeb, and C. Hackl, "Simple and robust direct-model predictive current control technique for pmsgs in variable-speed wind turbines," 2017, pp. 1–6.

[9] M. Abdelrahem, C. Hackl, R. Kennel, and J. Rodriguez, "Sensorless Predictive Speed Control of Permanent-Magnet Synchronous Generators in Wind Turbine Applications," 2019, pp. 1–8.

[10] A. Alesina and M. G. Venturini, "Analysis and design of optimum-amplitude nine-switch direct AC-AC converters," *IEEE Transactions on Power Electronics*, vol. 4, no. 1, pp. 101–112, 1989.

[11] M. Khosravi *et al.*, "Review of model predictive control strategies for matrix converters," *IET Power Electronics*, vol. 12, no. 12, pp. 3021-3032(11), Oct. 2019.

[12] L. Gugyi, *Static Power Frequency Changers; Thoery, Performace, and Application.* Wiley-Interscience, 1976.

[13] M. Y. Lee, "Three-level neutral-point-clamped matrix converter topology," 2009.

[14] B. K. Bose, *Power electronics and motor drives: advances and trends.* Elsevier, 2010.

[15] T. Friedli and J. W. Kolar, "Milestones in matrix converter research," *IEEJ Journal of industry applications*, vol. 1, no. 1, pp. 2–14, 2012.

[16] R. Alammari, Z. Aleem, A. Iqbal, and S. Winberg, "Matrix converters for electric power conversion: Review of topologies and basic control techniques," *International Transactions on Electrical Energy Systems*, vol. 29, no. 10, p. e12063, 2019.

[17] J. Holtz and U. Boelkens, "Direct frequency convertor with sinusoidal line currents for speed-variable AC motors," *IEEE Transactions on Industrial Electronics*, vol. 36, no. 4, pp. 475–479, 1989.

[18] L. Huber and D. Borojevic, "Space vector modulated three-phase to three-phase matrix converter with input power factor correction," *IEEE transactions on industry applications*, vol. 31, no. 6, pp. 1234–1246, 1995.

[19] J. W. Kolar, M. Baumann, F. Schafmeister, and H. Ertl, "Novel three-phase AC-DC-AC sparse matrix converter," 2002, vol. 2, pp. 777–791.

[20] P. Szczesniak, "Three-Phase AC–AC Power Converters Based on Matrix Converter Topology," *Springer*, 2013.

[21] M. Y. Lee, C. Klumpner, and P. Wheeler, "Experimental evaluation of the indirect three-level sparse matrix converter," 2008.

[22] B. Ge, Q. Lei, W. Qian, and F. Z. Peng, "A family of Z-source matrix converters," *IEEE Transactions on Industrial Electronics*, vol. 59, no. 1, pp. 35–46, 2011.

[23] X. P. Fang, Z. M. Qian, and F. Z. Peng, "Single-phase Z-source PWM ac-ac converters," *IEEE Power Electronics Letters*, vol. 3, no. 4, pp. 121–124, 2005.

[24] J. H. Lee, "Model predictive control: Review of the three decades of development," *International Journal of Control, Automation and Systems*, vol. 9, no. 3, p. 415, 2011.

[25] S. Vazquez, J. Rodriguez, M. Rivera, L. G. Franquelo, and M. Norambuena, "Model predictive control for power converters and drives: Advances and trends," *IEEE Transactions on Industrial Electronics*, vol. 64, no. 2, pp. 935–947, 2016.

[26] J. Holtz, "A predictive controller for the stator current vector of ac machines fed from a switched voltage source," *Proc. of IEE of Japan IPEC-Tokyo'83*, pp. 1665–1675, 1983.

[27] M. Niroomand and H. Karshenas, "Review and comparison of control methods for uninterruptible power supplies," 2010, pp. 18–23.

[28] E. F. Camacho and C. B. Alba, *Model predictive control*. Springer Science & Business Media, 2013.

[29] G. C. Goodwin, M. Seron, and J. De Dona, "Constrained control and estimation: and optimization approach/Graham C. Goodwin, María M. Seron, and José De Doná.," 2005.

[30] O. Begovich, V. Ruiz, G. Besancon, C. Aldana, and D. Georges, "Predictive control with constraints of a multi-pool irrigation canal prototype," *Latin American applied research*, vol. 37, no. 3, pp. 177–185, 2007.

[31] S. Vazquez *et al.*, "Model Predictive Control: A Review of Its Applications in Power Electronics," *IEEE Industrial Electronics Magazine*, vol. 8, no. 1, pp. 16–31, Mar. 2014, doi: 10.1109/MIE.2013.2290138.

[32] J. Rodriguez *et al.*, "State of the art of finite control set model predictive control in power electronics," *IEEE Transactions on Industrial Informatics*, vol. 9, no. 2, pp. 1003–1016, 2012.

[33] H. M. Basri, K. Lias, and S. Mekhilef, "Digital Predictive Current Control Fed by Three-Level Indirect Matrix Converter under Unbalanced Power Supply Condition."

[34] M. Uddin, S. Mekhilef, M. Rivera, and J. Rodriguez, "Predictive indirect matrix converter fed torque ripple minimization with weighting factor optimization," 2014, pp. 3574–3581.

[35] M. P. Akter, S. Mekhilef, N. M. L. Tan, and H. Akagi, "Modified model predictive control of a bidirectional AC–DC converter based on Lyapunov function for energy storage systems," *IEEE Transactions on Industrial Electronics*, vol. 63, no. 2, pp. 704–715, 2015.

[36] M. P. Akter, S. Mekhilef, N. M. L. Tan, and H. Akagi, "Model predictive control of bidirectional AC-DC converter for energy storage system," *Journal of Electrical Engineering & Technology*, vol. 10, no. 1, pp. 165–175, 2015.

[37] M. P. Akter, S. Mekhilef, N. M. L. Tan, and H. Akagi, "Stability and performance investigations of model predictive controlled active-front-end (AFE) rectifiers for energy storage systems," *Journal of Power Electronics*, vol. 15, no. 1, pp. 202–215, 2015.

[38] H. Akagi, A. Nabae, and S. Atoh, "Control Strategy of Active Power Filters Using Multiple Voltage-Source PWM Converters," *IEEE Transactions on Industry Applications*, vol. IA-22, no. 3, pp. 460–465, May 1986, doi: 10.1109/TIA.1986.4504743.

[39] P. Zanchetta, P. Cortes, M. Perez, J. Rodriguez, and C. Silva, "Finite States Model Predictive Control for Shunt Active Filters," in *IECON 2011 - 37th Annual Conference of the IEEE Industrial Electronics Society*, Nov. 2011, pp. 581–586, doi: 10.1109/IECON.2011.6119375.

[40] R. P. Aguilera *et al.*, "Selective Harmonic Elimination Model Predictive Control for Multilevel Power Converters," *IEEE Transactions on Power Electronics*, vol. 32, no. 3, pp. 2416–2426, Mar. 2017, doi: 10.1109/TPEL.2016.2568211.

[41] H. Aggrawal, J. I. Leon, L. G. Franquelo, S. Kouro, P. Garg, and J. Rodríguez, "Model predictive control based selective harmonic mitigation technique for multilevel cascaded H-bridge converters," 2011, pp. 4427–4432.

[42] M. Rivera *et al.*, "A Comparative Assessment of Model Predictive Current Control and Space Vector Modulation in a Direct Matrix Converter," *IEEE Transactions on Industrial Electronics*, vol. 60, no. 2, pp. 578–588, Feb. 2013, doi: 10.1109/TIE.2012.2206347.

[43] J. Rodriguez *et al.*, "Predictive Current Control of a Voltage Source Inverter," *IEEE Transactions on Industrial Electronics*, vol. 54, no. 1, pp. 495–503, Feb. 2007, doi: 10.1109/TIE.2006.888802.

[44] A. Benachour, E. M. Berkouk, and M. O. Mahmoudi, "Study and comparison between two DTC strategies of induction machine fed by direct matrix converter," *Journal of Renewable and Sustainable Energy*, vol. 9, no. 5, p. 055501, 2017.

[45] J. Holtz, "The representation of AC machine dynamics by complex signal flow graphs," *IEEE Transactions on Industrial Electronics*, vol. 42, no. 3, pp. 263–271, Jun. 1995, doi: 10.1109/41.382137.

[46] M. Siami, D. A. Khaburi, M. Rivera, and J. Rodriguez, "An experimental evaluation of predictive current control and predictive torque control for a PMSM fed by a matrix converter," *IEEE Transactions on Industrial Electronics*, vol. 64, no. 11, pp. 8459–8471, 2017.

[47] H.-N. Nguyen, M.-K. Nguyen, T.-D. Duong, T.-T. Tran, Y.-C. Lim, and J.-H. Choi, "A Study on Input Power Factor Compensation Capability of Matrix Converters," *Electronics*, vol. 9, no. 1, p. 82, 2020.

[48] F. Blaschke, "The principle of field orientation applied to the new transvector closed-loop control system for rotating field machines," *Power Electron*, vol. 2, no. 2, pp. 26–28, 2004.

[49] I. Takahashi and T. Noguchi, "A new quick-response and high-efficiency control strategy of an induction motor," *IEEE Transactions on Industry applications*, no. 5, pp. 820–827, 1986.

[50] N. El Ouanjli *et al.*, "Modern improvement techniques of direct torque control for induction motor drives-a review," *Protection and Control of Modern Power Systems*, vol. 4, no. 1, p. 11, 2019.

[51] F. Wang, Z. Chen, P. Stolze, R. Kennel, M. Trincado, and J. Rodriguez, "A comprehensive study of direct torque control (DTC) and predictive torque control (PTC) for high performance electrical drives," *EPE Journal*, vol. 25, no. 1, pp. 12–21, 2015.

Appendices

Appendix A

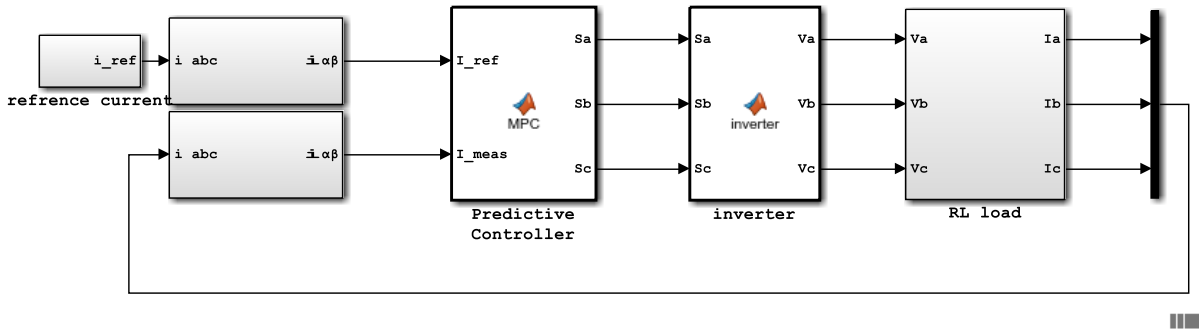Figure A.1: Simulink model of MPCC of a 2LVSI-fed RL-load

Table A.1: Simulation parameters for the MPCC of an inverter-fed RL-load

Parameter	Value
Fixed-step size	5 μs
Solver	ode3
Tasking mode	SingleTasking
Resistance	50 Ω
Inductance	20 mH
DC voltage	300 V

Appendix B

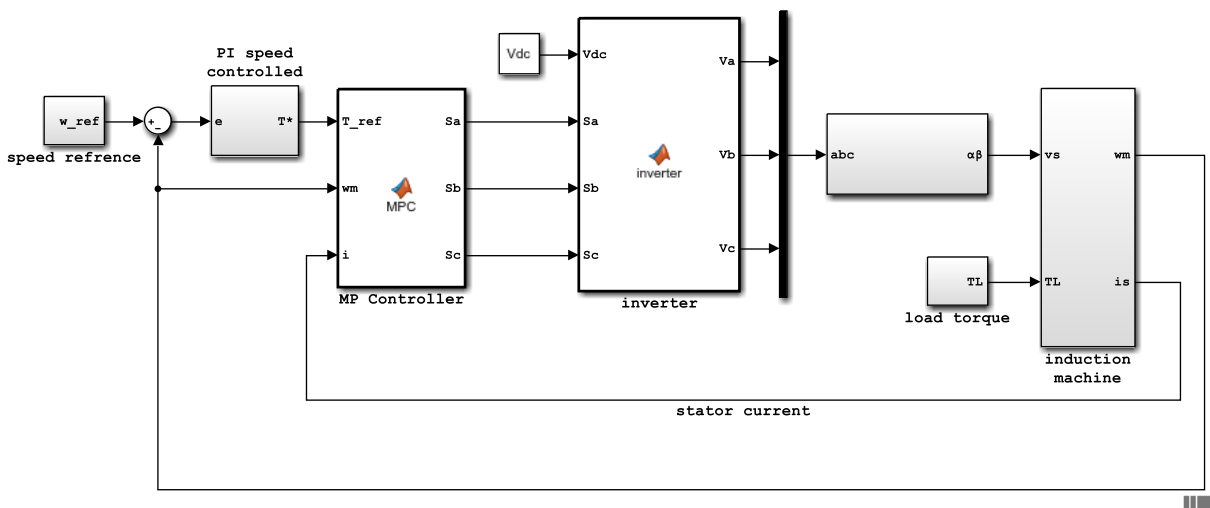Figure B.1: Simulink model of MPTC of a 2LVSI-fed induction machine

Table B.1: Machine parameters

Description	Variables	Values
Rated power	P_{nom}	1.5 kW
Rated torque	T_{nom}	15 N.m
Rated speed	Ω_{nom}	157 rad/s
Rated stator current (RMS)	I_{nom}	6.7 A
Stator resistance	R_s	4.85 Ω
Stator inductance	L_s	0.274 H
Rotor resistance	R_r	6.3 Ω
Rotor inductance	L_r	0.274 H
Magnetizing inductance	L_m	0.258 H
Pole pairs	p	2
Dry friction coefficient	k_f	N.m.s.rad^{-1}
Moment of inertia	J	0.031 kg.m^2

Table B.2: Simulation parameters for the MPTC of an inverter-fed induction motor

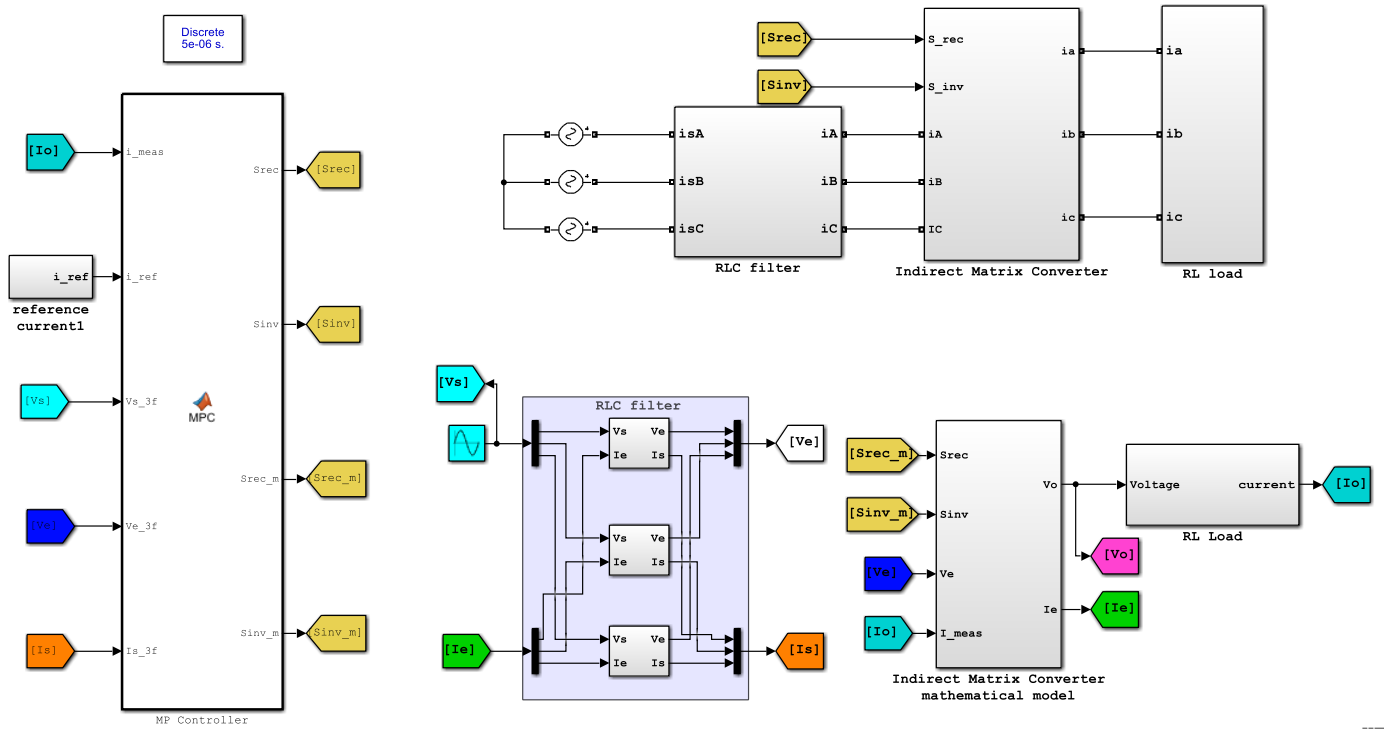| Description	Variables	Values
Fixed-step size	-	5 μs
Solver	-	ode3
Tasking mode	-	SingleTasking
Supply voltage	V_{DC}	500 V
Damping coefficient	ξ	0.7
Natural circular pulse	ω_n	100π rad/s
	λ_T	0.0667 N^{-1}m^{-1}
Weighting factors	λ_φ (case 1)	1.2195 Wb^{-1}
	λ_φ (case 2)	3.6585 Wb^{-1}

Appendix C

Figure C.1: Simulink model of MPCC of an IMC-fed RL-load

Figure C.2: Simulink model of MPCC of a DMC-fed RL-load

Table C.1: Simulation parameters for the MPCC of a MC-fed RL-load

Description	Variables	Values
Fixed-step size	-	5 μs
Solver	-	ode3
Tasking mode	-	SingleTasking
Supply voltage (RMS)	v_s	220 V
Weighting factor	λ_Q	0.035

Table C.2: Filter parameters

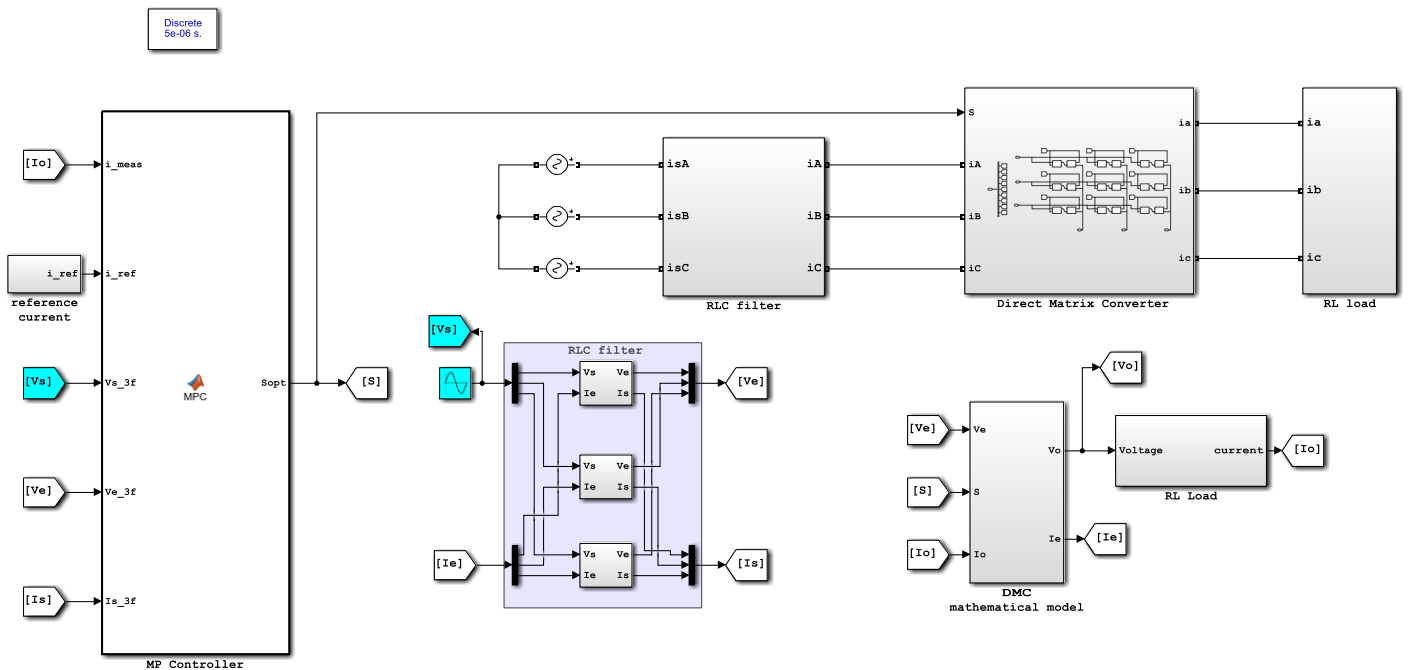| Description	Variables	Values
Filter resistor	R_f	0.5 Ω
Filter inductor	L_f	400 µH
Filter capacitor	C_f	21 µF

Appendix D

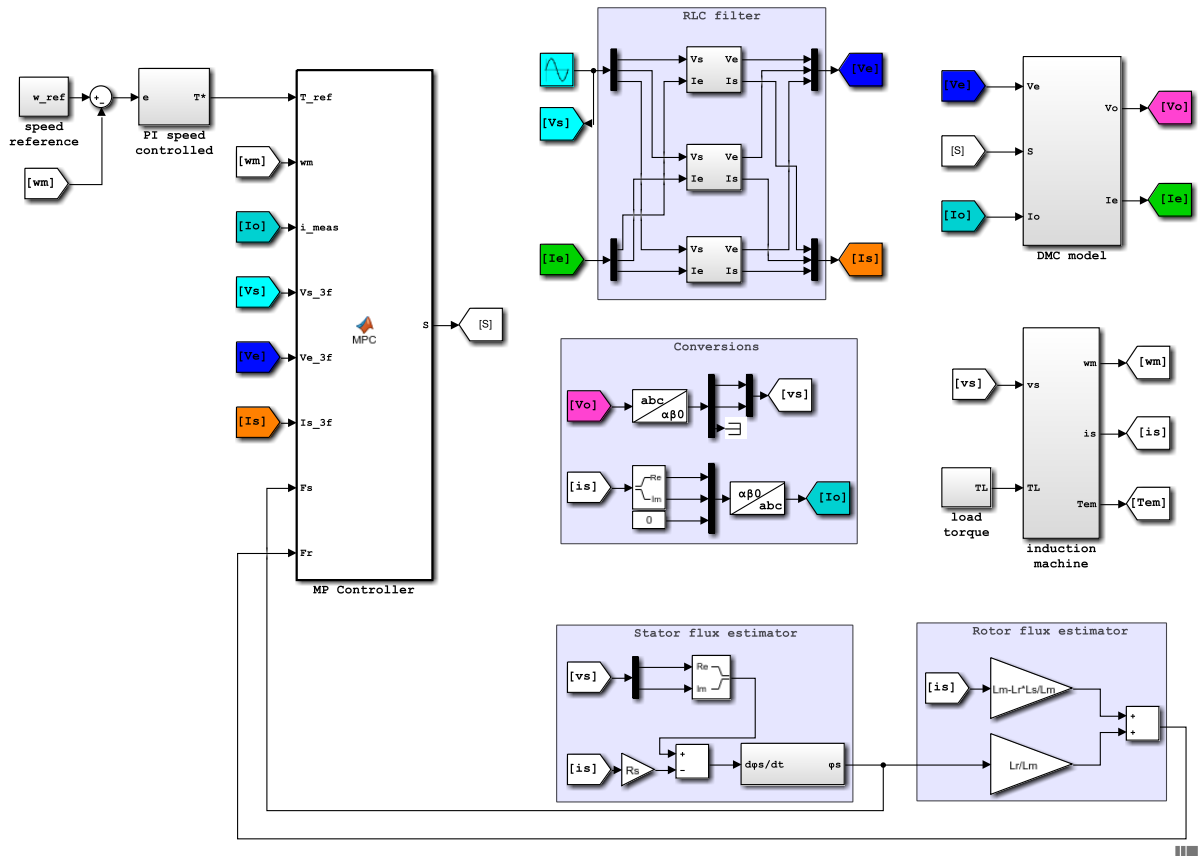Figure D.1: Simulink model of MPTC of an IMC-fed induction machine

Figure D.2: Simulink model of MPTC of a DMC-fed induction machine

Table D.1: Simulation parameters for the MPTC of a MC-fed induction machine

Description	Variables	Values
Fixed-step size	-	5 μs
Solver	-	ode3
Tasking mode	-	SingleTasking
Sampling frequency	f_s	100 kHz
Supply voltage (RMS)	v_s	220 V
Damping coefficient	ξ	0.7
Natural circular pulse	ω_n	100π rad/s
	λ_T	200
Weighting factor	λ_φ	10000
	λ_Q	1
Flux hysteresis band	h_φ	0.01 Wb
Torque hysteresis band	h_T	0.2 N.m
	$< \sin(\Psi) >^*$	0